NASA CR-121144

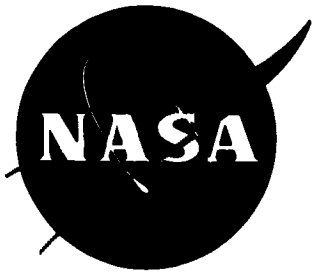

THERMOPHYSICAL PROPERTIES OF PLASMA SPRAYED COATINGS

by

K. E. Wilkes and J. F. Lagedrost

BATTELLE
Columbus Laboratories
505 King Avenue
Columbus, Ohio 43201

prepared for

NATIONAL AERONAUTICS AND SPACE ADMINISTRATION

NASA Lewis Research Center
Contract NAS3-13329

1. Report No.	2. Government Accession No.	3. Recipient's Catalog No.
NASA CR 121144		

4. Title and Subtitle	5. Report Date
Thermophysical Properties of Plasma Sprayed Coatings	March 1973
	6. Performing Organization Code

7. Author(s)	8. Performing Organization Report No.
K. E. Wilkes and J. F. Lagedrost	
	10. Work Unit No.

9. Performing Organization Name and Address	11. Contract or Grant No.
Battelle Columbus Laboratories 505 King Avenue Columbus, OH 43201	NAS3-13329
	13. Type of Report and Period Covered
12. Sponsoring Agency Name and Address	Contract Report
National Aeronautics and Space Administration Washington, DC 20546	14. Sponsoring Agency Code

15. Supplementary Notes

Project Manager, William L. Jones, V/STOL and Noise Division, NASA Lewis Research Center, Cleveland, Ohio

16. Abstract

Thermophysical properties of plasma sprayed materials were determined for the following plasma sprayed materials: CaO - stabilized ZrO_2, Y_2O_3 - stabilized ZrO_2, Al_2O_3, H_fO_2 Mo, nichrome, NiAl, Mo-ZrO_2, and $MoAl_2O_3$ mixtures. In all cases the thermal conductivity of the as-sprayed material was found to be considerably lower than that of the bulk material. The "flash-laser" thermal diffusivity technique was used both for diffusivity determination of single-layer materials and to determine the thermal contact resistance at the interface of two-layer specimens.

17. Key Words (Suggested by Author(s))	18. Distribution Statement
Thermophysical properties Thermal diffusivity Thermal conductivity Plasma sprayed materials	Unclassified - Unlimited

19. Security Classif. (of this report)	20. Security Classif. (of this page)	21. No. of Pages	22. Price*
Unclassified	Unclassified	140	$3.00

* For sale by the National Technical Information Service, Springfield, Virginia 22151

TABLE OF CONTENTS

LIST OF TABLES

TABLE OF CONTENTS (CONTINUED)

LIST OF FIGURES

LIST OF FIGURES (CONTINUED)

LIST OF FIGURES (CONTINUED)

LIST OF FIGURES (CONTINUED)

LIST OF FIGURES (CONTINUED)

THERMOPHYSICAL PROPERTIES OF PLASMA SPRAYED COATINGS

by

K. E. Wilkes and J. F. Lagedrost

SUMMARY

The objective of this program was to determine the thermophysical properties of plasma sprayed materials that were considered for use as thermally insulating coatings on rocket nozzles.

Thermal conductivity values were determined for the following plasma sprayed materials: CaO-stabilized ZrO_2, Y_2O_3-stabilized ZrO_2, Al_2O_3, HfO_2, Mo, nichrome, NiAl, and Mo-ZrO_2, and Mo-Al_2O_3 mixtures. The thermal conductivity values were derived from separately measured values of thermal diffusivity, specific heat, and density. The main emphasis was placed upon property determinations in the temperature range from about 1200 K to about 2300 K, although many determinations were made at lower temperatures. In all cases, the thermal conductivity of the as-sprayed material was found to be considerably lower than that of the bulk material and was found to increase as a result of heat treatment at high temperature. For example, the thermal conductivity of as-sprayed CaO-stabilized ZrO_2 near 550 K was found to be about a factor of three lower than the values obtained after high-temperature heat treatment. Similarly, near 1300 K, the initial conductivity of plasma sprayed Al_2O_3 is about a factor of two lower than the values after heat treatment (the postheat treatment values are within some 10 to 20 percent of the bulk values for Al_2O_3). Similar effects were observed with plasma-sprayed metals. The thermal conductivity of as-sprayed Mo is lower than values for the pure bulk material by factors of about seven and three at temperatures of 500 K and 1300 K, respectively. Following final heat treatment at 2273 K, the conductivity of plasma-sprayed Mo is about 35 percent lower than that of pure bulk Mo. The apparent explanation for these effects is that poor thermal contact exists between individual particles in the as-sprayed condition and that the thermal contact improves at high temperatures due to sintering effects. The sintering effects also result in significant dimension shrinkages. The following tabulation summarizes some thermal conductivity values of the plasma sprayed materials following heat treatment:

Thermal Conductivity

Temperature, K	Watt m^{-1} K^{-1}										
	CaO Stab. ZrO_2	Y_2O_3 Stab. ZrO_2	Al_2O_3	HfO_2	Mo	Nichrome	NiAl	75 Mo-25 ZrO_2	25 Mo-75 ZrO_2	75 Mo-25 Al_2O_3	25 Mo-75 Al_2O_3
1000	1.65	—	—	—	—	15.0	22.0	—	—	—	—
1200	1.60	—	—	—	69	17.0	23.0	85	21.0	73	15.0
1400	1.55	2.00	6.4	2.00	67	18.5	23.5	84	22.5	72	14.5
1600	1.50	1.90	6.0	2.15	64	—	—	81	23.0	70	13.5
1800	1.50	1.75	5.5	2.35	62	—	—	78	23.5	67	12.5
2000	1.50	1.70	5.0	2.45	59	—	—	74	23.5	63	11.0
2200	1.50	1.65	—	2.40	57	—	—	65	22.5	—	—

Thermal conductivity increases were found to be functions of heat treatment temperature and heat treatment time. The heat treatment temperature appears to be the major variable, with the heat treatment time producing relatively minor effects. In some cases, the measuring atmosphere (i.e., type and pressure of gas) has a significant influence on the thermal conductivity. High-temperature heat treatments reduce the effect of the atmosphere. It was found that plasma-sprayed coatings containing molybdenum contain significant amounts of oxygen which is removed by heat treatment in hydrogen at fairly moderate temperatures. However, since the water vapor formed by this reaction would probably be removed from the coating system, this effect might not be deleterious to coating performance.

No obvious trend was found for thermal conductivity versus coating thickness for Y_2O_3-stabilized ZrO_2, Al_2O_3, and HfO_2. Thus, thermal conductivity gradients, if present at all, are relatively small.

The "flash-laser" thermal diffusivity technique, normally used for single layer homogeneous materials, was extended to enable the determination of the thermal contact resistance at the interface of a two-layer specimen. The thermal contact conductance (the reciprocal of the contact resistance) between a stainless steel substrate and a layer of plasma-sprayed molybdenum was found to vary between 1.5×10^5 and 6×10^5 Watt m^{-2} K^{-1}. Corresponding thermal contact resistances would be between 6.7×10^{-6} and 1.7×10^{-6} $Watt^{-1}$ m^2 K. At most, this contact resistance would yield a thermal resistance equivalent to a layer of plasma-sprayed ZrO_2 about 1.3×10^{-5} m (about 0.0005 in.) thick.

INTRODUCTION

The heat flux levels of current NERVA type nuclear rocket nozzles are at a level sufficiently high to cause the regenerative cooled tubes of the nozzles to operate at temperatures near the limiting value for conventional stainless steel materials. Advanced nuclear rockets will operate at higher gas temperatures and heat flux levels. These conditions will impose a more difficult job of cooling for the nuclear nozzle. One method of reducing the cooling requirements is by the use of thermally insulating coatings. Such coatings have the potential for reducing the heat flux to the nozzle by 50 percent or more.

In the development of reliable thermally insulating coating systems for rocket engines, an accurate knowledge of the thermophysical properties of the coating system is necessary in order to determine the thermal gradient and surface temperature of the system. For a graded layer coating system, these properties include the thermal conductivity of each of the layers and the thermal contact resistance between the stainless steel substrate and the first sprayed layer.

Plasma-sprayed coatings are applied to cooled substrate materials and are built up to the desired thickness by a succession of spray passes. Thus, each succeeding spray pass becomes insulated from the cooled substrate by the previous passes. This process could result in changes in the coating structure and thus produce density and thermal conductivity variations (or gradients) with thickness. Thus, a knowledge of possible thermal conductivity gradients is necessary.

The objectives of this program were:

(1) To determine the thermal conductivity of a number of selected plasma-sprayed materials over a range of temperatures and gas pressures.

(2) To determine possible changes in thermal conductivity of plasma-sprayed coatings as a function of time at temperature.

(3) To determine possible thermal conductivity gradients in plasma-sprayed coatings.

(4) To determine possible thermal contact resistances between stainless steel substrates and plasma-sprayed metal coatings.

MATERIALS

All plasma-sprayed specimens used in this program were prepared by the Rocket Cooling Section, Chemical Rocket Division, NASA Lewis Research Center, under the direction of Mr. William L. Jones, who was also NASA Project Manager for this program. Spray powders used in the preparation of specimens were:

(1) CaO-stabilized ZrO_2: Metco No. 201-B

(2) Y_2O_3-stabilized ZrO_2: Zyttrite

(3) Al_2O_3: Plasmalloy 331-F

(4) HfO_2: Cerac 1547

(5) Molybdenum: Metco No. 63

(6) Nichrome: Atlantic Equipment Engineers

(7) NiAl: Metco No. 405.

With the exception of the nichrome, all the spray powders were processed to an average particle size of 30 microns prior to spraying. The nichrome powder was processed to an average particle size of 44 microns.

TECHNICAL APPROACH

There exist several techniques for determining the thermal conductivity of solid materials. One of the most versatile is that known as the "flash-laser" diffusivity technique. With this technique, the thermal conductivity is not measured directly. Rather, the thermal diffusivity is measured and the conductivity is calculated by the relation:

$$\lambda = \alpha \, Cp \, d \quad , \tag{1}$$

where

λ = thermal conductivity
α = thermal diffusivity
Cp = specific heat
d = density.

This technique is particularly well suited for the determination of the thermal conductivity of plasma-sprayed coatings, since the technique can employ relatively small samples.

With the "flash-laser" thermal diffusivity technique, a disk-shaped specimen is placed in the isothermal zone of a furnace and the front face is heated with a short-duration pulse from a ruby laser. As the heat pulse travels through the specimen, the back-face temperature rise is recorded as a function of time. This temperature-time history of the back face is directly related to the thermal diffusivity of the specimen. Assuming that heat flow is one-dimensional and that the incident energy from the laser is uniformly absorbed at the front surface of an opaque homogeneous specimen, this time-temperature relationship is given by:

$$\Delta T = \frac{4Q\ell}{\lambda a} \sum_{n=1}^{\infty} \left[\frac{\sin\mu_n \exp\left(-\mu_n^2 \theta t/a\right)}{\left(\frac{\mu_n^2 + \beta^2}{\mu_n}\right)\sin^2 \mu_n + 2\beta\mu_n} \right] \left[\frac{\exp\left(\mu_n^2\theta\right)-1}{\mu_n^2\theta} - 1 \right] \qquad (2)$$

where

μ_n = roots of the transcendental equation

$\tan \mu_n = 2\beta\mu_n/(\mu_n^2 - \beta^2)$

$\theta = \alpha a/\ell^2$

α = thermal diffusivity

t = time from start of the laser pulse

a = pulse time of laser (laser pulse is adequately described as a negative-going saw-tooth with a base of about 1-1/3 milliseconds)

Q = total energy per unit area in laser pulse

ℓ = specimen thickness

λ = thermal conductivity

$\beta = \gamma\ell/\lambda$

γ = coefficient of heat transfer off the specimen faces.

Equation (2) may be solved numerically for α and β using ΔT and t as input data. In practice, it is easiest to solve for α and β by Cowan's method[1], by determining: (1) $t_{1/2}$, the time at which ΔT reaches one-half of its maximum value, and (2) the ratio $\Delta T\ (5t_{1/2})/\ \Delta T\ (t_{1/2})$. These two experimentally determined parameters provide sufficient information to derive the thermal diffusivity.

---

(1) References at end.

Larson and Koyama[2] have extended the analysis of the pulse laser technique to samples consisting of two layers of different materials with no thermal contact resistance at the interface. With the assumption of no heat losses from the specimen surfaces, the rear face temperature-time relationship for a two-layer system using the above described laser input is given by

$$\Delta T \left(\frac{Q}{C_1 d_1 \ell_1 + C_2 d_2 \ell_2}\right)^{-1} = 1 + 4 \sum_{n=1}^{\infty} \left\{ \frac{\exp\left(-\beta_n^2 \theta \frac{t}{a}\right) \left[\frac{\exp\left(\beta_n^2 \theta\right) - 1}{\beta_n^4 \theta^2} - \frac{1}{\beta_n^2 \theta}\right]}{\cos X\beta_n \cos\beta_n - \left(\frac{X + \frac{H}{X}}{H + 1}\right) \sin X\beta_n \sin\beta_n} \right\} \quad (3)$$

where

β_n = roots of the transcendental equation: $\frac{X}{H} \tan\beta_n + \tan X\beta_n = 0$

$X = \frac{\ell_1}{\ell_2} \left(\frac{\alpha_2}{\alpha_1}\right)^{1/2}$

$H = \frac{C_1 d_1 \ell_1}{C_2 d_2 \ell_2}$

$\theta = \frac{\alpha_2 a}{\ell_2^2}$

α_i = thermal diffusivity of i^{th} layer

C_i = specific heat of i^{th} layer

d_i = density of i^{th} layer

ℓ_i = thickness of i^{th} layer

t = time from start of laser pulse

a = pulse time of laser

Q = total energy per unit area in laser pulse.

If the condition of no thermal contact resistance at the interface is relaxed, Equation (3) may be generalized to

$$\Delta T \left(\frac{Q}{C_1 d_1 \ell_1 + C_2 d_2 \ell_2} \right)^{-1} = 1 + 4 \sum_{n=1}^{\infty} \frac{\exp(-\beta_n^2 \theta \frac{t}{a}) \left[\frac{\exp(\beta_n^2 \theta) - 1}{\beta_n^4 \theta^2} - \frac{1}{\beta_n^2 \theta} \right]}{\left[\cos X\beta_n \cos\beta_n - \frac{X + \frac{H}{X} + \frac{X}{B}}{H + 1} (\sin X\beta_n \sin\beta_n) \right] \left[- \frac{\beta_n X}{B(H+1)} (X \sin\beta_n \cos X\beta_n + \sin X\beta_n \cos\beta_n) \right]} \quad (4)$$

where

β_n = roots of the transcendental equation

$$\beta_n \frac{X^2}{HB} \tan X\beta_n \tan\beta_n - \left(\frac{X}{H} \tan\beta_n + \tan X\beta_n\right) = 0$$

$$B = \frac{h\ell_1}{\lambda_1}$$

h = thermal contact conductance at the interface

λ_1 = thermal conductivity of layer 1, and the symbols are as defined in Equation (3).

Thus, if the properties and thicknesses of both layers of a two-layer composite are known, it is possible to determine the thermal contact conductance (or its reciprocal, the thermal contact resistance) between the two layers by using the pulse laser technique.

Two thermal diffusivity apparatuses were used in the present program. The first is a low pressure apparatus shown schematically in Figure 1. It consists of a double-walled tantalum tube furnace surrounded by tantalum thermal radiation shielding. The specimen is held in a tantalum holder. Temperatures are read with a thermocouple which is in contact with the specimen holder. With this apparatus, diffusivity measurements can be made in vacuum or in inert gas atmospheres up to about 45 psia. The temperature-time history of the rear face of the specimen is determined by an infrared detector-optics system which is focused on a small spot in the center of the rear face of the sample. The detector is placed in a biasing or bridge circuit, the unbalance of which is displayed on an oscilloscope. A photograph of the oscilloscope trace provides a record of the temperature-time relationship. Infrared detectors used with this system include indium antimonide, lead sulfide, and silicon devices.

The second apparatus, shown schematically in Figure 2, was designed for diffisivity determinations in hydrogen at pressures up to about 515 psia and at temperatures from about 1200 to 2500 K. It consists of a tungsten mesh furnace

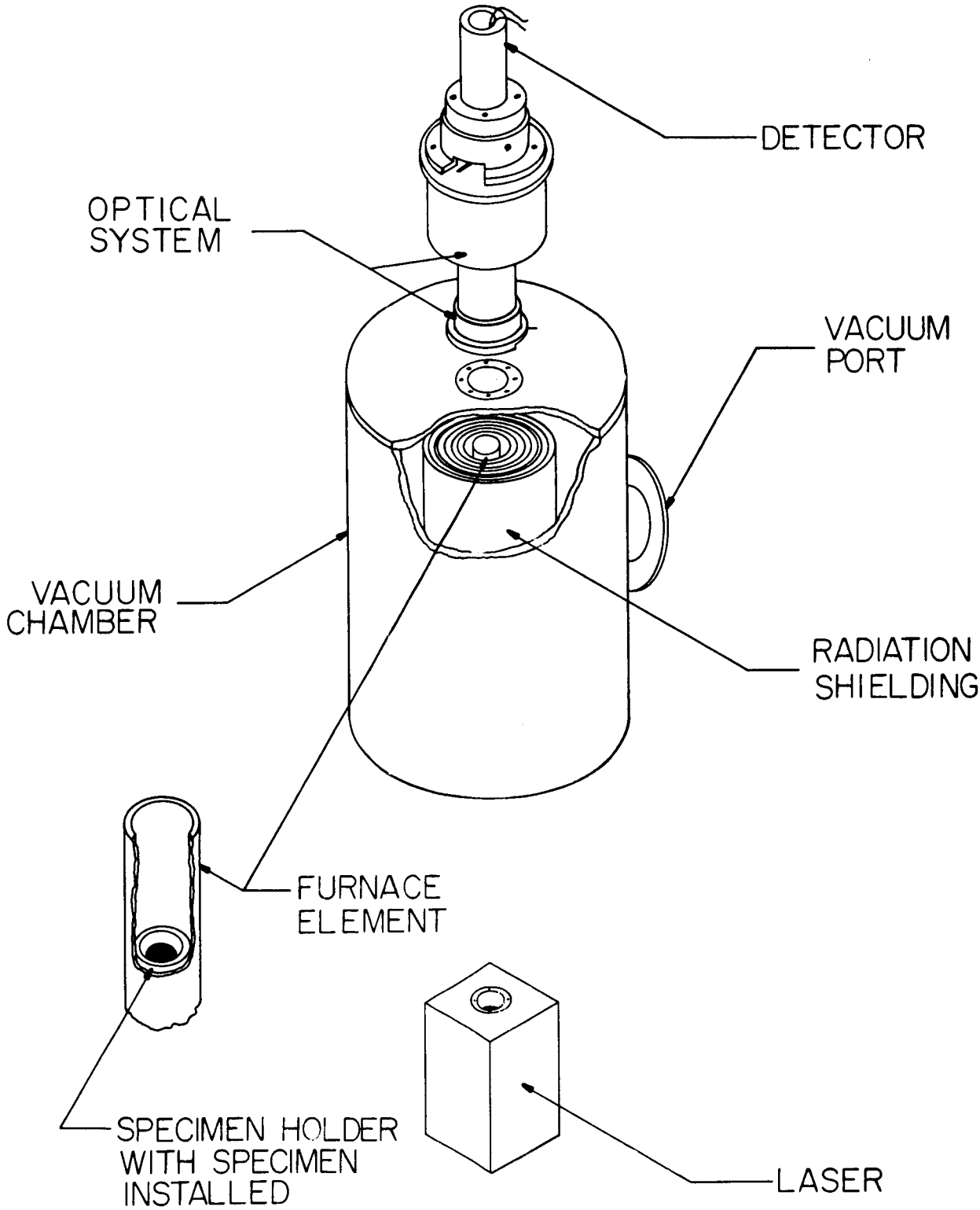

FIGURE 1. LASER FLASH THERMAL DIFFUSIVITY MEASUREMENT APPARATUS

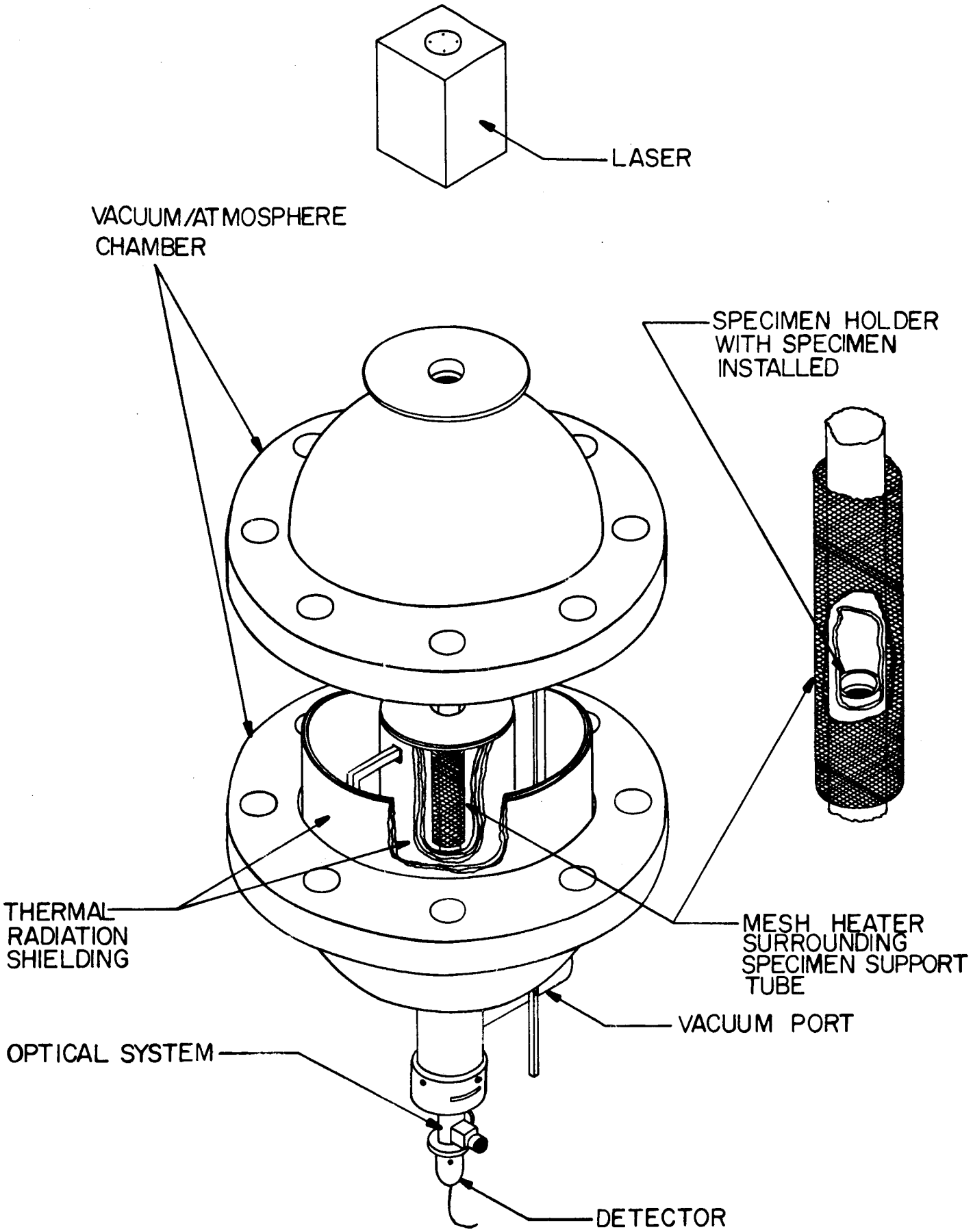

FIGURE 2. HIGH TEMPERATURE, VACUUM-HIGH PRESSURE THERMAL DIFFUSIVITY MEASUREMENT APPARATUS

surrounded by tungsten and molybdenum radiation shielding. The specimen is held in a tungsten holder and temperatures are determined with a calibrated optical pyrometer system. Rear face temperature-time histories are determined in a manner similar to that used with the low pressure apparatus.

In the case of translucent materials, it is often necessary to coat the faces of the specimens with thin ($\sim$8000 Å) coatings of an opaque metal in order to satisfy the assumed boundary conditions of the diffusivity technique. The coating on the front face assures that the energy from the laser is absorbed at the specimen surface, while the coating on the rear face assures that the infrared detector monitors the temperature at the surface rather than temperatures within the specimen. All the oxides studied in this program are translucent at room temperature. It was found that the ZrO_2 and HfO_2 specimens became sufficiently opaque at high temperatures so that coatings were not needed. Sputtered coatings of tungsten were applied to both faces of Samples 1, 2, and 3 of CaO-stabilized ZrO_2 and to all the Al_2O_3 samples.

Based on experience with standard materials, the uncertainty in thermal diffusivity values measured in the low-pressure apparatus is believed not to exceed ±5 percent. Uncertainties in values measured in the high pressure apparatus are believed not to exceed ±5 to 10 percent, with the higher uncertainties being associated with the higher gas pressures.

Specific heat values were determined from enthalpy data measured in a Bunsen ice calorimeter. Figure 3 is a sketch of the calorimeter well. In the Bunsen ice calorimeter, heat given up by the specimen and capsule melts ice which is in equilibrium with water in the closed calorimeter well. As the ice melts to water, a reduction in volume occurs. Mercury entering the system from an external accounting system to make up the volume change is accurately weighed. Both Battelle-Columbus and the National Bureau of Standards have measured the ice-calorimeter heat-quantity versus mercury-weight constant to be 270.48 joules per gram. This is the constant of the measuring method and should not vary among Bunsen ice calorimeters. It is a function of the volume change of ice melting to water and the heat of fusion involved in the change of state. All heat transfer is measured at the ice point as ice melts to water; temperatures are not measured in the calorimeter well.

All oxide, molybdenum, and molybdenum-oxide mixture specimens were wrapped in molybdenum foil and then encapsulated in tantalum capsules. The NiAl and nichrome specimens were encapsulated in Type 304 stainless steel. The capsules were sealed under helium at about one-half atmospheric pressure. The encapsulated specimen was heated in a furnace above the calorimeter well and was then dropped into the well and allowed to cool. Separate drops of an empty capsule of the same material and surface emittance conditions as the specimen capsule determined the contribution of heat of the specimen by difference. The process was repeated through the temperature range of interest to establish an enthalpy-versus-temperature curve. Specific heat was obtained graphically using enthalpy and temperature data.

Calibration of the apparatus is checked with National Bureau of Standards Al_2O_3 as the specimen standard. Measured enthalpies agree routinely with NBS values for this standard to within about 1/2 percent. The nominal uncertainty in the specific heat values computed in the above manner is approximately ±2 percent.

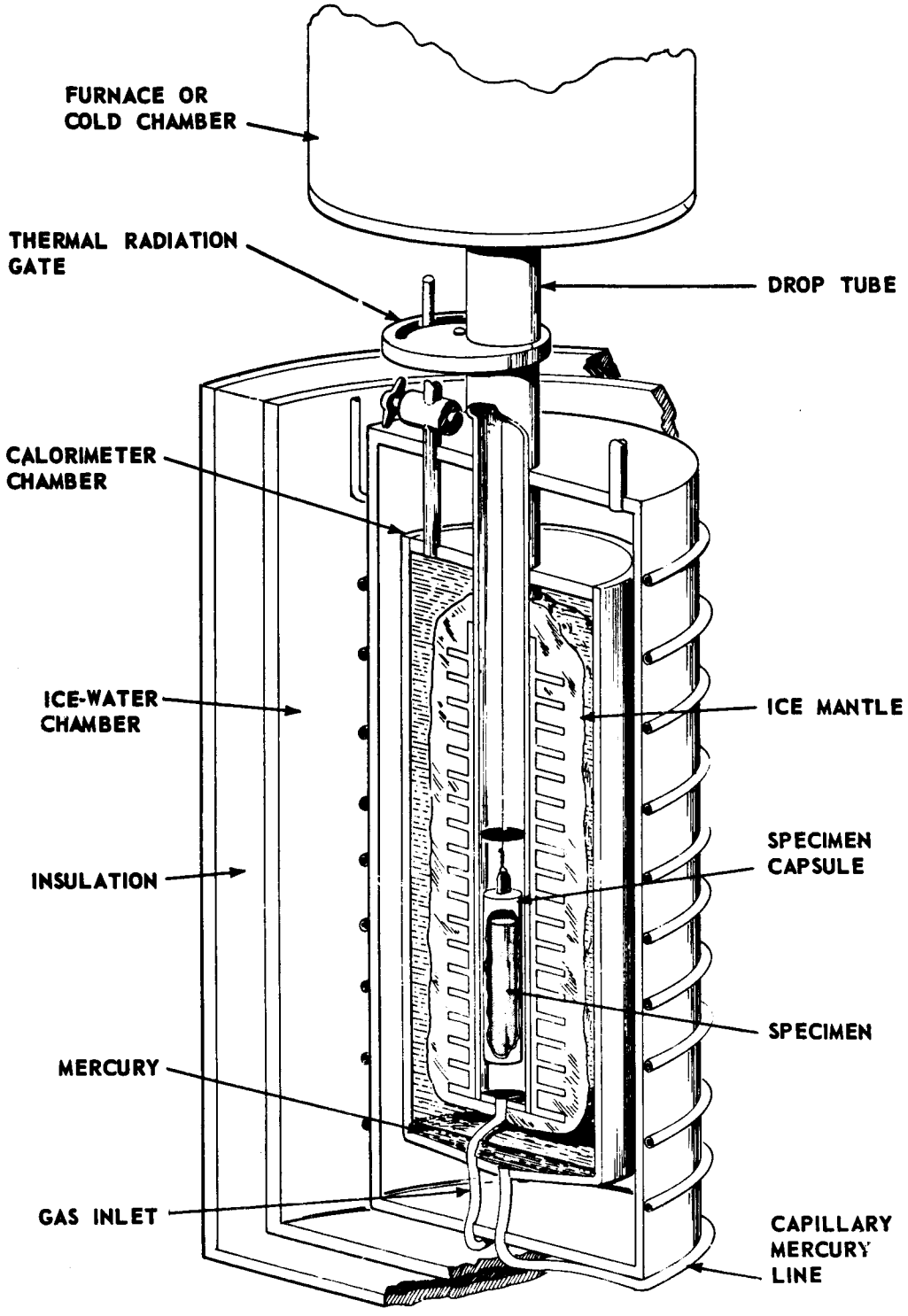

FIGURE 3. BUNSEN ICE CALORIMETER

Linear thermal expansion measurements were made in a direct view dilatometer as illustrated schematically in Figure 4. In this method, two telemicroscopes fitted with filar eyepieces are used to view fiducial marks on tantalum end caps located on both ends of the specimen but separated from the specimen by thin molybdenum disks. The expansion (or shrinkage) of the specimen is determined by subtracting the known expansion of the tantalum and molybdenum end pieces from the total observed value. The specimens were heated with a tantalum resistance furnace. Measurements below about 1600 K were made in helium at atmospheric pressure, while higher temperature measurements were made under a vacuum of about 10^{-6} torr. Uncertainties in this apparatus are determined by the measurement of standard materials of known linear thermal expansion, supplied by NBS. Uncertainties associated with these measurements are believed to be less than about ±1 percent of the total expansion.

Room temperature density measurements were made on the thermal diffusivity specimens both before and after the diffusivity measurements. These measurements were performed by immersion in mercury. Since mercury does not penetrate into the open pores, this immersion technique yields the true bulk density of the specimen. These density values, along with suitable corrections for thermal expansion and shrinkage effects, were used in the calculation of thermal conductivity by Equation (1).

Chemical analyses of the specimens were performed by the Environmental and Materials Characterization Division of Battelle. The analyses for CaO and Y_2O_3 content of the ZrO_2 specimens were performed by X-ray fluorescence with an accuracy of about ±5 percent. Impurity contents were determined by optical emission spectrometry with an accuracy of about ±50 percent. Hydrogen and oxygen contents, when reported, were determined by vacuum fusion with an accuracy of about ±10 percent. The nickel contents of the NiAl and nichrome specimens were determined by wet chemical analysis.

RESULTS OF THERMOPHYSICAL PROPERTY MEASUREMENTS

Thermal Conductivity Phase I

The materials studied in this phase were those with potential for use as the outermost layer of a coating system. These materials are CaO-stabilized ZrO_2, Y_2O_3-stabilized ZrO_2, Al_2O_3, and HfO_2.

CaO-Stabilized ZrO_2

Since ZrO_2 has the greatest potential for use on the hot side of the coating system, a large effort was directed at understanding its properties. A chemical analysis of a typical as-sprayed sample of CaO-stabilized ZrO_2 is given in Table 1. Photomicrographs of an as-sprayed sample are shown in Figures 5 and 6. As can be seen from the photomicrographs, the sample consists of loosely connected solid particles with a fine interpenetrating void network, along with larger voids.

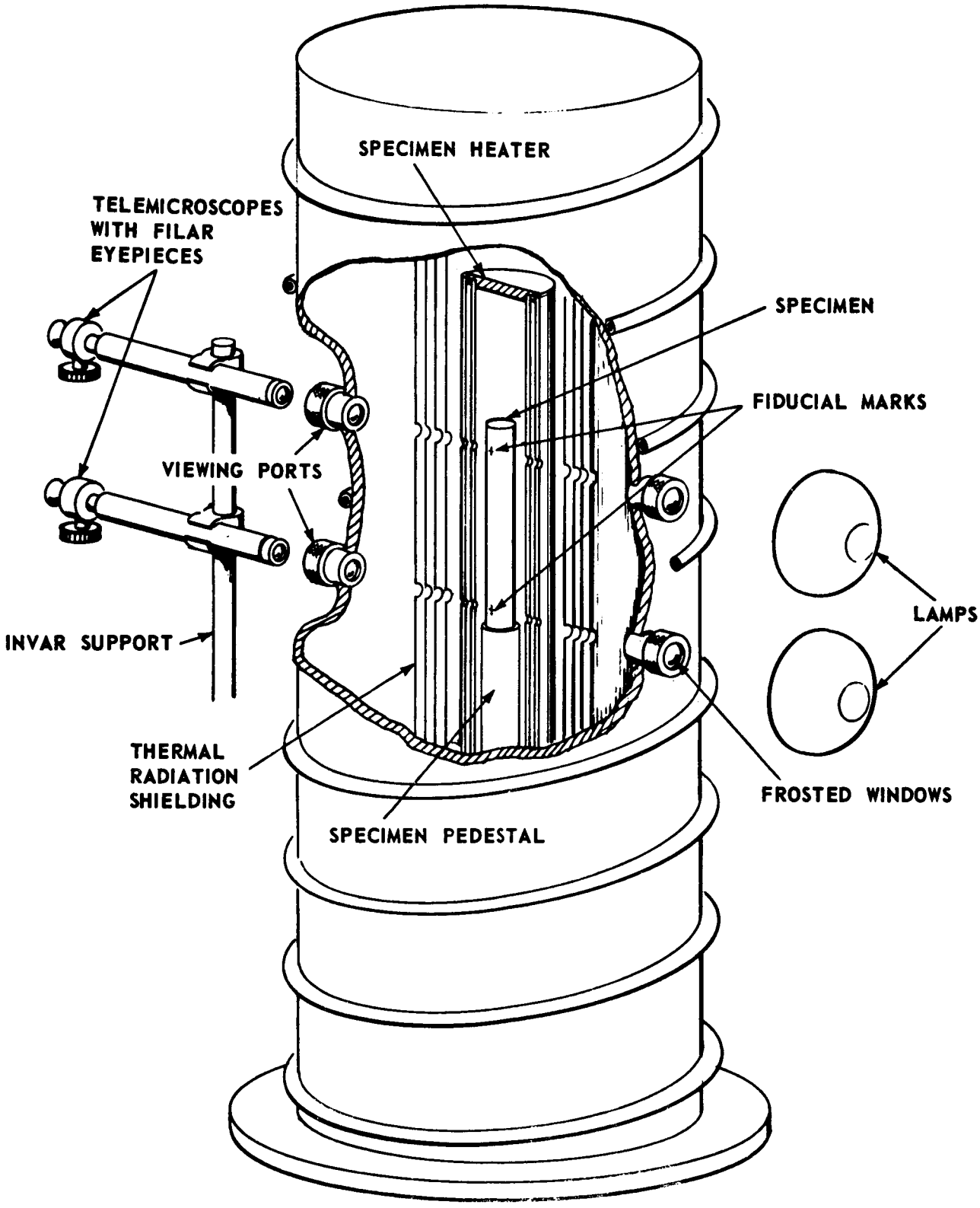

FIGURE 4. HIGH-TEMPERATURE DILATOMETER AS USED FOR DIRECT-VIEW EXPANSION MEASUREMENTS

TABLE 1. CHEMICAL ANALYSES OF CaO-STABILIZED ZrO_2 SAMPLES

Element	Weight percent					
	As-Sprayed	Sample 2	Sample 3	Sample 4	Expansion Sample (As-Sprayed)	Expansion Sample Companions
CaO	4.8	2.70	2.70	2.63	5.2	3.3
Fe	0.1	<0.01	<0.01	0.03	0.1	<0.001
Si	0.04	0.005	<0.005	0.005	0.1	<0.001
Ta	<0.1	0.2	0.3	<0.1	<0.03	0.2
Mg	0.4	0.01	0.02	0.01	0.3	0.003
Al	0.08	0.01	0.01	0.01	0.005	0.002
Cu	<0.005	<0.005	<0.005	<0.005	<0.001	<0.001
Ti	0.06	0.04	0.03	0.05	0.03	0.02
Ni	<0.01	<0.01	<0.01		0.002	<0.001
Cr				0.01	0.001	<0.001
W				<0.03		
H				0.019		
Ba					0.002	<0.001
Mn					0.001	<0.001
Pb					0.003	<0.001
Sn					0.002	<0.001
Mo					<0.001	<0.001
Na					0.02	<0.005

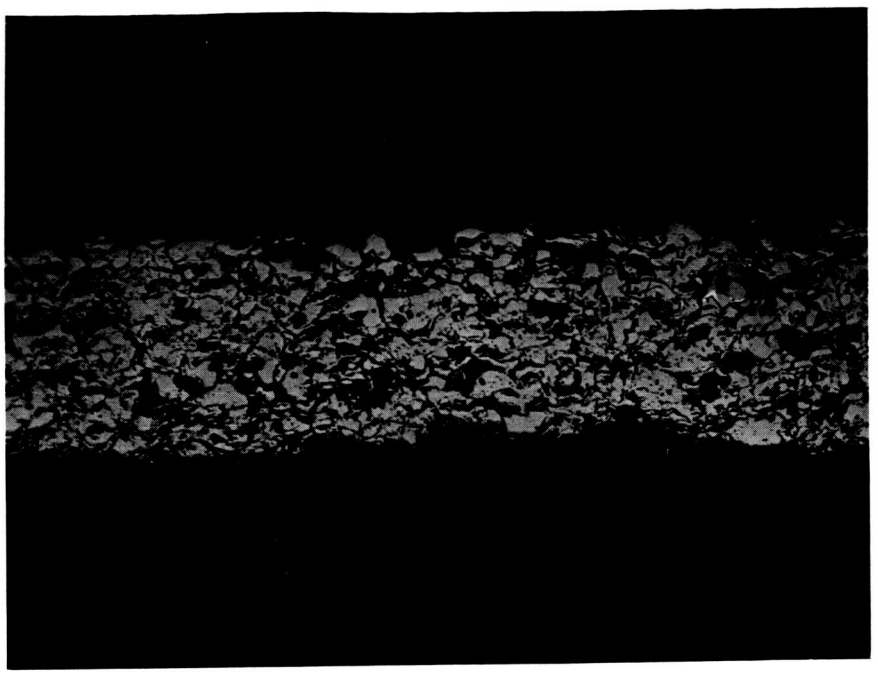

100X OF860

250X OF861

FIGURE 5. MICROSTRUCTURE OF AS-SPRAYED CaO-STABILIZED ZrO_2, LONGITUDINAL SECTION (AS-POLISHED)

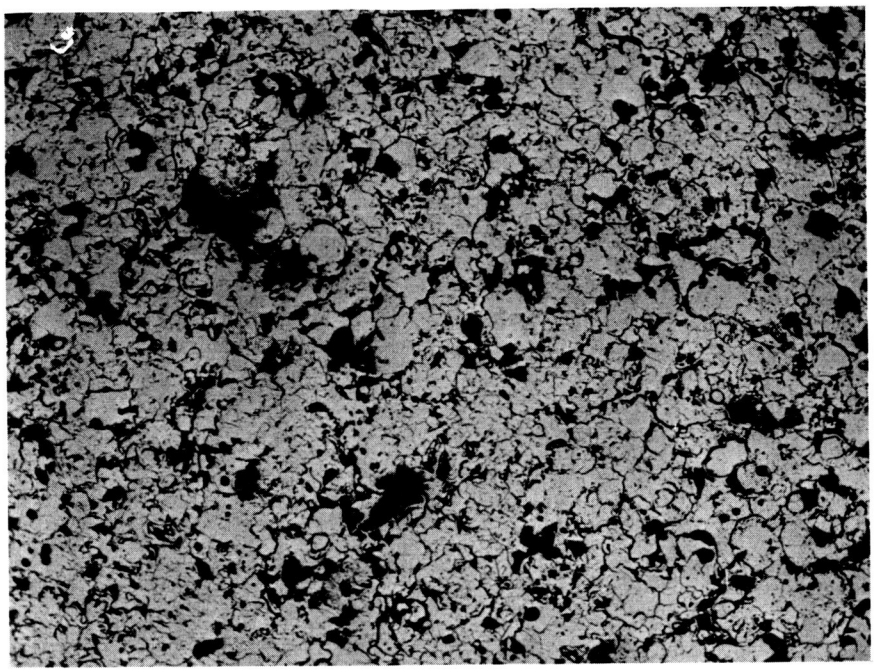

100X OF863

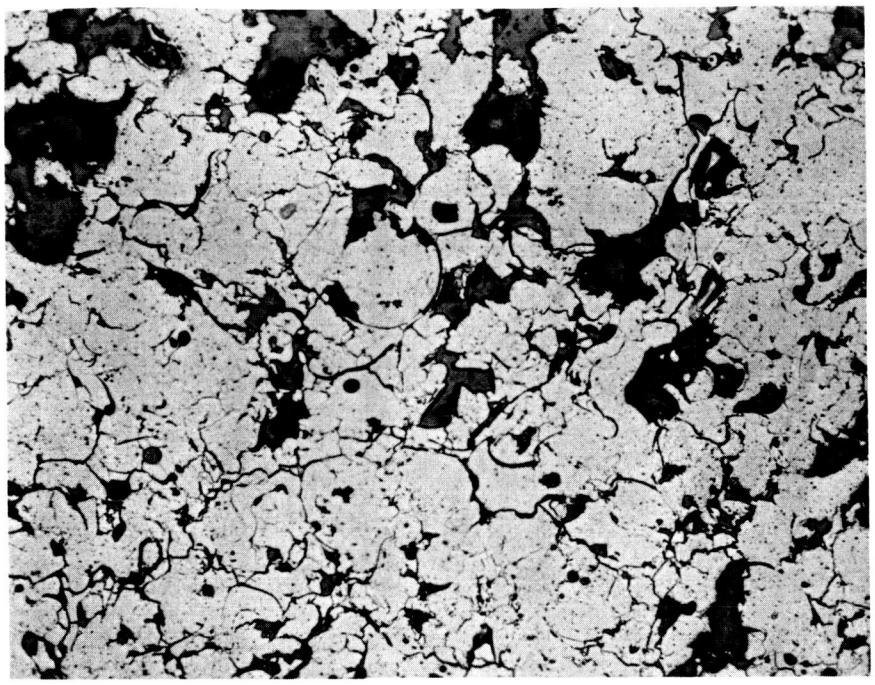

250X OF864

FIGURE 6. MICROSTRUCTURE OF AS-SPRAYED CaO-STABILIZED ZrO_2, TRANSVERSE SECTION (AS-POLISHED)

In order to determine the effects of atmosphere on the thermal conductivity, thermal diffusivity measurements on Sample 1 were made under four atmospheres: vacuum ($\sim 5 \times 10^{-5}$ torr), argon at atmospheric pressure, helium at atmospheric pressure, and helium at two atmospheres pressure. These measurements were made under each of the four atmospheres at each temperature before proceeding to the next higher temperature. In this manner, the effects of variability from sample to sample may clearly be separated from the effects of atmosphere and heat treatment.

Thermal conductivity results on Sample 1 are given in Figures 7 and 8. The results in Figure 7 were obtained as the specimen was heated from about 550 to 2200 K, while the results in Figure 8 were obtained as the specimen was cooled back to the starting temperature. From these Figures, it is seen that the effect of atmosphere is greatest on the unheat-treated material at the lowest temperatures. The conductivity in two atmospheres helium is about twice as great as in a vacuum. As the temperature was increased, the effect of the atmosphere became progressively smaller. The second point to be noted is that the conductivity is greatly increased as a result of the high-temperature heat treatment. The conductivity in vacuum is increased by a factor of about three at the lowest temperatures. These results may be partially understood by comparing the postmeasurement microstructure of Sample 1, shown in Figures 9 and 10, with the microstructure of the as-sprayed sample, shown in Figures 5 and 6. The solid phase is seen to be much more continuous in Sample 1 than in the as-sprayed sample. The fine void network in the as-sprayed material apparently presents a large barrier to heat flow, especially under vacuum conditions. As a gas is introduced, these thermal barriers are partially bridged, resulting in higher thermal conductivities. As the sample is heat treated, the fine voids seem to disappear due to sintering and the thermal contact between the solid particles is greatly improved. This improvement in thermal contact leads to a substantial lessening of the effect of the gaseous environment.

Thermal diffusivity measurements were made on Sample 2 in order to determine the variability of thermal conductivity between two supposedly identical specimens, and to determine the effects of repeated thermal cycling on the thermal conductivity. Thermal diffusivity measurements on Sample 2 were made over four complete thermal cycles between about 550 and 2220 K, in vacuum and in helium at two atmospheres pressure. Occasional measurements were made in argon and helium at atmospheric pressure. These results, shown in Figures 11 through 18, indicate the same trends as observed on Sample 1. A large increase in conductivity is experienced after the first heating to 2220 K. After this first heat treatment, only minor changes take place in the thermal conductivity. The agreement between Samples 1 and 2 is generally better than about ±12 percent over the entire temperature range for the first complete thermal cycle. The total spread in all the data generated at a given temperature after the first heat treatment is about 20 percent. The peculiar shapes of the thermal conductivity curves are at least partly due to the anomaly in the specific heat curve used to calculate conductivity from measured values of diffusivity. The thermal properties of stabilized ZrO_2 are subject to changes caused by destabilization due to loss of stabilizing agent, destabilization due to the material being initially in a nonequilibrium condition, and changes in stoichiometry due to loss of oxygen. In the case of a partially stabilized ZrO_2, the properties can also depend upon whether the sample is being heated or cooled through the phase transformations.

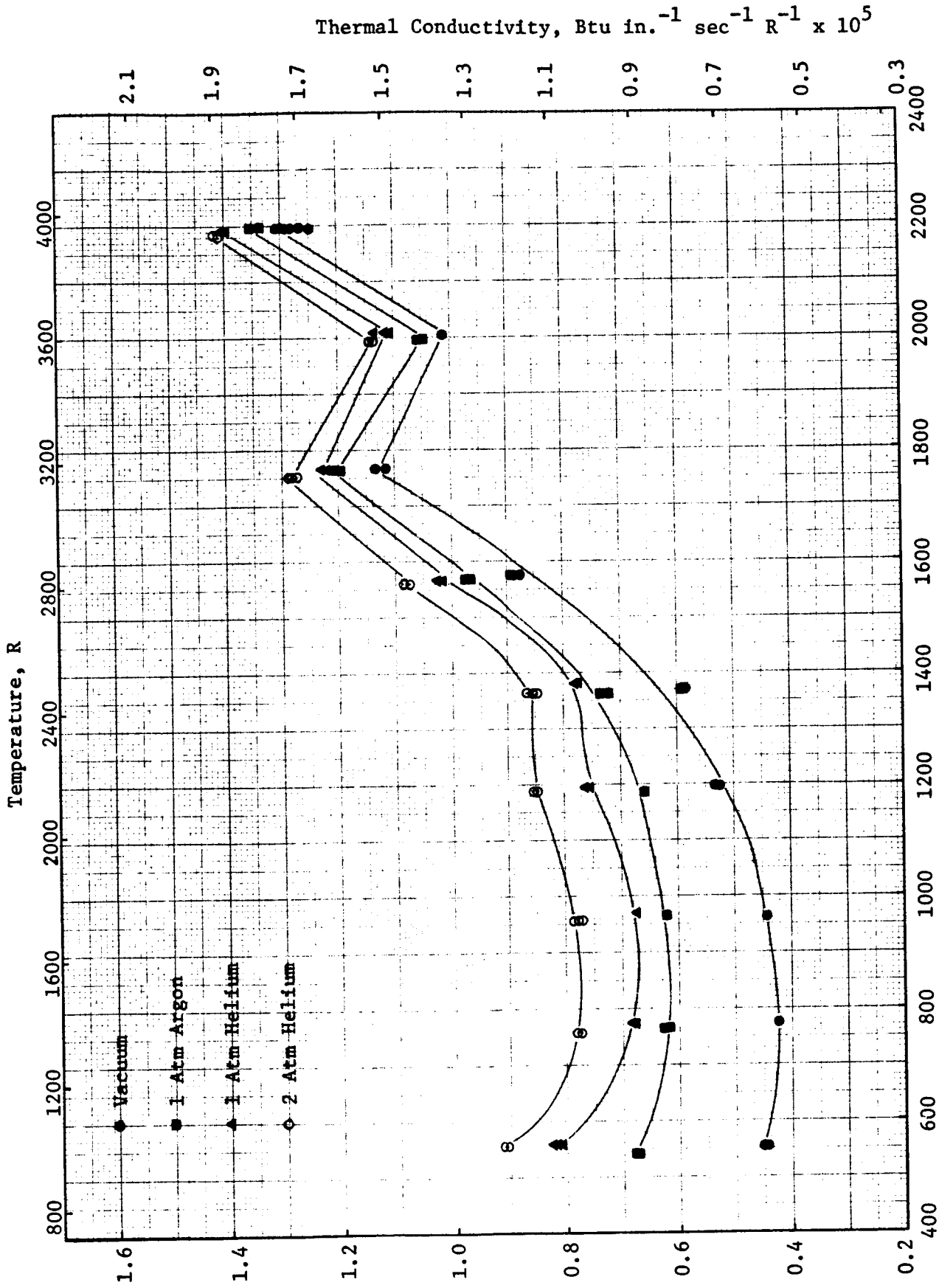

FIGURE 7. THERMAL CONDUCTIVITY OF CaO-STABILIZED ZrO_2, SAMPLE 1, HEATING PART OF CYCLE

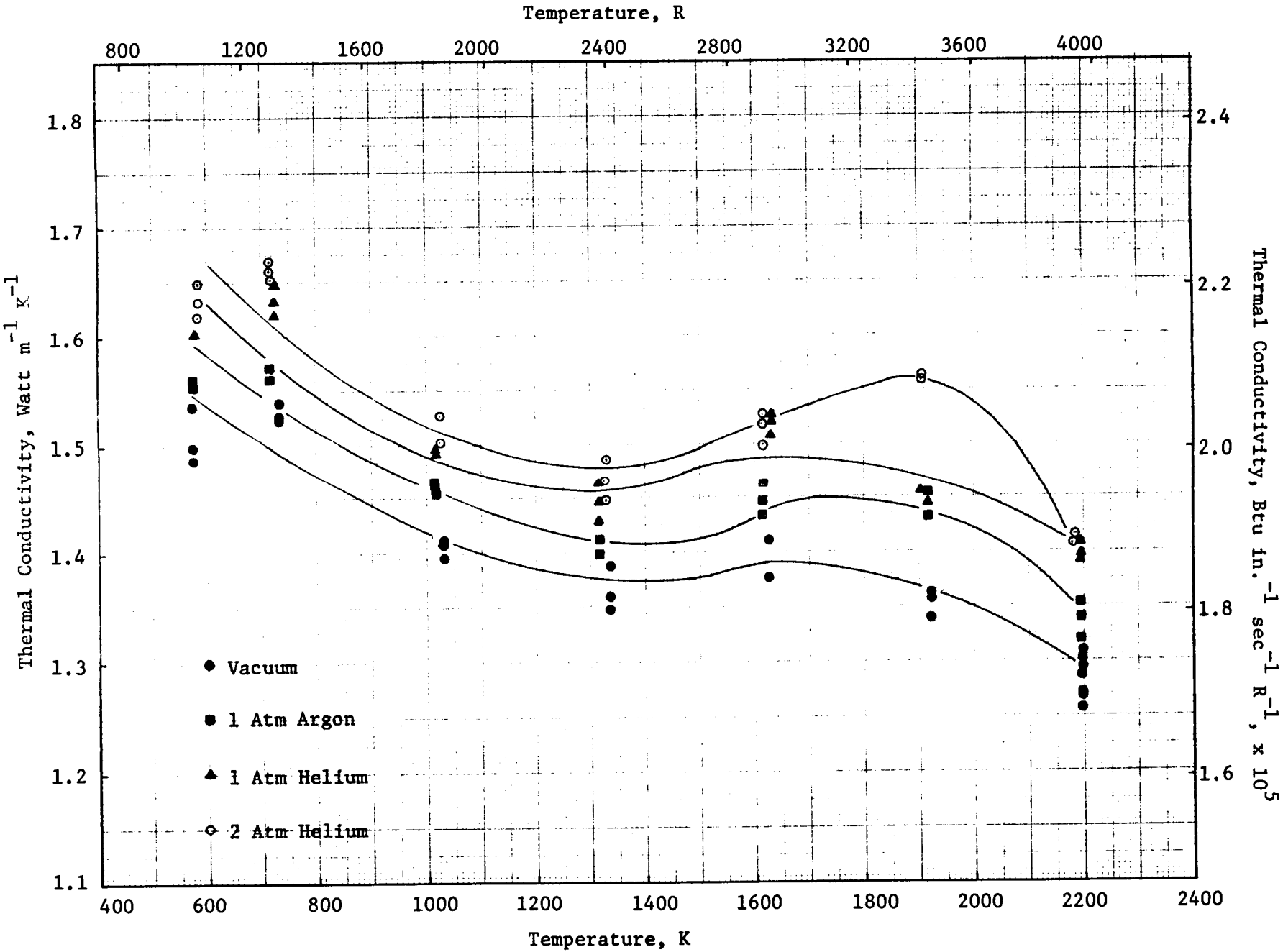

FIGURE 8. THERMAL CONDUCTIVITY OF CaO-STABILIZED ZrO_2, SAMPLE 1, COOLING PART OF CYCLE

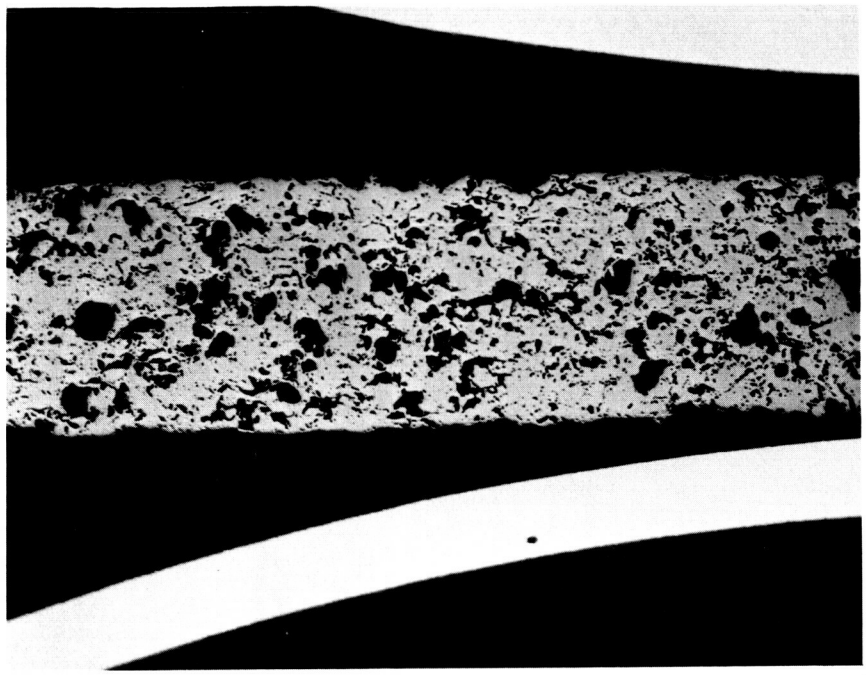

100X OF746

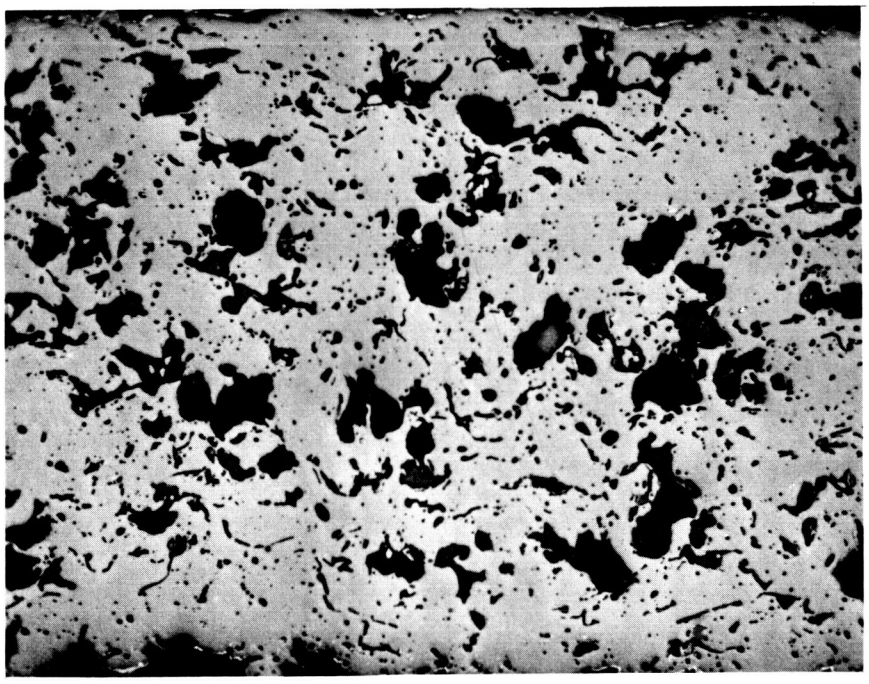

250X OF747

FIGURE 9. POSTMEASUREMENT MICROSTRUCTURE OF CaO-STABILIZED ZrO_2, SAMPLE 1, LONGITUDINAL SECTION (AS-POLISHED)

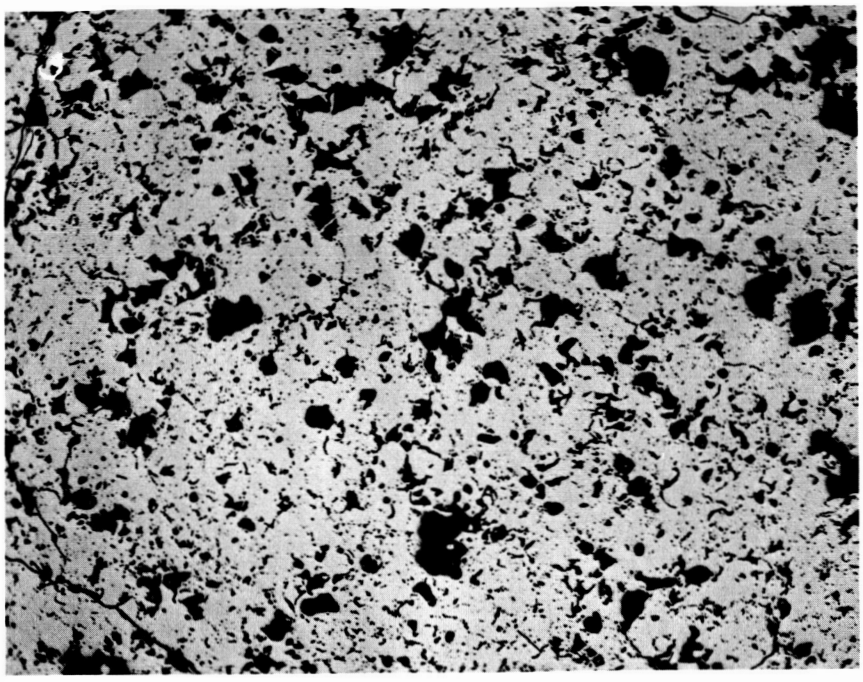

100X OF743

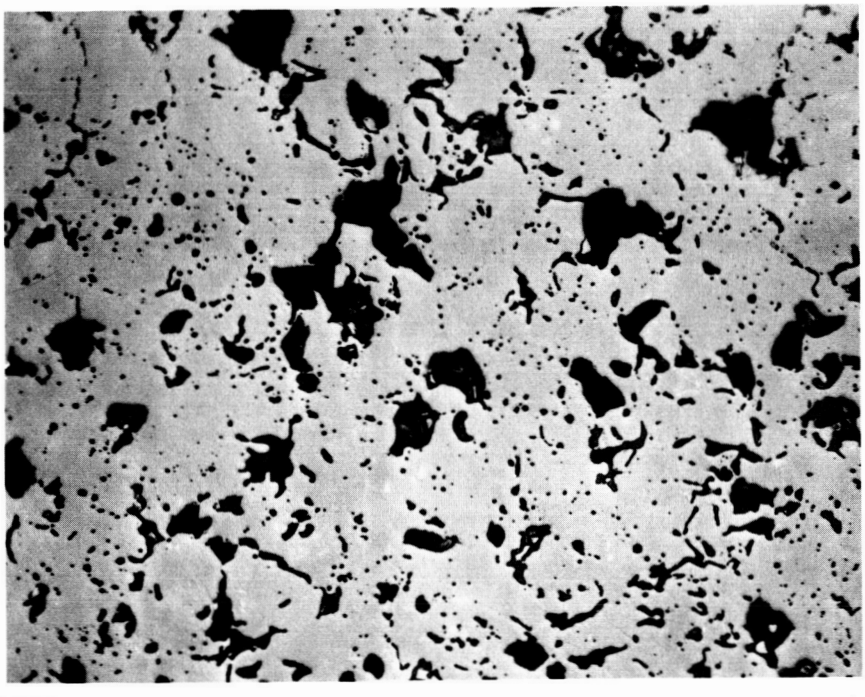

250X OF744

FIGURE 10. POSTMEASUREMENT MICROSTRUCTURE OF CaO-STABILIZED ZrO_2, SAMPLE 1, TRANSVERSE SECTION (AS-POLISHED)

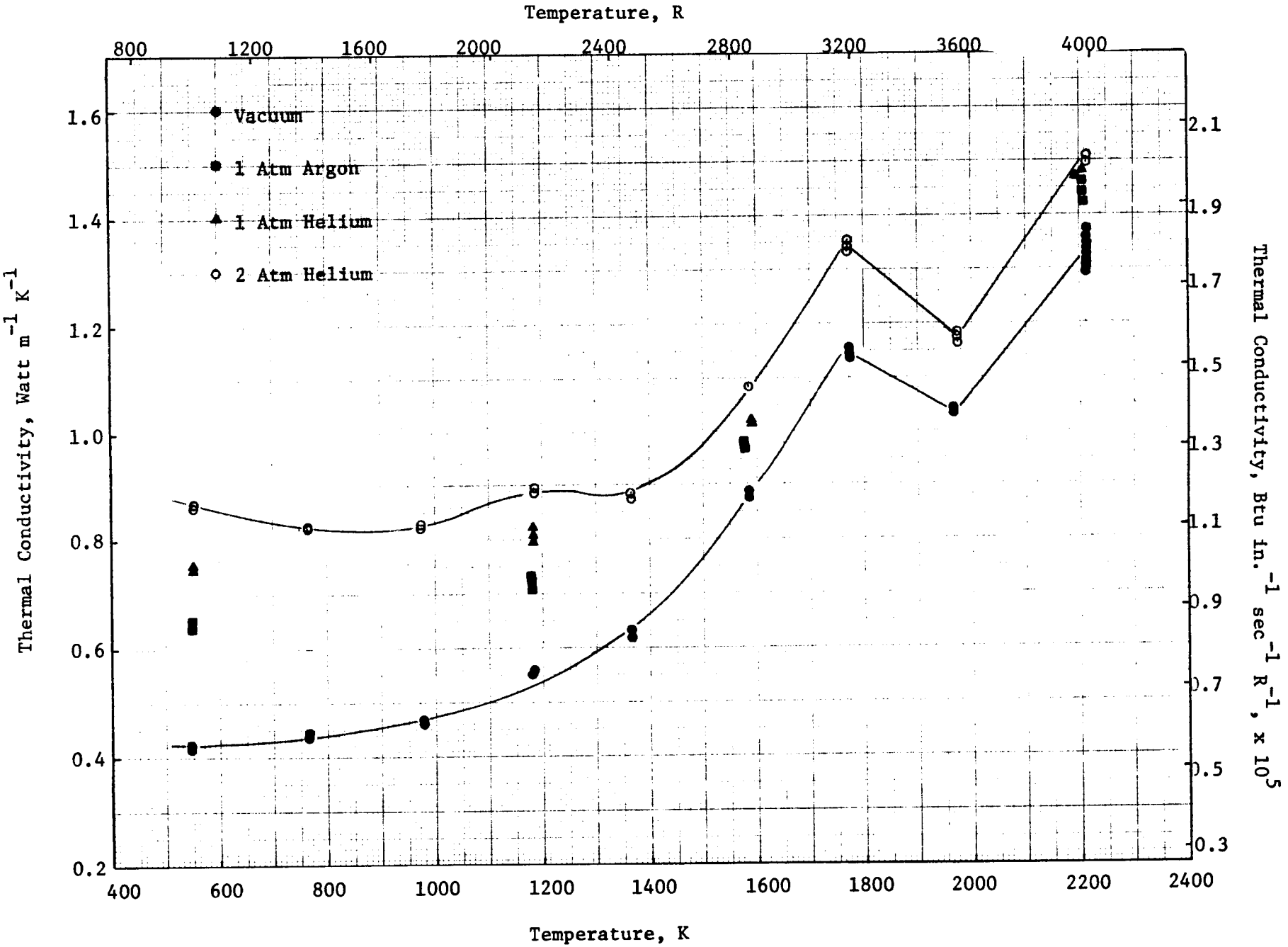

FIGURE 11. THERMAL CONDUCTIVITY OF CaO-STABILIZED ZrO_2, SAMPLE 2, HEATING PART OF FIRST CYCLE

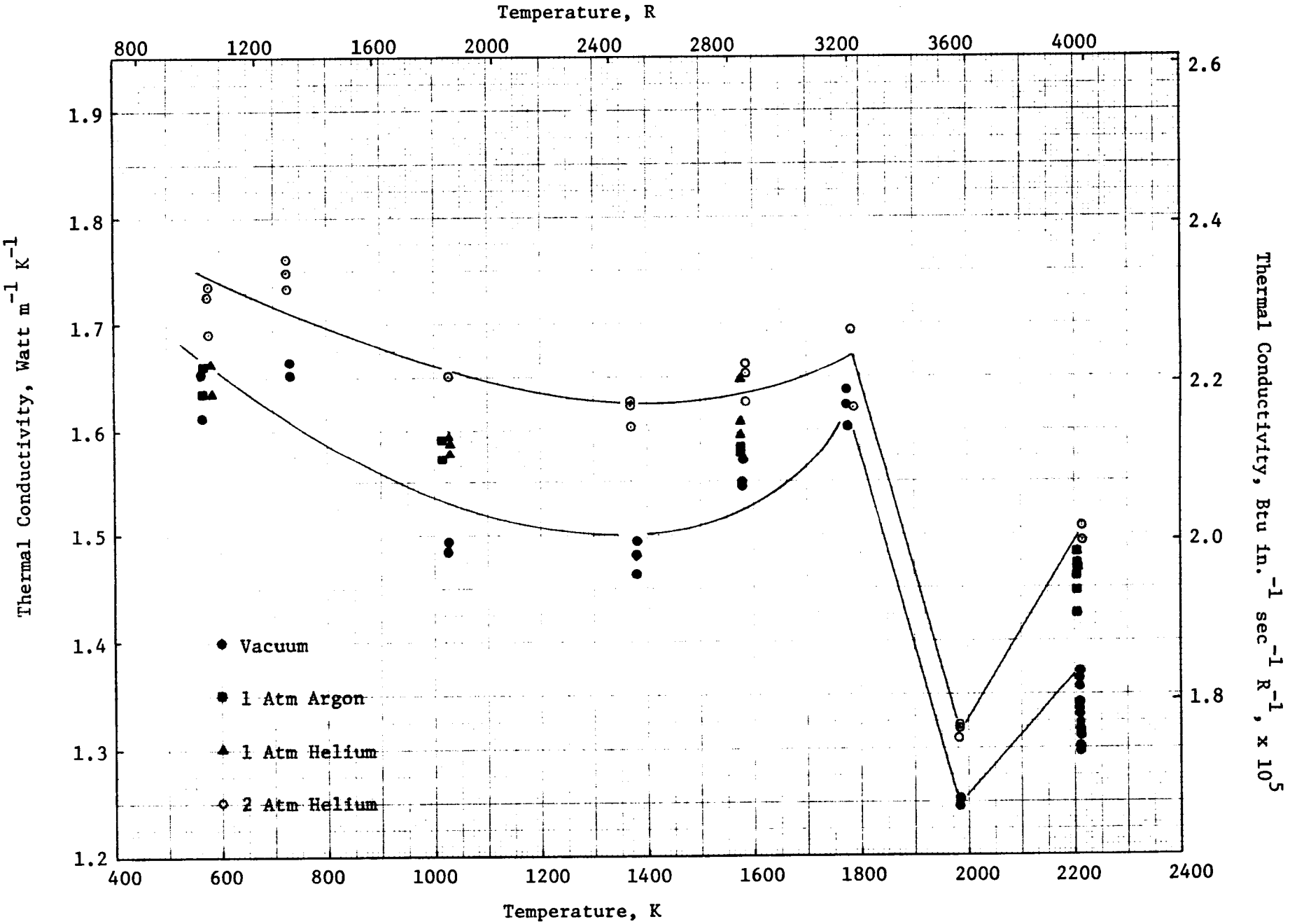

FIGURE 12. THERMAL CONDUCTIVITY OF CaO-STABILIZED ZrO_2, SAMPLE 2, COOLING PART OF FIRST CYCLE

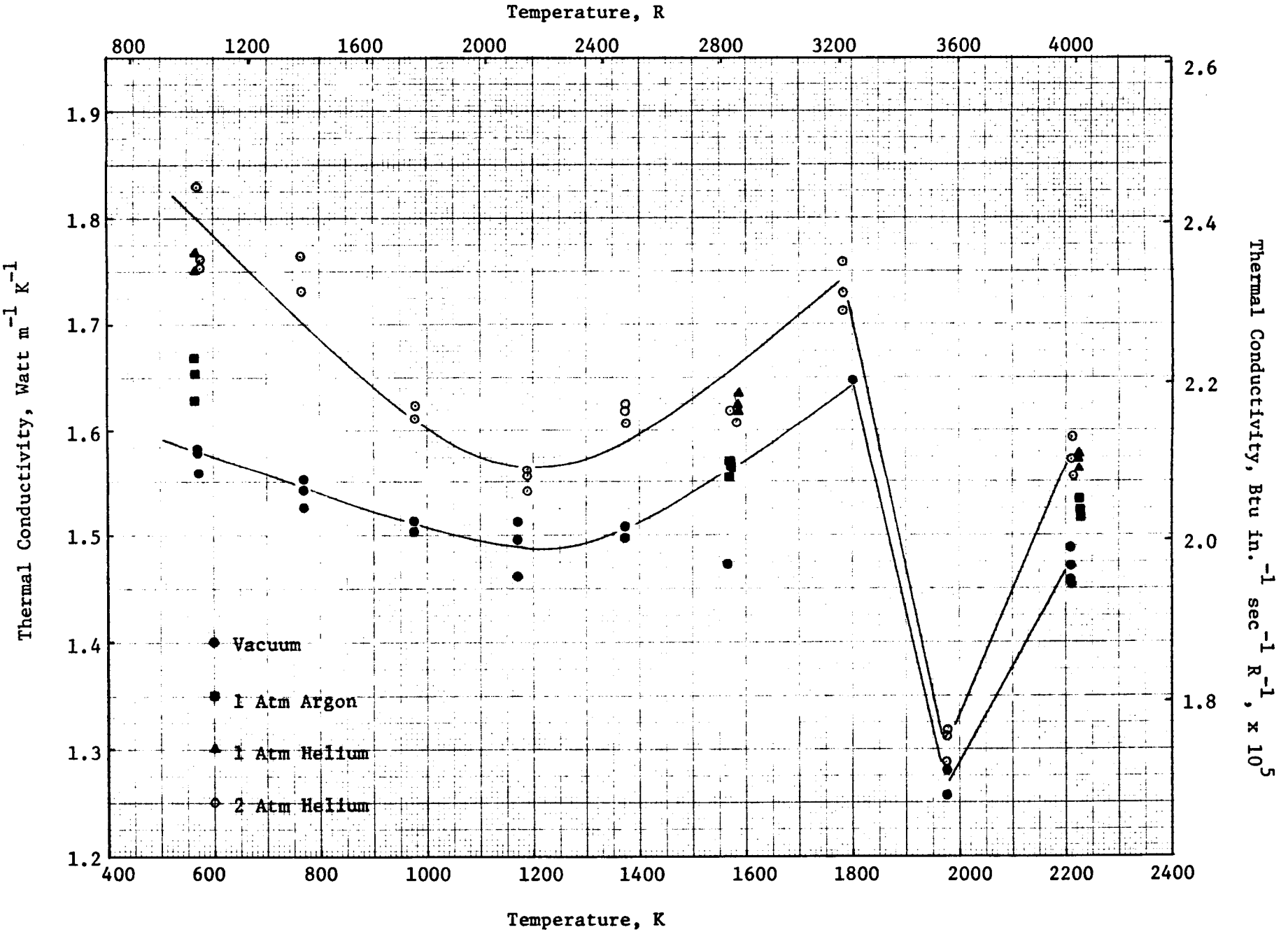

FIGURE 13. THERMAL CONDUCTIVITY OF CaO-STABILIZED ZrO_2, SAMPLE 2, HEATING PART OF SECOND CYCLE

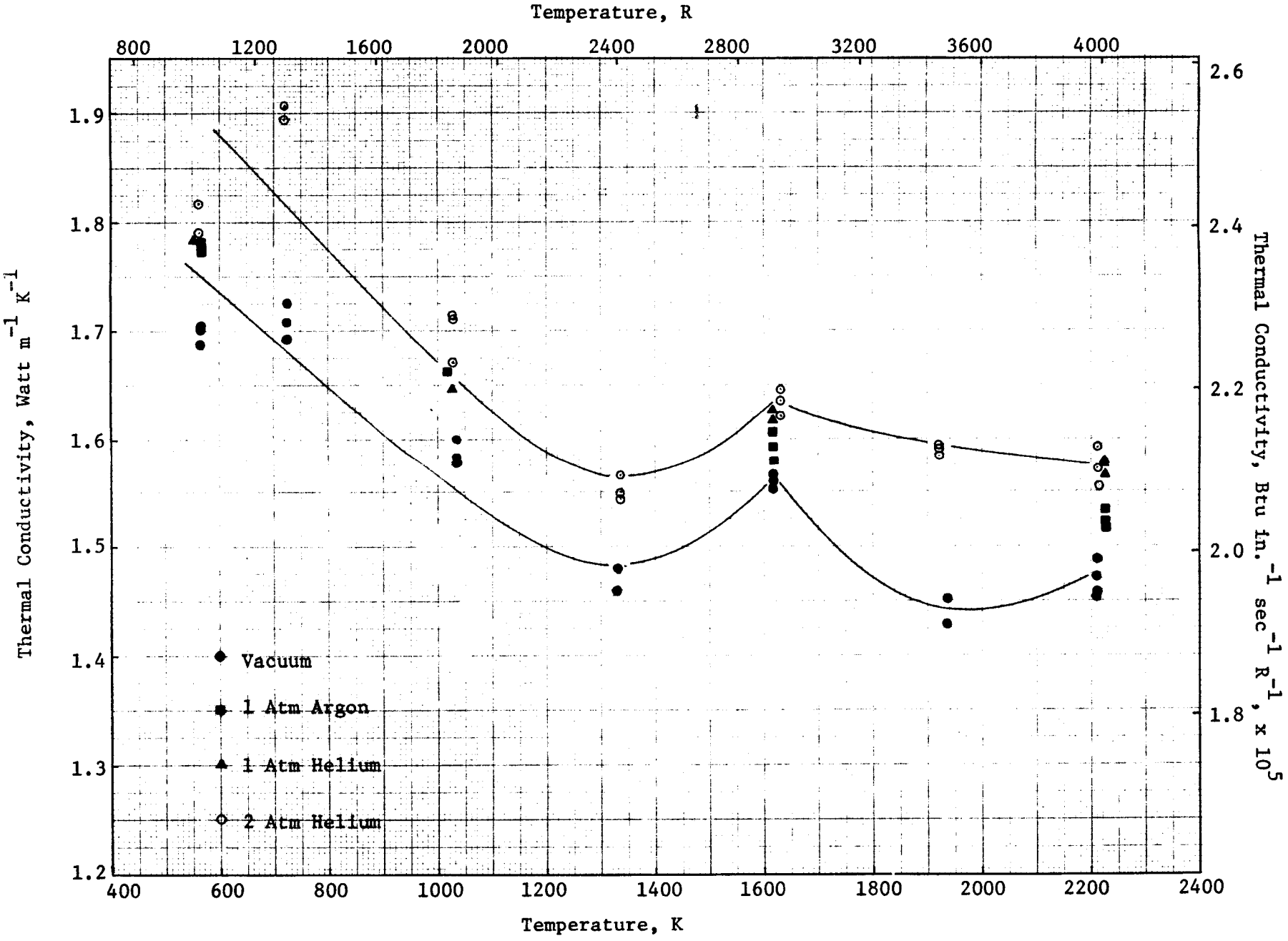

FIGURE 14. THERMAL CONDUCTIVITY OF CaO-STABILIZED ZrO_2, SAMPLE 2, COOLING PART OF SECOND CYCLE

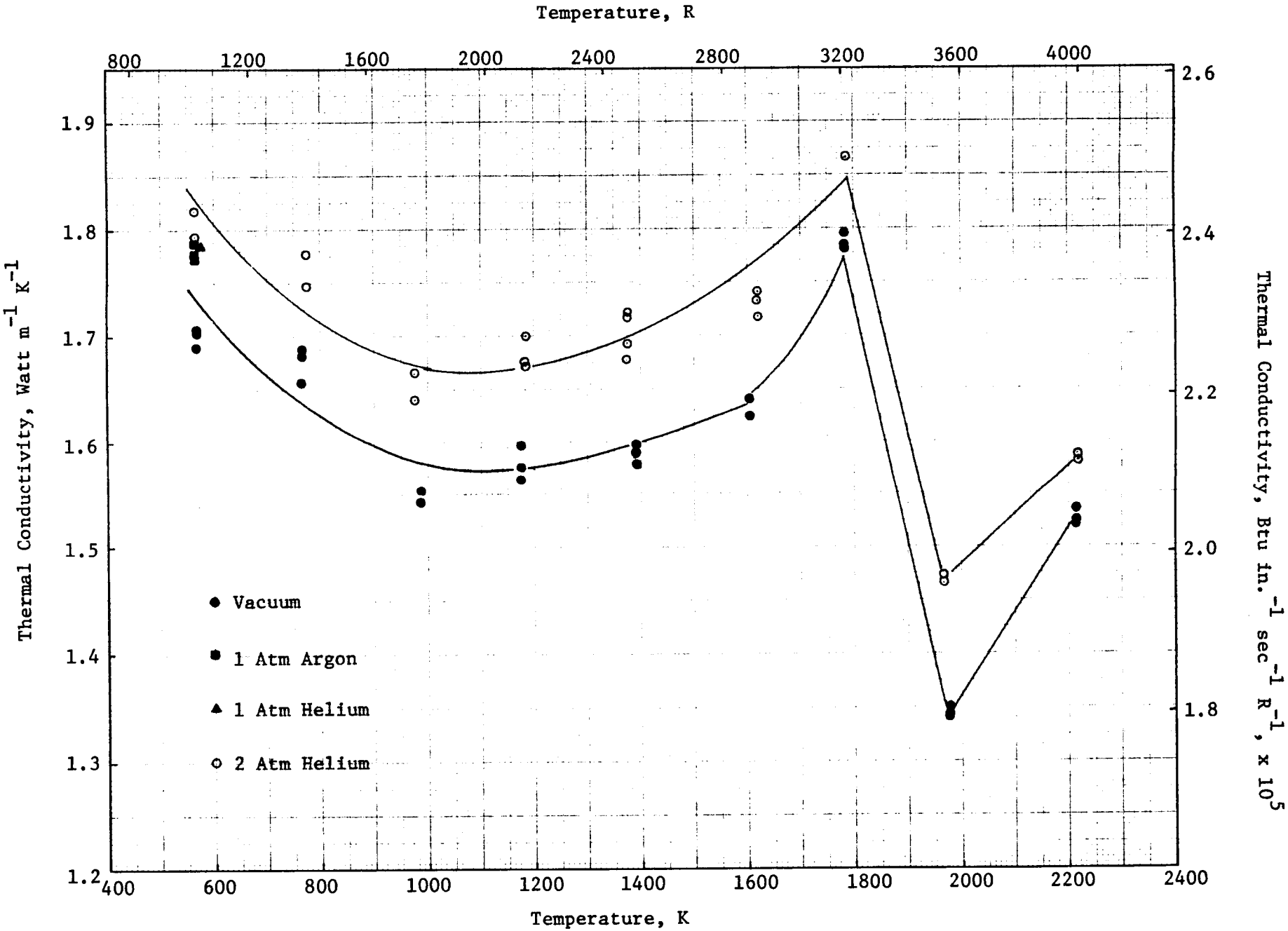

FIGURE 15. THERMAL CONDUCTIVITY OF CaO-STABILIZED ZrO_2, SAMPLE 2, HEATING PART OF THIRD CYCLE

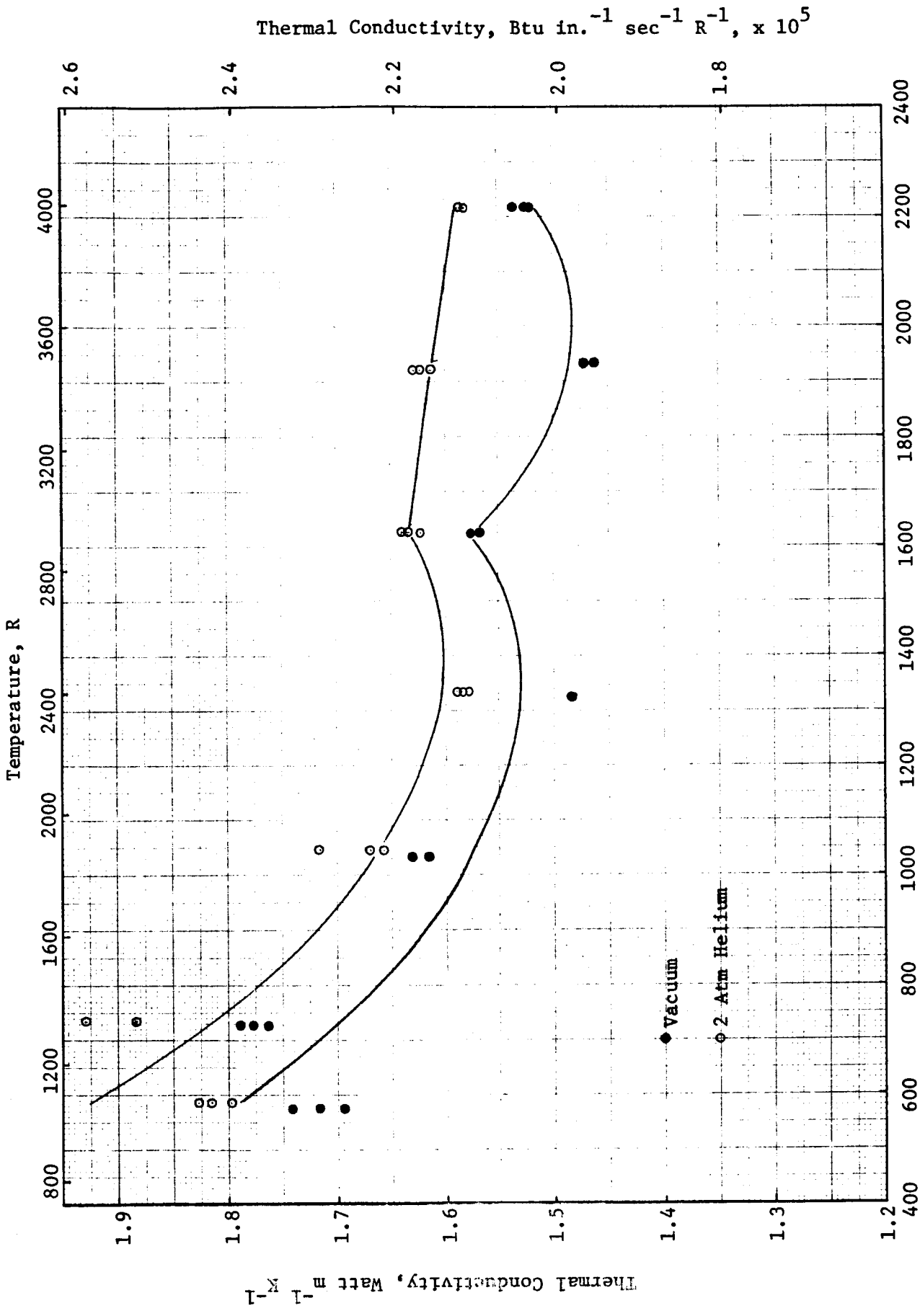

FIGURE 16. THERMAL CONDUCTIVITY OF CaO-STABILIZED ZrO_2, SAMPLE 2, COOLING PART OF THIRD CYCLE

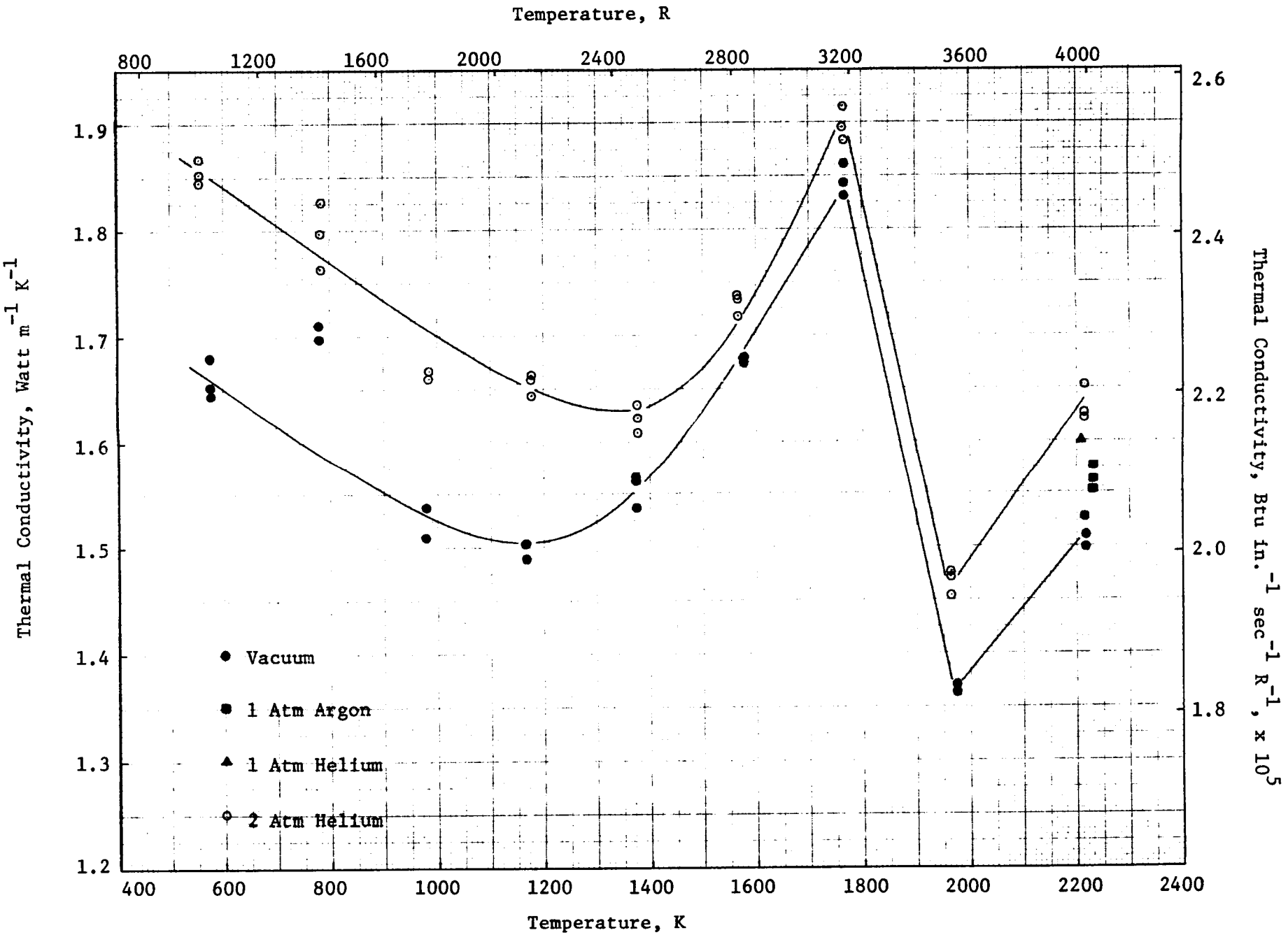

FIGURE 17. THERMAL CONDUCTIVITY OF CaO-STABILIZED ZrO_2, SAMPLE 2, HEATING PART OF FOURTH CYCLE

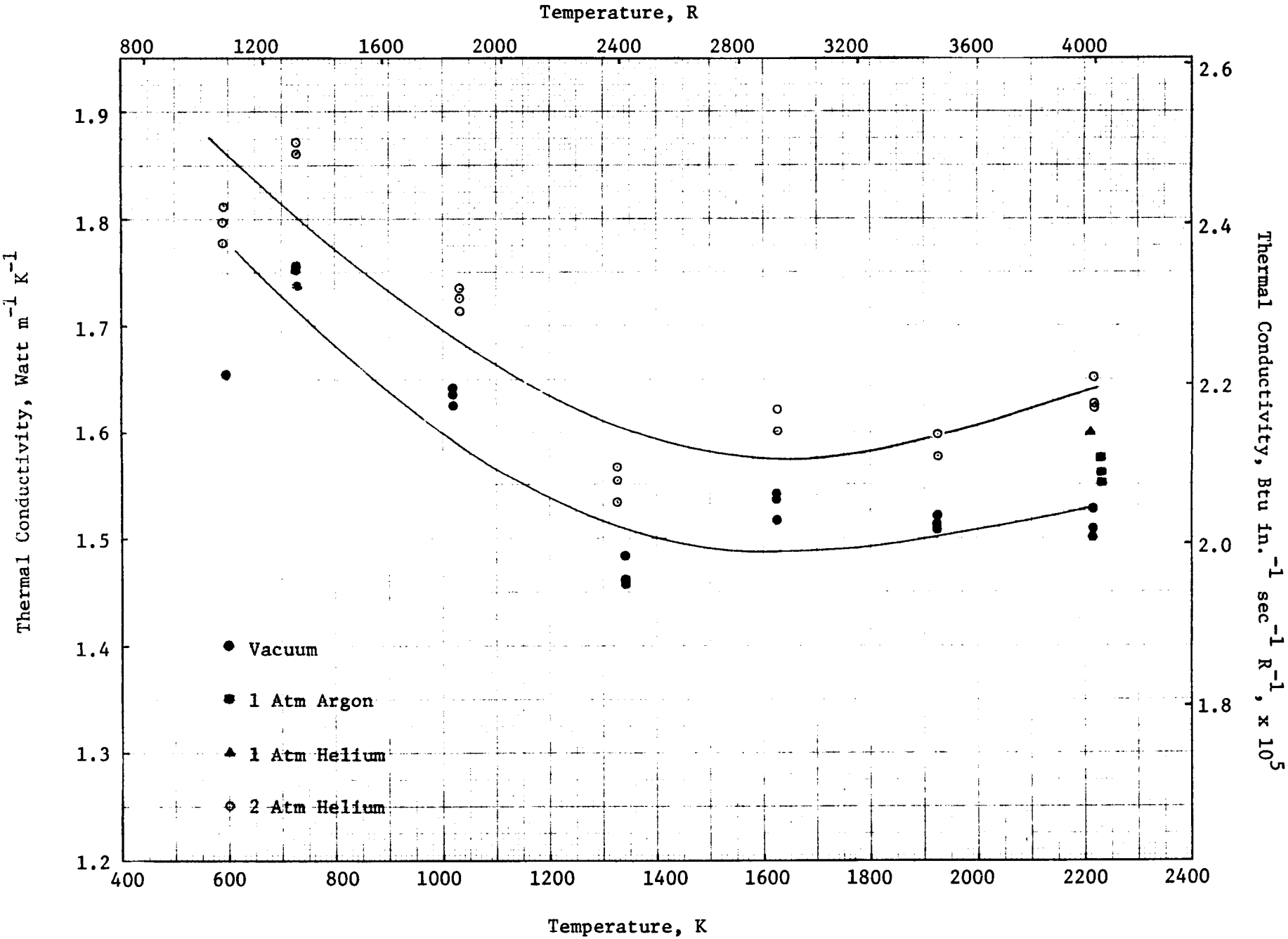

FIGURE 18. THERMAL CONDUCTIVITY OF CaO-STABILIZED ZrO_2, SAMPLE 2, COOLING PART OF FOURTH CYCLE

As indicated by Garvie[3], the phase diagram of the $CaO-ZrO_2$ system is poorly understood. However, the as-sprayed material containing 4.8 weight percent CaO appears unlikely to be in a completely stabilized condition. A postmeasurement analysis of Sample 2, given in Table 1, indicates a CaO content of only 2.70 weight percent. This loss of CaO and subsequent destabilization probably account for some of the changes in the thermal conductivity of Sample 2 during repeated thermal cycling. It should be noted that Samples 2 through 4 have about the same final CaO content.

The thermal conductivity of Sample 2 at 550 K prior to heat treatment is shown in Figure 19 as a function of helium pressure. These measurements, made at nominally the same temperature, indicate that the conductivity is independent of pressure up to about 1 torr and at higher pressures rises continually with pressure up to at least 1420 torr (2 atmospheres). These data show the same trend observed at low gas pressures (i.e. pressures at which the mean free path of the gas molecules is greater than or of the same magnitude as interparticle separations) for fibrous and powdered insulations.[4] At about 100 torr, the mean free path of the helium molecules is about equal to the width of the fine cracks in the as-sprayed sample. At higher pressures, one would expect the conductivity to again become independent of pressure. This large variation with pressure led to the decision to study the properties of the coatings in high-pressure hydrogen to more closely simulate the conditions during the anticipated application.

Kinetic effects were studied on Sample 3. All measurements were made under vacuum (5×10^{-5} torr). The sample was first heated to 560 K where measurements were made. The sample was then heated rapidly to near 2200 K. The first data point was taken within 4.5 minutes after the start of the heat-up period. The data, shown in Figure 20, were taken rapidly at first (at intervals of about 1.5 minutes) and more slowly later. Conductivity measurements were made over a six-hour heat treat period. After the initial stages of heat treatment, the conductivity continued to rise approximately linearly with time, with no indication of saturation. The conductivity increased by about 27 percent over the period of heat treatment. Following the heat treatment, the sample was cooled and data were taken at 1383 and 578 K. These data, shown in Figure 21 are in fairly good agreement with the data obtained on Samples 1 and 2.

In order to more closely simulate the conditions in the anticipated application, the fourth sample of CaO-stabilized ZrO_2 was measured in hydrogen. The results of these measurements are given in Figure 22. The sample was first heated to 1918 K in 46 psia hydrogen. Data taken at this temperature over a period of about one hour show no apparent dependence upon time at temperature and pressure. The sample was next heated to 2281 K under 46 psia, and data were taken over a period of about one-half hour with little apparent time dependence. The pressure was then raised to 85 psia while holding the temperature constant, and the measurements were repeated. Again no time dependence was apparent as measurements were made over a one-half hour period. The difference between the data under the two different pressures is less than 10 percent. Following this heat treatment, the sample was cooled and several data points were taken at lower temperatures. The data on Sample 4 taken under hydrogen are close to the mean of the data taken on Samples 1 through 3 in vacuum and inert gases, indicating that the effect of a hydrogen environment on the thermal conductivity of CaO-stabilized ZrO_2 is small at these temperatures and pressures. The postmeasurement chemical analysis of Sample 4 indicates about the same amount

TABLE 2. PHYSICAL CHARACTERISTICS OF CaO-STABILIZED ZrO_2 THERMAL DIFFUSIVITY SAMPLES

	Thickness, cm		Weight, g		Density, g cm^{-3}		Color
	Pretest	Posttest	Pretest	Posttest	Pretest	Posttest	
Sample 1	0.0356	0.0348	0.1846	0.1809	4.36	4.62	Turned slightly darker
Sample 2	0.0343	0.0338	0.1783	0.1732	4.42	4.75	Turned slightly darker
Sample 3	0.0325	0.0323	0.1790	0.1723	4.46	4.76	Turned dark grey
Sample 4	0.0312	0.0310	0.1748	0.1704	4.40	4.45	Turned dark grey

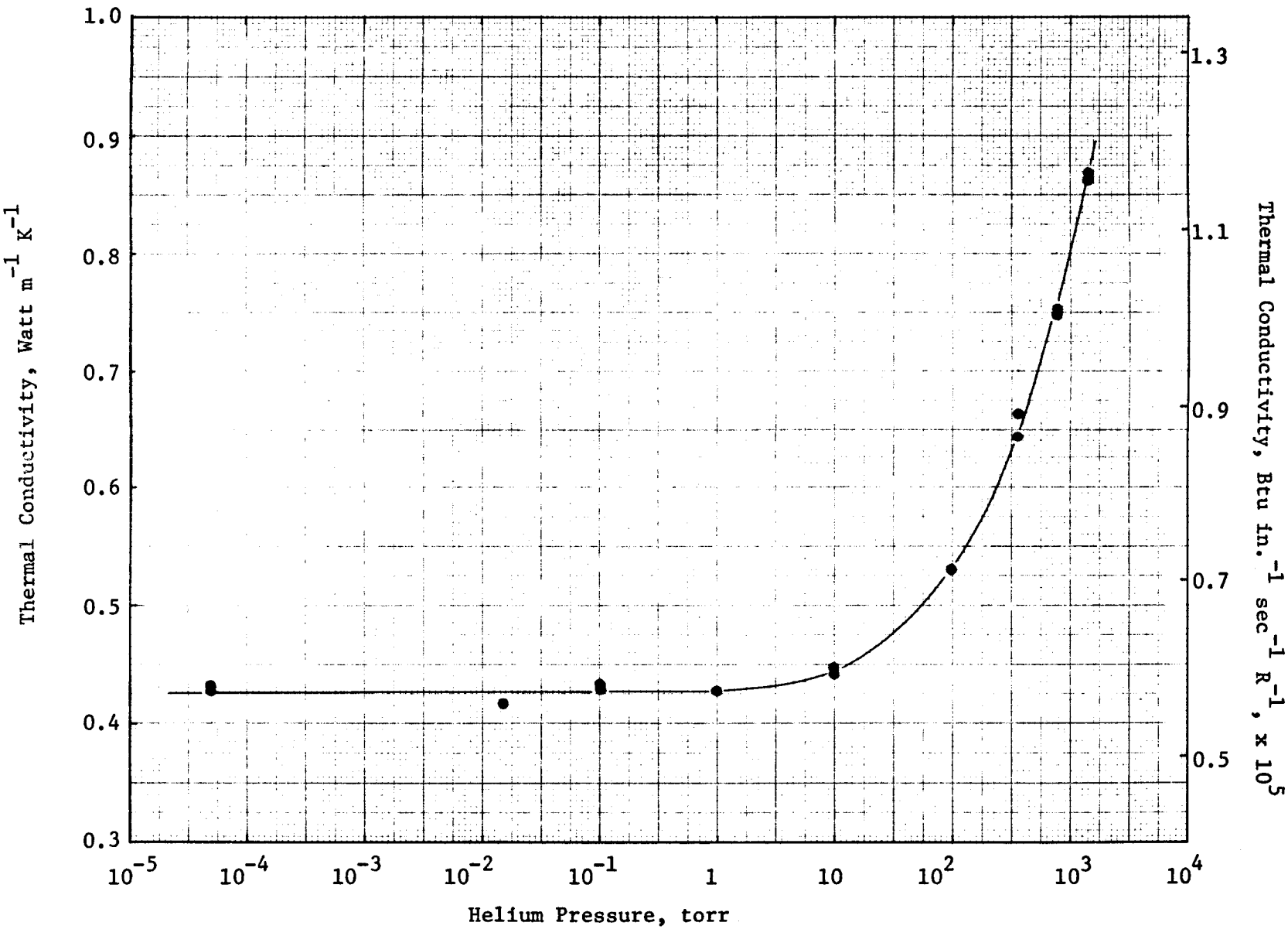

FIGURE 19. THERMAL CONDUCTIVITY OF CaO-STABILIZED ZrO_2, SAMPLE 2, AT ABOUT 550 K AS A FUNCTION OF HELIUM PRESSURE, BEFORE HEAT TREATMENT

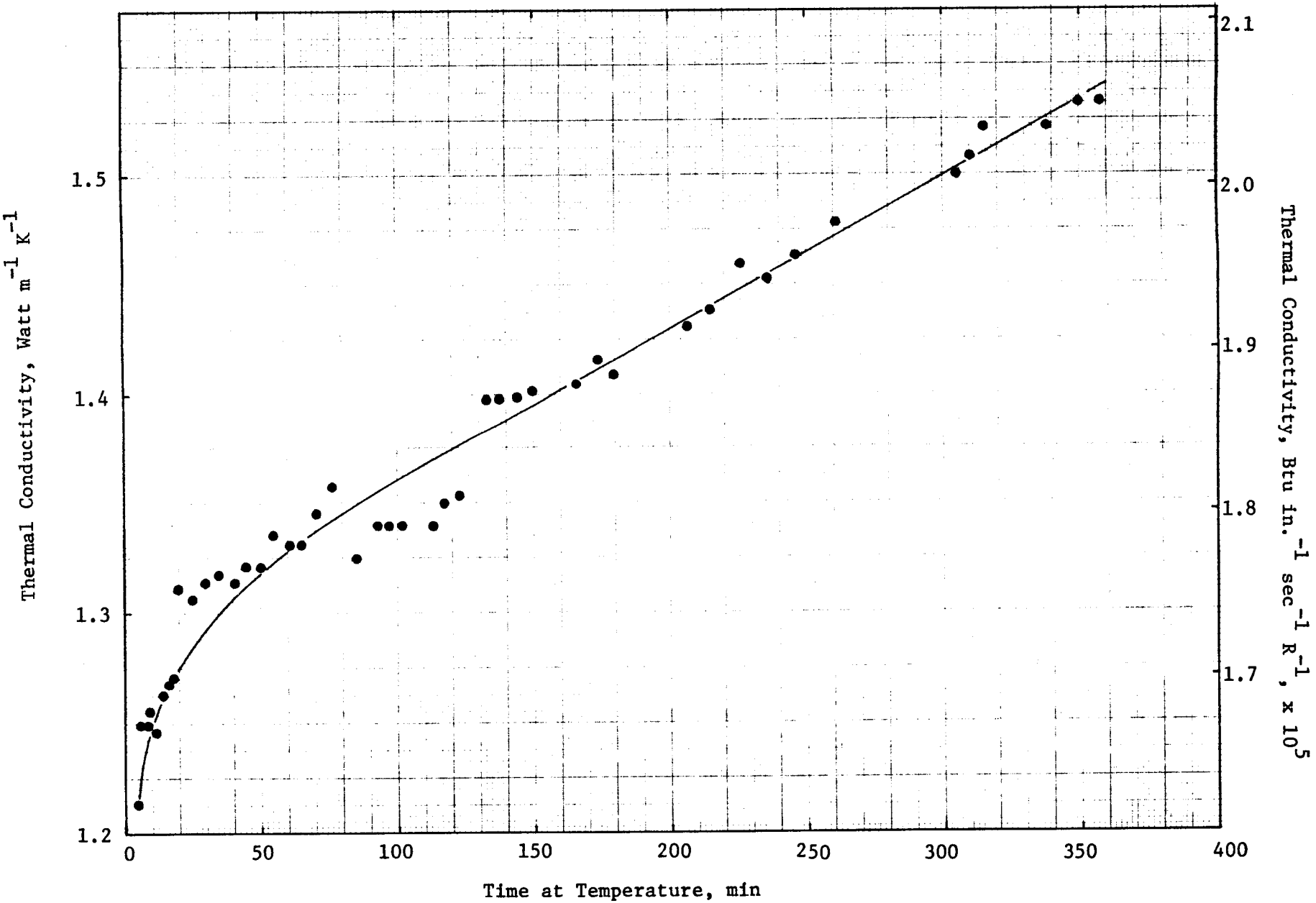

FIGURE 20. THERMAL CONDUCTIVITY OF CaO-STABILIZED ZrO_2, SAMPLE 3, DURING ISOTHERMAL HEAT TREATMENT IN VACUUM NEAR 2200 K

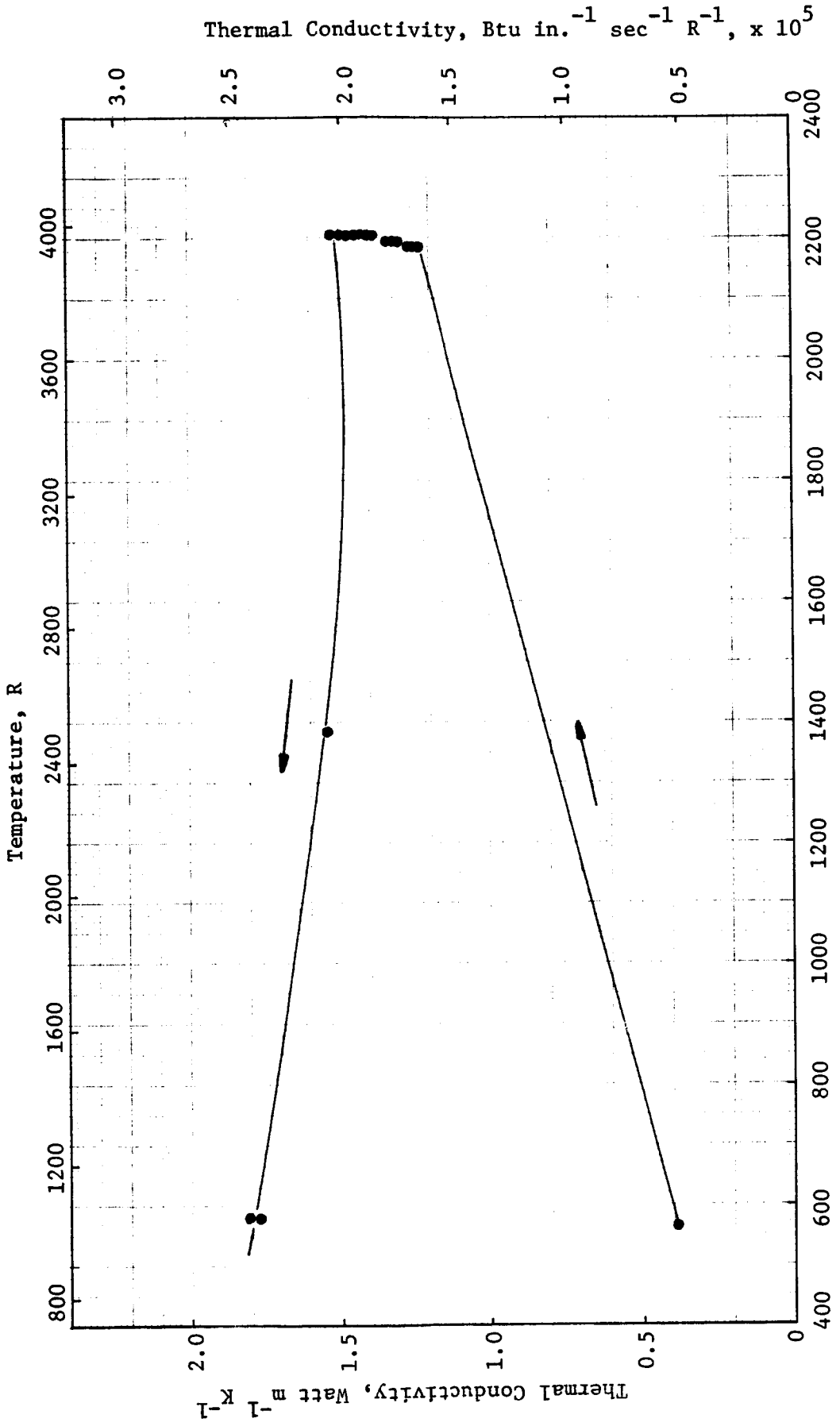

FIGURE 21. THERMAL CONDUCTIVITY OF CaO-STABILIZED ZrO_2, SAMPLE 3, IN VACUUM

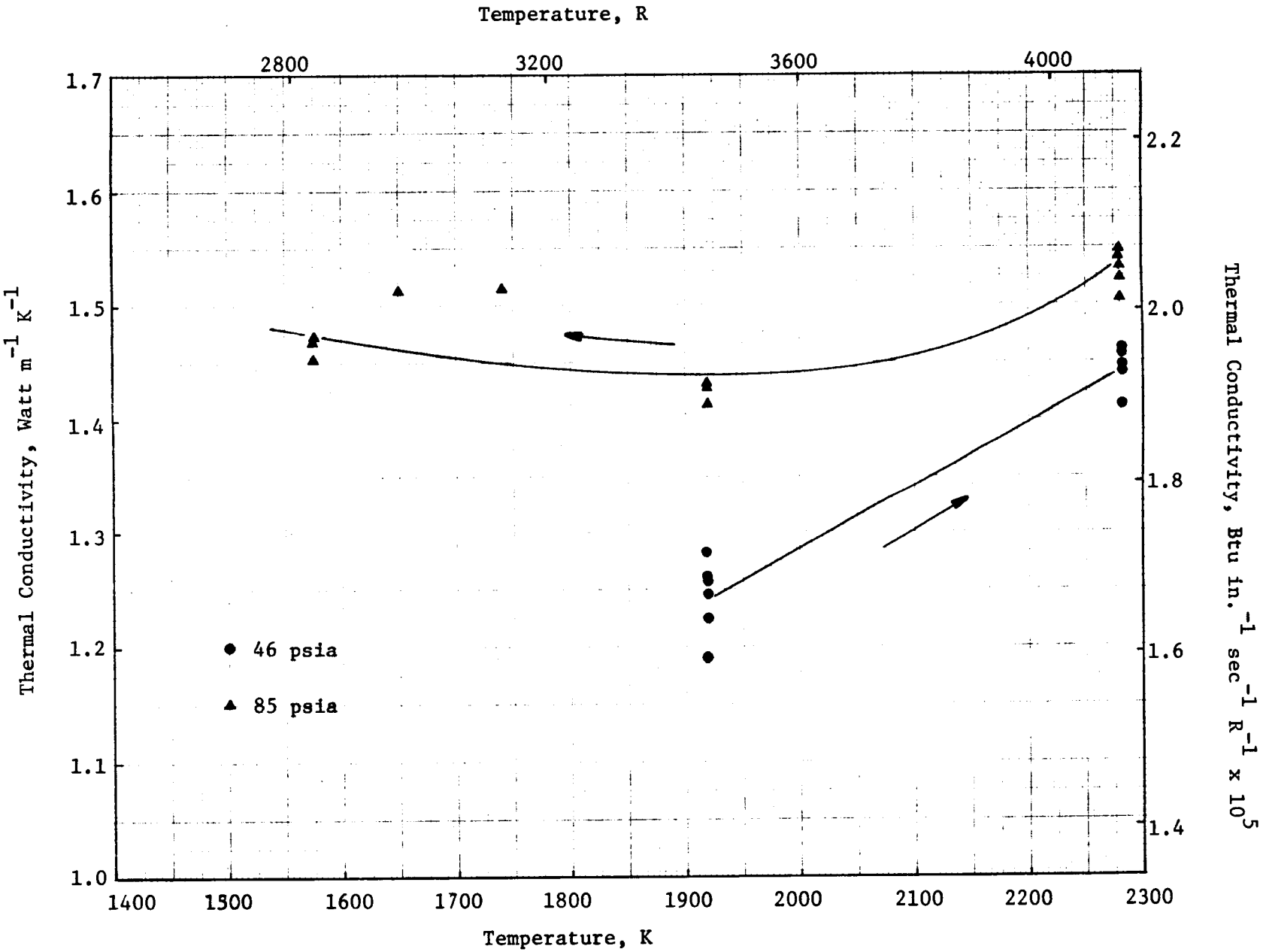

FIGURE 22. THERMAL CONDUCTIVITY OF CaO-STABILIZED ZrO_2, SAMPLE 4, IN HYDROGEN

of CaO loss as for Samples 2 and 3. The hydrogen content is about 0.75 atomic percent. While this amount of hydrogen may be significant for some properties, it probably does not significantly alter the already extremely low thermal conductivity of ZrO_2. The postmeasurement microstructure of Sample 4 is shown in Figure 23. The as-polished condition is very similar to that of Sample 1. The etchant used for the second photomicrograph was boiling NH_4F. The uniformly sized, equiaxed grains tend to indicate that the hydrogen causes no anisotropy or heterogeneity of properties. In addition, as shown in Table 2, the weight loss, thickness shrinkage, and color change of Sample 4 are similar to those of the first three samples.

It is difficult to compare the present thermal conductivity results with the literature. The data shown by Touloukian[5] for CaO-stabilized ZrO_2 containing from 2.2 to 5 w/o CaO and having porosities less than 28 percent vary from about 0.8 to 3.6 Watt m^{-1} K^{-1}. After the first heat treatment, all the present data fall between 1.2 and 1.95 Watt m^{-1} K^{-1} and are thus within the lower part of the range shown by Touloukian.

The results of specific heat measurements on CaO-stabilized ZrO_2 are given in Figure 24. An anomaly is seen to exist in the curve between about 1875 and 1975 K. Much of the anomalous behavior of the thermal conductivity curves can be attributed to the shape of this specific heat curve. As mentioned above, the specific heat is influenced by changes such as destabilization. For comparison, Figure 24 also shows the results of two earlier investigations. Levinstein's[6] sample contained about 5.25 w/o CaO, and his results are seen to be in fairly good agreement with the present work. The results of measurements by Borovik and Usikova[7] on two supposedly identical samples containing 2.99 w/o CaO are shown in this figure. The results on their Sample 1 form a smooth curve while the results on their Sample 2 show a large anomaly. These results illustrate the difficulties involved in making accurate physical property measurements on CaO-stabilized ZrO_2.

Linear thermal expansion measurements were performed on one sample of CaO-stabilized ZrO_2. These results are shown in Figure 25 and Table 3. Evidence of steady shrinkage at constant temperatures was noted above about 1275 K. At two selected temperatures, the shrinkage was measured as a function of time. These values are also given in Table 3. Following heat treatment, the specimen showed a permanent shrinkage of 1.68 percent. Small ZrO_2 chips were placed near the expansion specimen during measurement, thus being subjected to the same environment and temperature history as the expansion sample. Chemical analyses were performed on these chips and on chips broken off a spare expansion sample which had not been heat treated. The results of these analyses are given in Table 1. Two points concerning the analyses should be noted. First, the heat-treated chips had a considerably lower CaO content than the unheat-treated sample, probably due to loss of CaO by vaporization at high temperatures. Second, the heat-treated sample has a considerably higher tantalum content, probably due to a reaction between the specimen and the tantalum holder. The shrinkage of the linear expansion sample may thus be due to a combination of two effects: loss of CaO and subsequent partial destabilization, and sintering. With the present data, it is not possible to clearly separate the contribution of these two effects.

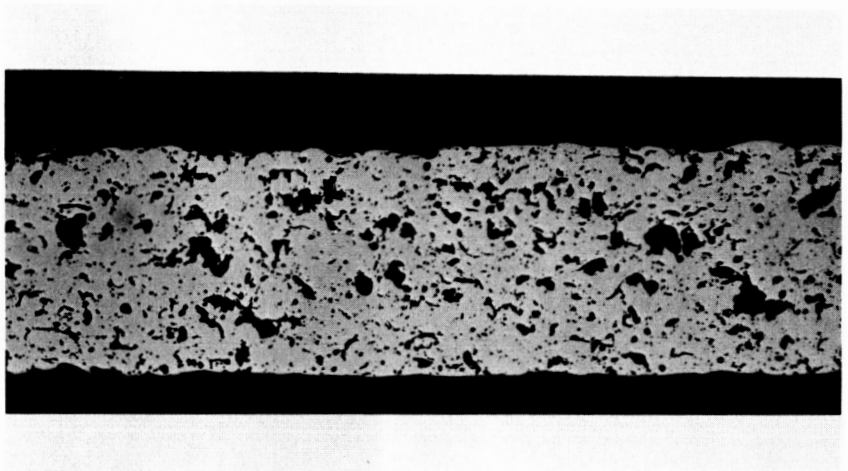

100X As-Polished 4F454

250X Etched 4F450

FIGURE 23. POSTMEASUREMENT MICROSTRUCTURE OF CaO-STABILIZED ZrO_2, SAMPLE 4, LONGITUDINAL SECTION

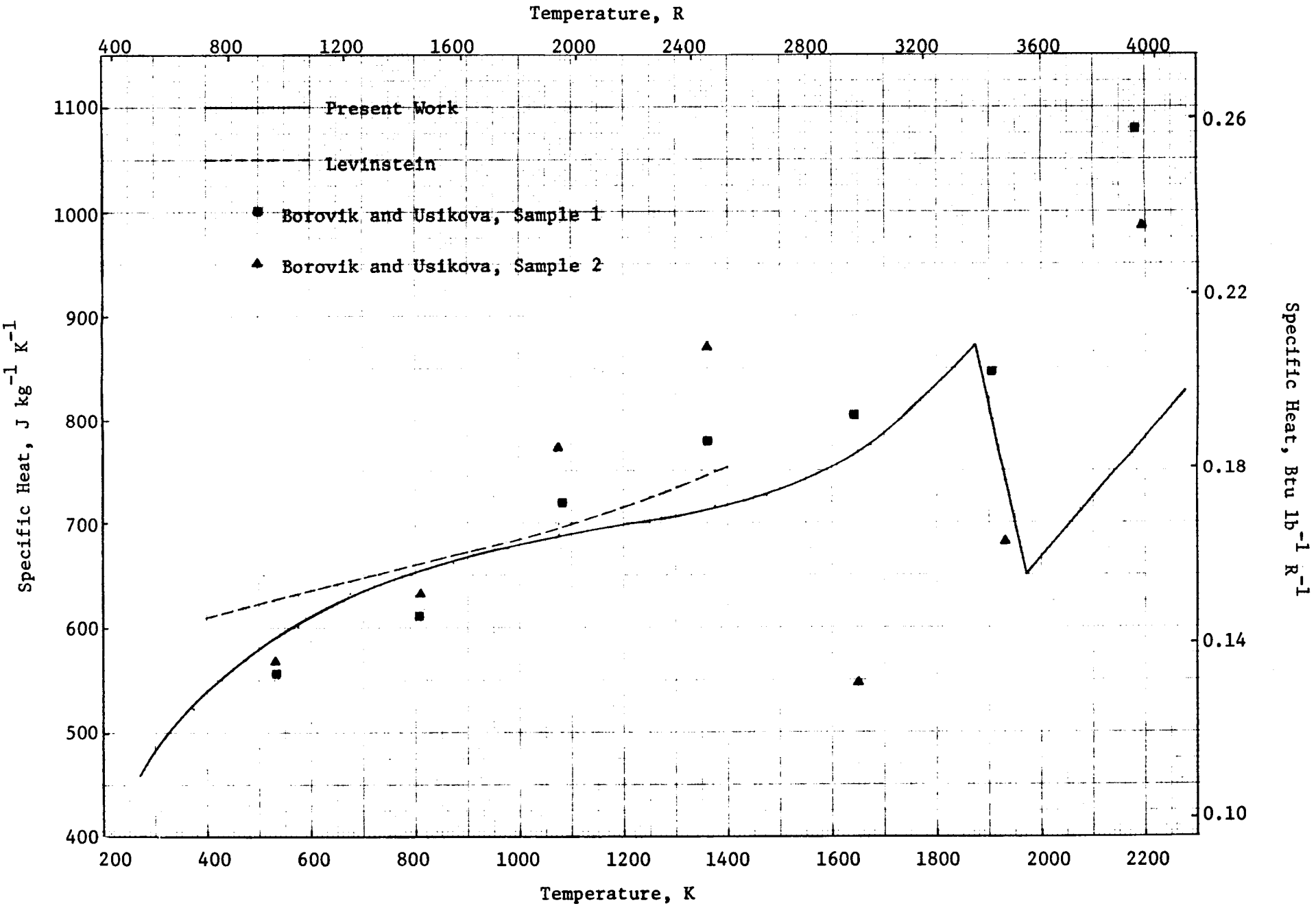

FIGURE 24. SPECIFIC HEAT OF CaO STABILIZED ZrO_2

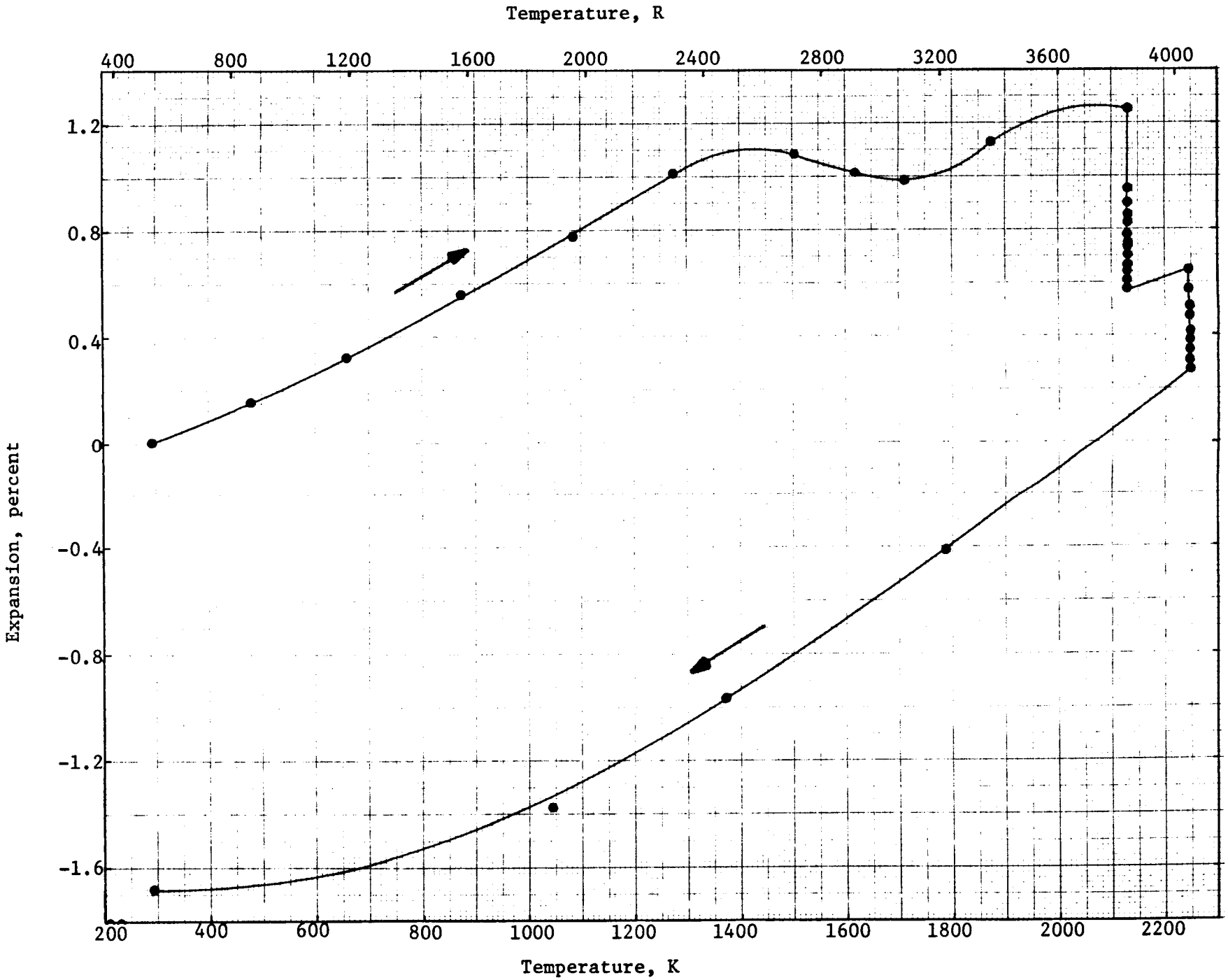

FIGURE 25. LINEAR THERMAL EXPANSION OF CaO-STABILIZED ZrO_2

TABLE 3. LINEAR THERMAL EXPANSION OF CaO-STABILIZED ZrO_2

Temperature, K	Expansion, percent	Accumulated Time, min
293	0	0
479	0.155	40
657	0.327	100
874	0.557	140
1083	0.777	180
1274	1.006	225
1509	1.082	270
1618	1.007	295
1712	0.981	325
1873	1.128	345
2130	1.253	360
2130	0.951	375
	0.892	379
	0.848	383
	0.822	387
	0.789	391
	0.753	395
	0.733	399
	0.703	403
	0.677	407
	0.646	411
	0.628	415
	0.602	419
	0.578	425
	0.572	429
2244	0.644	440
	0.568	445
	0.507	450
	0.470	455
	0.419	460
	0.387	465
	0.350	470
	0.304	475
	0.271	480
1780	-0.415	495
1370	-0.972	515
1041	-1.368	540
293	-1.68	- -

Y_2O_3-Stabilized ZrO_2

An alternative to CaO as a stabilizing agent for ZrO_2 is Y_2O_3. The material used in the present investigation was obtained from Dr. K. S. Mazdiyazni of the Air Force Materials Laboratory and is sometimes referred to as Zyttrite. A chemical analysis of a typical as-sprayed sample is given in Table 4; 11.6 weight percent is equivalent to about 6.7 mole percent Y_2O_3, in good agreement with the value of 6.5 mole percent Y_2O_3 determined by the Air Force Materials Laboratory on similar material. Photomicrographs of an as-sprayed sample are shown in Figures 26 and 27. The great number of both large and small pores is again evident.

Thermal diffusivity measurements on Sample 1 were made under hydrogen pressures ranging between 115 and 515 psia, the pressure being partly determined by the pressure-temperature limitations of the furnace. The results of these measurements are given in Figure 28. Measurements during and after the first heat treatment were made under 515 psia. No increase in the conductivity was noted due to the second heat treatment. The third heat treatment was carried out for about one-half hour at 2080 K under 415 psia while the data upon subsequent cooling were again taken under 515 psia. The increase in conductivity due to this heat treatment is about 12 percent. The sample was next heated to 2269 K under 315 psia and then to 2426 K under 115 psia where it was held for a period of about 15 minutes. The sample was then cooled to 2082 K under 115 psia, after which the pressure was increased to 415 psia and the temperature changed to 2061 K. Data taken under these conditions are in close agreement, indicating that the pressure has little influence on the conductivity. Further data taken near 1825 K under 415 and 515 psia again indicate little influence of pressure. The posttest chemical analysis of Sample 1 shows that the Y_2O_3 content is essentially the same as for the as-sprayed materials. Photomicrographs, Figures 29 and 30, show that the solid phase is much more continuous than the as-sprayed material. As indicated in Table 5, very little weight loss was experienced with this sample. The slight weight loss could be due to loss of oxygen, as evidenced by the sample color turning slightly gray.

Measurements were performed on a second sample of Y_2O_3-stabilized ZrO_2 in an effort to determine whether long-term effects in high pressure, high temperature hydrogen are significant compared to the short-term effects investigated with the first sample. The sample was first heated to 1530 K under 225 psia hydrogen. The conductivity results here, shown in Figure 31, are lower than similar results on Sample 1. The sample was then heated rapidly to 2269 K under 325 psia hydrogen, where diffusivity measurements were made at intervals over a period of about 4-1/2 hours. These results, shown in Figure 32, indicate an increase in conductivity of less than 10 percent during the heat treatment. The final conductivity value agrees very well with the results on Sample 1 at this temperature. The good agreement between these measurements and those obtained on Sample 1 indicate that long-term effects in high pressure hydrogen are fairly insignificant compared with short-term effects.

Following the high temperature measurements, the sample was cooled to about 1541 K and measurements were made at 225 psia hydrogen and at 3.5×10^{-5} torr. The results in these two atmospheres are in fairly good agreement, again

TABLE 4. CHEMICAL ANALYSES OF Y_2O_3-STABILIZED ZrO_2 SPECIMENS

Element	Weight percent			
	As-Sprayed	Sample 1	Sample 2	Specific Heat Sample
Y_2O_3	11.6	11.85	11.80	12.0
Si	0.005	<0.01	<0.01	0.03
Mg	<0.0005			<0.0005
Pb				<0.001
W				<0.01
Ni	0.002			0.002
Al	0.003			<0.001
Mo	0.007			0.003
Ca	0.001	<0.005	<0.005	<0.0005
Cr	<0.001			<0.001
Ta				<0.03
B	<0.0005			
Fe	0.001			
Cu	<0.0005			

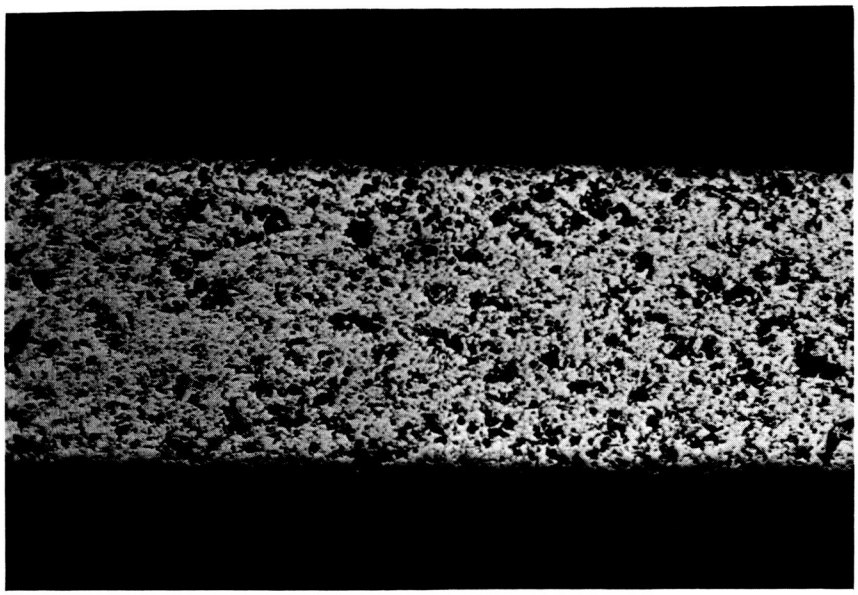

100X 2G310

FIGURE 26. MICROSTRUCTURE OF AS-SPRAYED Y_2O_3-STABILIZED ZrO_2, LONGITUDINAL SECTION (AS-POLISHED)

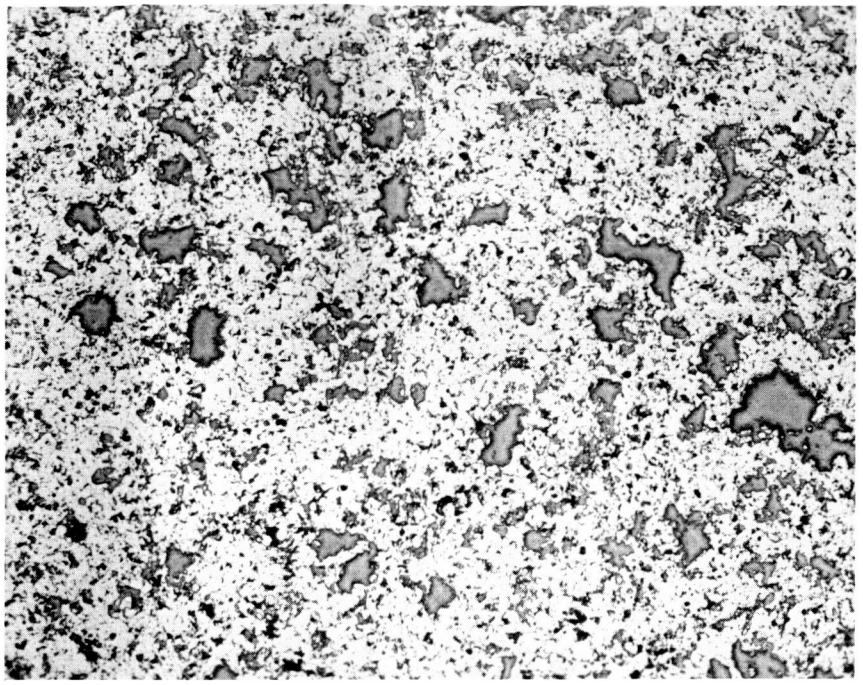

100X 2G311

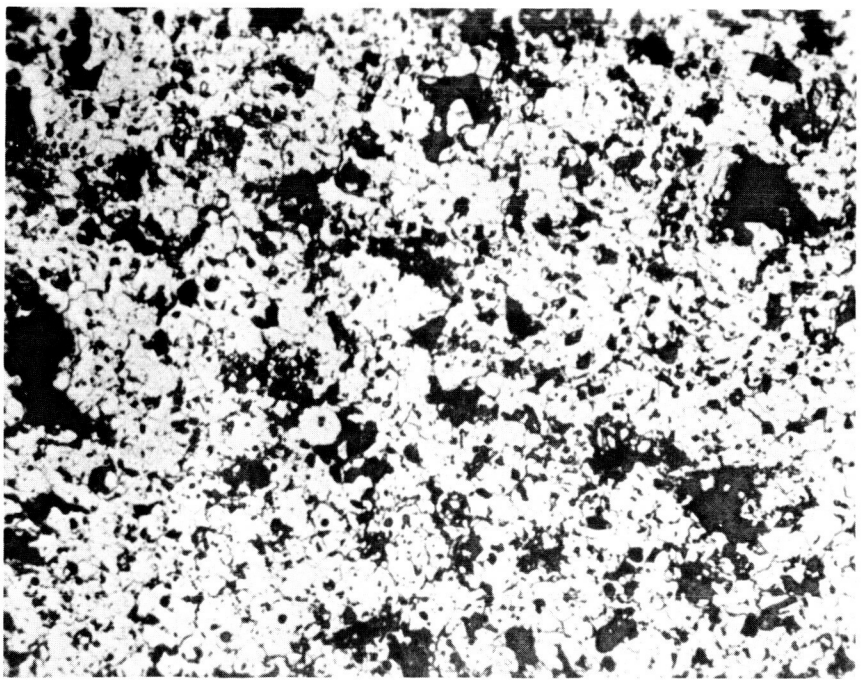

250X 2G312

FIGURE 27. MICROSTRUCTURE OF AS-SPRAYED Y_2O_3-STABILIZED ZrO_2, TRANSVERSE SECTION (AS-POLISHED)

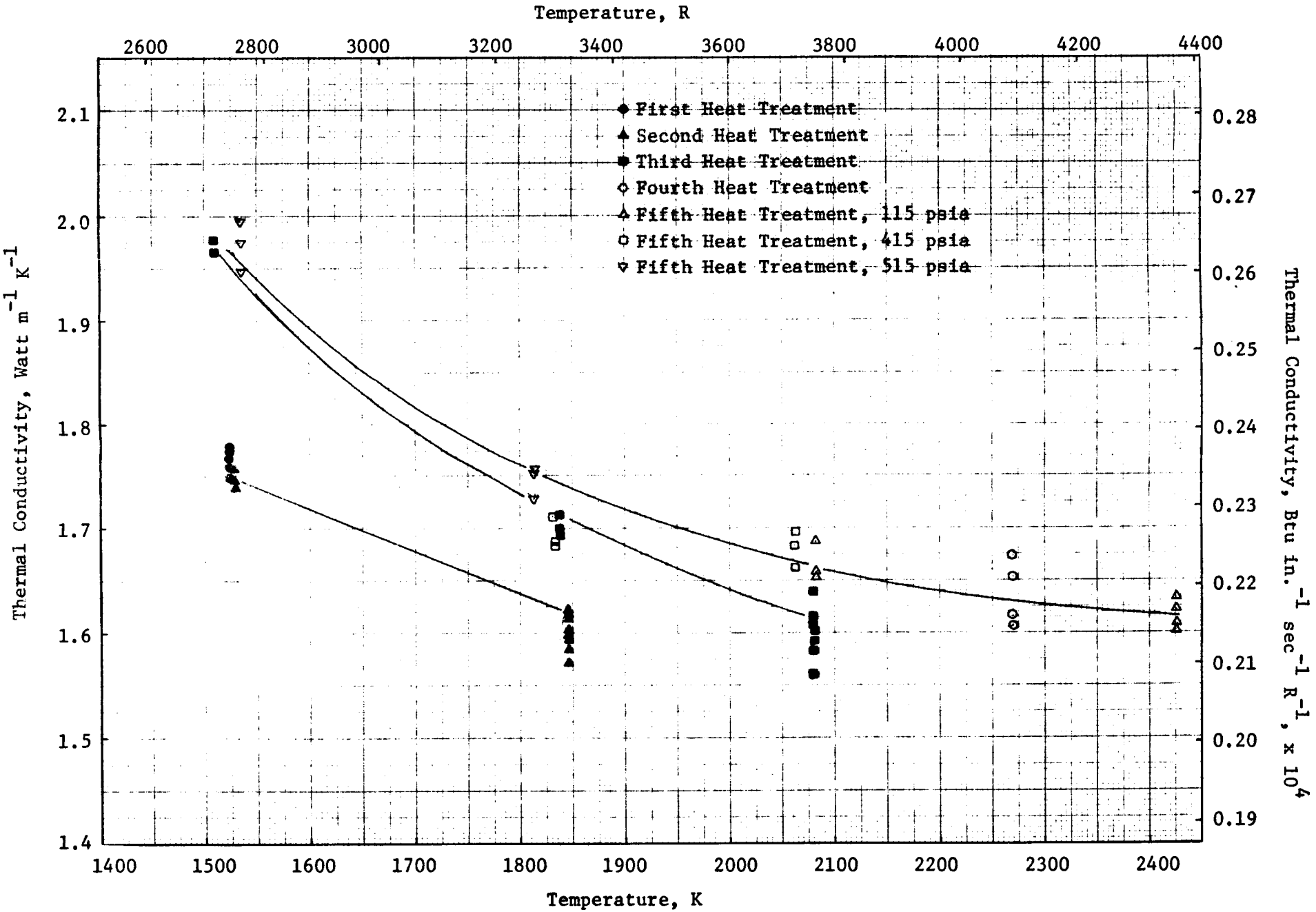

FIGURE 28. THERMAL CONDUCTIVITY OF Y_2O_3-STABILIZED ZrO_2, SAMPLE 1, IN HYDROGEN

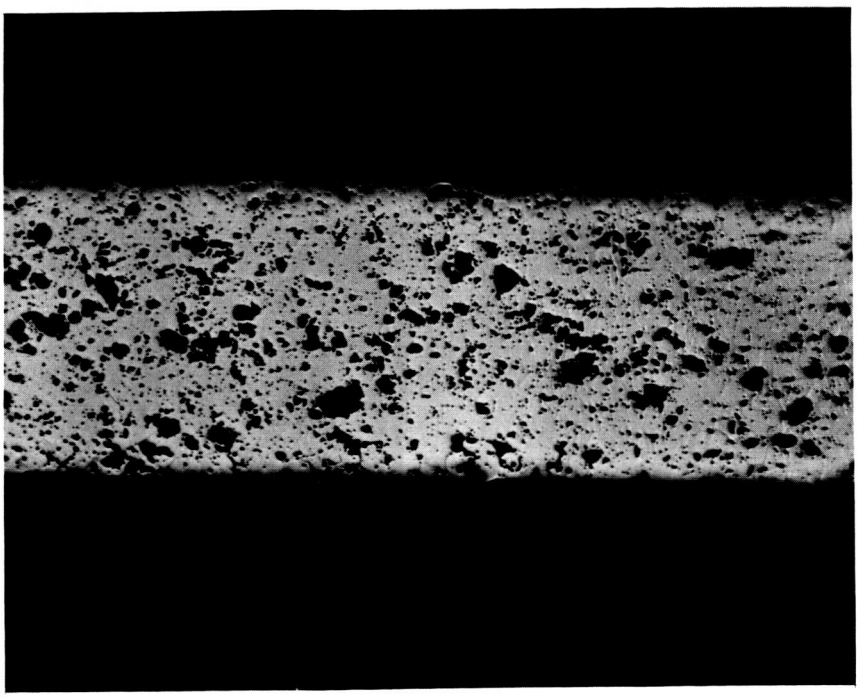

100X 2G313

FIGURE 29. POSTMEASUREMENT MICROSTRUCTURE OF Y_2O_3-STABILIZED ZrO_2, SAMPLE 1, LONGITUDINAL SECTION (AS-POLISHED)

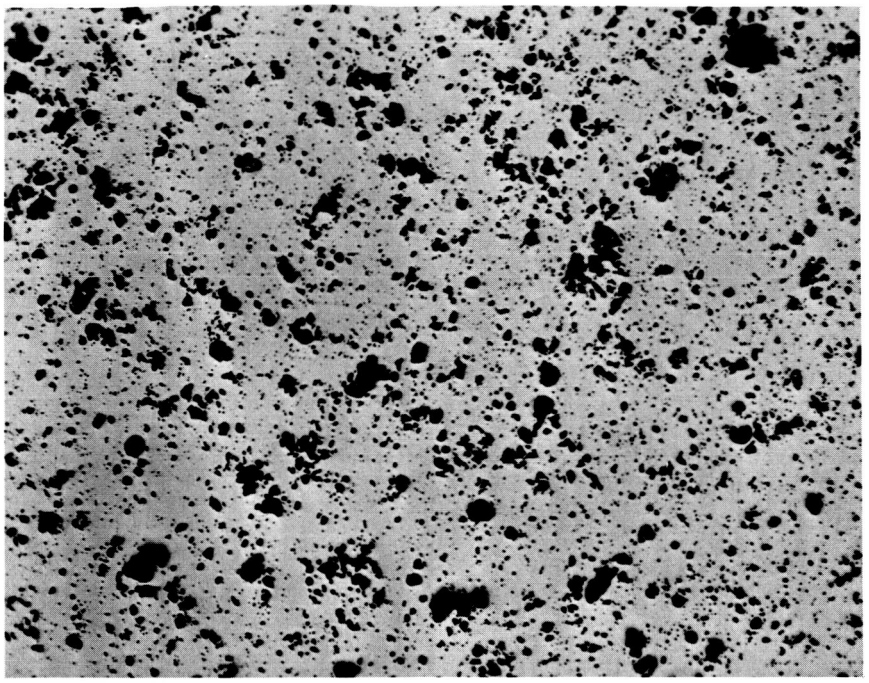

100X 2G314

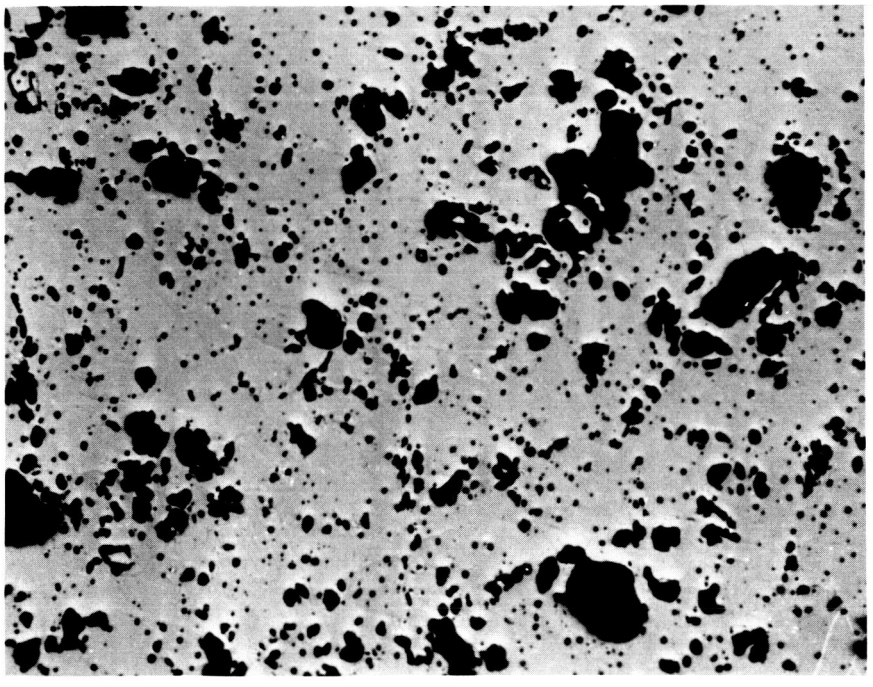

250X 2G315

FIGURE 30. POSTMEASUREMENT MICROSTRUCTURE OF Y_2O_3-STABILIZED ZrO_2, SAMPLE 1, TRANSVERSE SECTION (AS-POLISHED)

TABLE 5. PHYSICAL CHARACTERISTICS OF Y_2O_3-STABILIZED ZrO_2 THERMAL DIFFUSIVITY SAMPLES

	Thickness, cm		Diameter, cm		Weight, g		Density, g cm^{-3}		Posttest Color
	Pretest	Posttest	Pretest	Posttest	Pretest	Posttest	Pretest	Posttest	
Sample 1	0.0444	0.0432	1.2718	1.2448	0.2698	0.2695	4.975	5.362	Turned light gray
Sample 2	0.0422	0.0411	1.2652	1.2390	0.2581	0.2577	5.040	5.379	Turned light gray

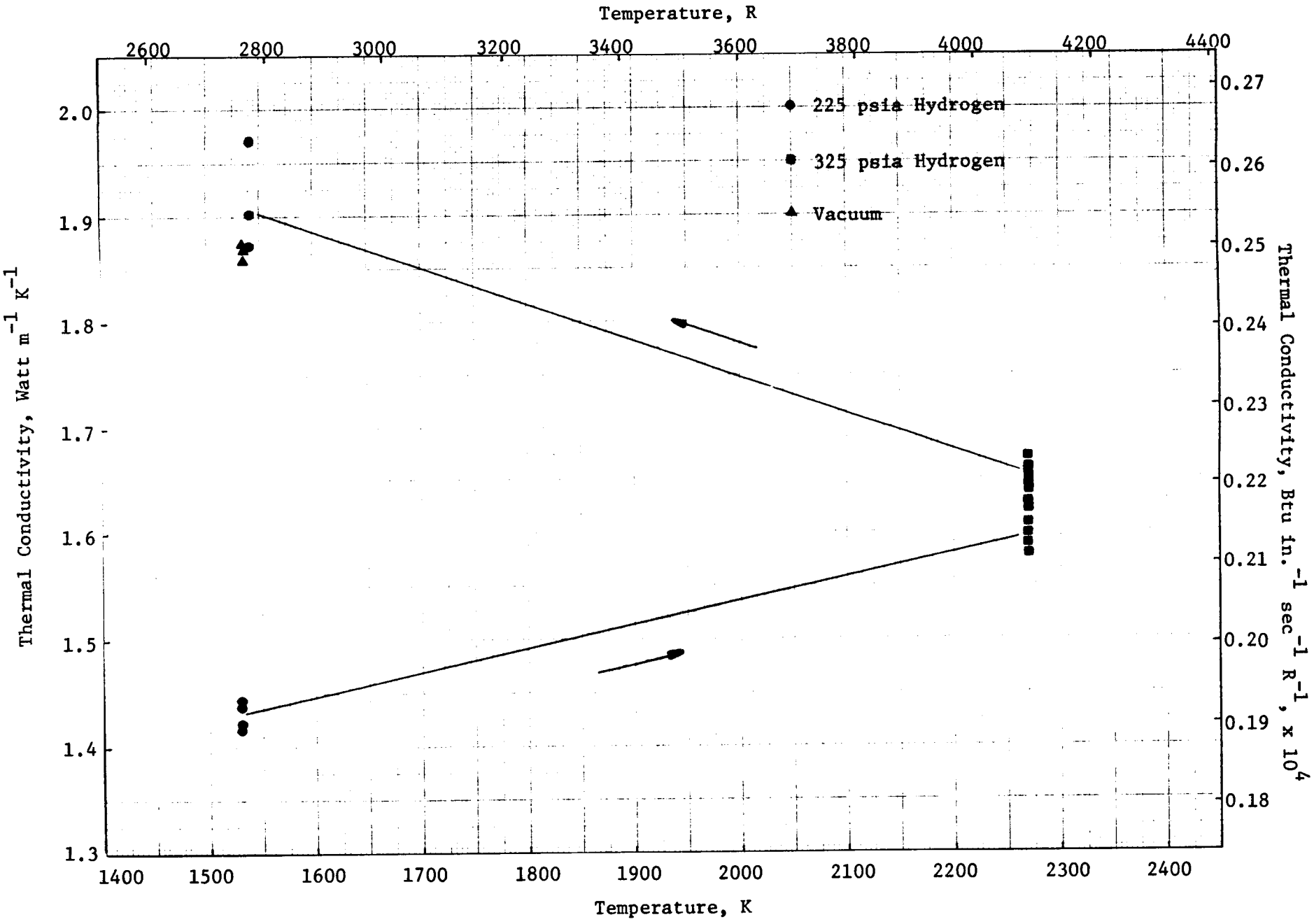

FIGURE 31. THERMAL CONDUCTIVITY OF Y_2O_3-STABILIZED ZrO_2, SAMPLE 2

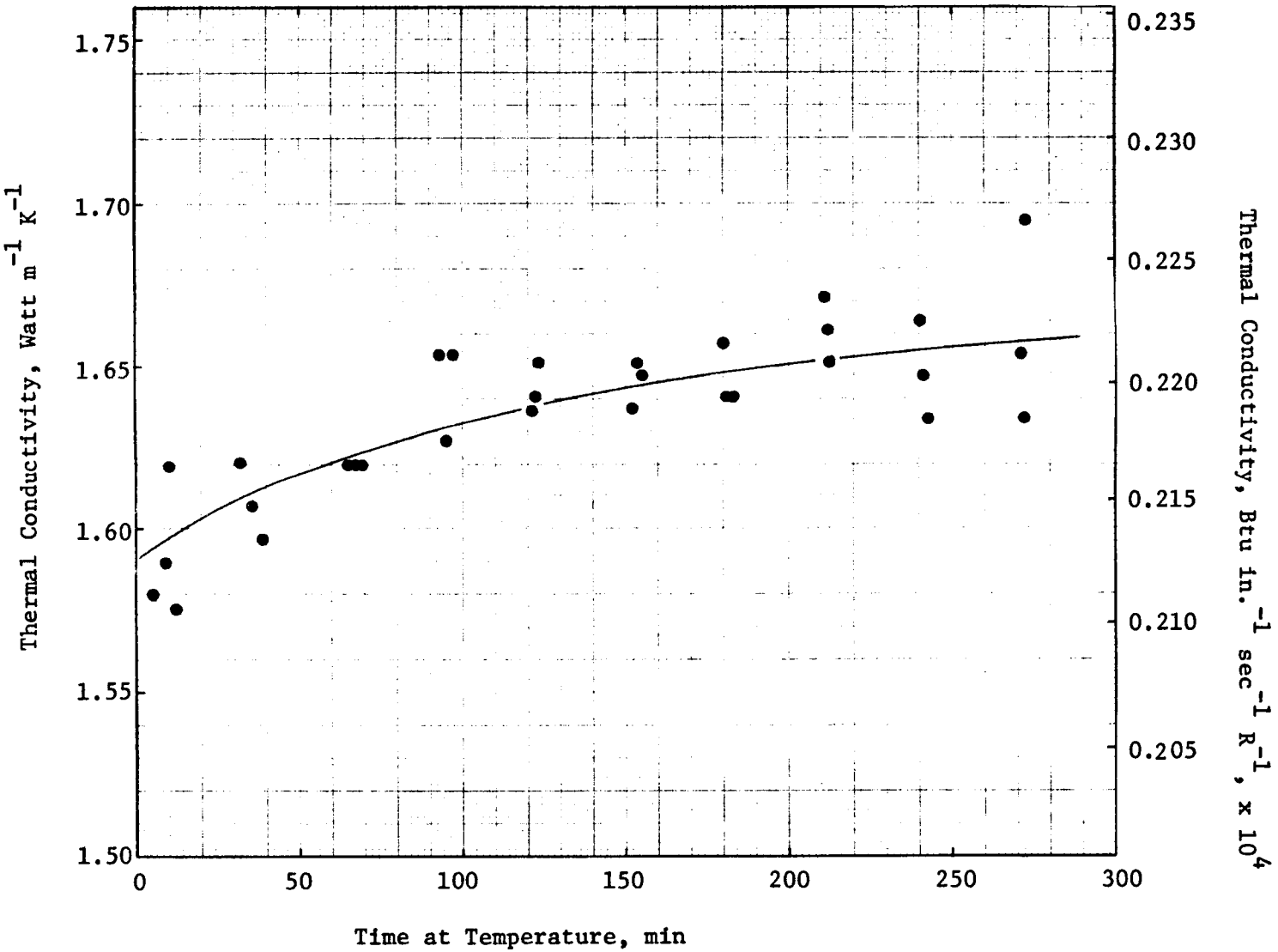

FIGURE 32. THERMAL CONDUCTIVITY OF Y_2O_3-STABILIZED ZrO_2, SAMPLE 2, DURING ISOTHERMAL HEAT TREATMENT IN 325 PSIA HYDROGEN NEAR 2269 K

indicating an insensitiveness of conductivity to pressure. Chemical analyses on this sample showed no loss of Y_2O_3, and the microstructure, shown in Figure 33, is very similar to that of Sample 1.

The present data may be compared to the results of Fitzsimmons[8], and Hobbs, et al[9], for ZrO_2 + 15 percent Y_2O_3 of 87 percent density. These values increase steadily from about 1.5 Watt m^{-1} K^{-1} at 400 K to about 1.65 at 1367 K. The present results are in fairly good agreement, although they start at a somewhat higher value and have an opposite slope. It is conceivable that part of this difference could be due to differences in specimen compositions, purities, and densities.

The results of specific heat measurements on Y_2O_3-stabilized ZrO_2 are shown in Figure 34. The values above about 2100 K are somewhat uncertain due to an apparent reaction which occurred above this temperature. Since this reaction occurred near the upper temperature limitations of the apparatus, it was not possible to accurately define the curve at the very highest temperatures. Thus, the lower temperature data were extrapolated for use in calculating thermal conductivity. An effort was made to determine the nature of the irreversible changes which were observed. A postmeasurement chemical analysis was performed on a portion of the specific heat sample. The results, given in Table 4, show that no Y_2O_3 was lost, indicating that the changes are not related to loss of stabilizer. The Mo content of the sample is lower than that of the as-sprayed material, indicating that no perceptible reaction occurred between the sample and the Mo foil within which it was wrapped. After being wrapped in Mo foil, the sample had been sealed in a tantalum capsule. Although the <0.03 weight percent Ta may have been picked up from the capsule, it seems unlikely that this small amount would have a noticable effect. The sample changed in color from white to dark gray, presumably due to a change in stoichiometry. This loss of oxygen and subsequent gettering by the tantalum capsule may explain the changes observed.

The results of linear thermal expansion measurements are given in Figure 35 and in Table 6. The results are given in chronological order in the table. The sample was held at a number of elevated temperatures for long periods of time. Steady shrinkage, presumably due to sintering was noted at each of these high temperatures. The final shrinkage at room temperature was found to be 2.082 percent

Al_2O_3

Al_2O_3 was also being considered for use on the hot side of the coating system. A chemical analysis of a typical as-sprayed Al_2O_3 sample is given in Table 7. Also given in Table 7 are postmeasurement chemical analyses of the two thermal diffusivity specimens. The as-sprayed material is indicated to be 99.67 percent Al_2O_3 by difference, while the two diffusivity samples are somewhat purer, being around 99.95 percent Al_2O_3. Photomicrographs of an as-sprayed sample are shown in Figures 36 and 37. The structure is similar to that of other sprayed oxides, consisting of loosely connected solid particles.

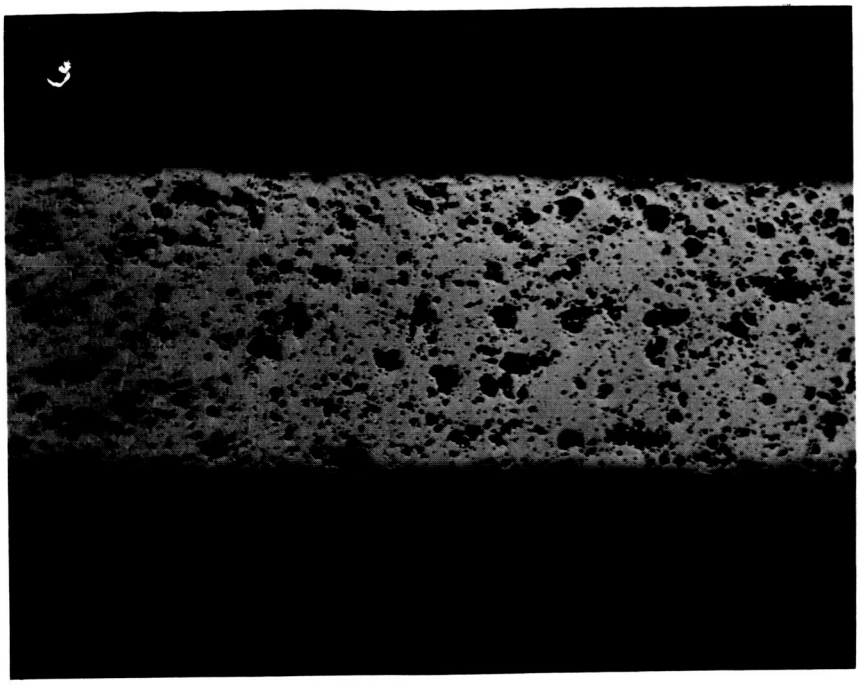

100X LONGITUDINAL SECTION 2G316

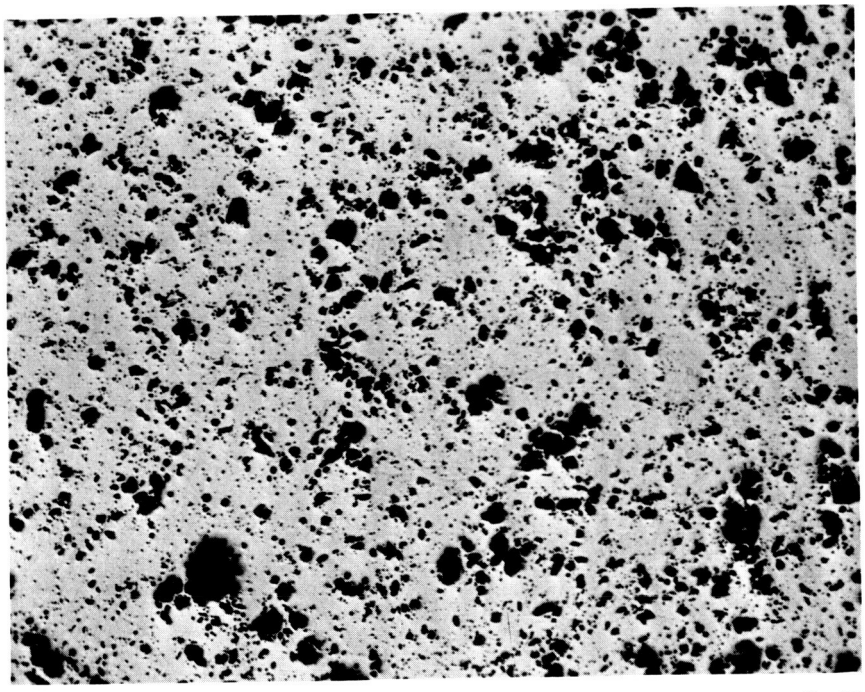

100X TRANSVERSE SECTION 2G317

FIGURE 33. POSTMEASUREMENT MICROSTRUCTURE OF Y_2O_3-STABILIZED ZrO_2, SAMPLE 2 (AS-POLISHED)

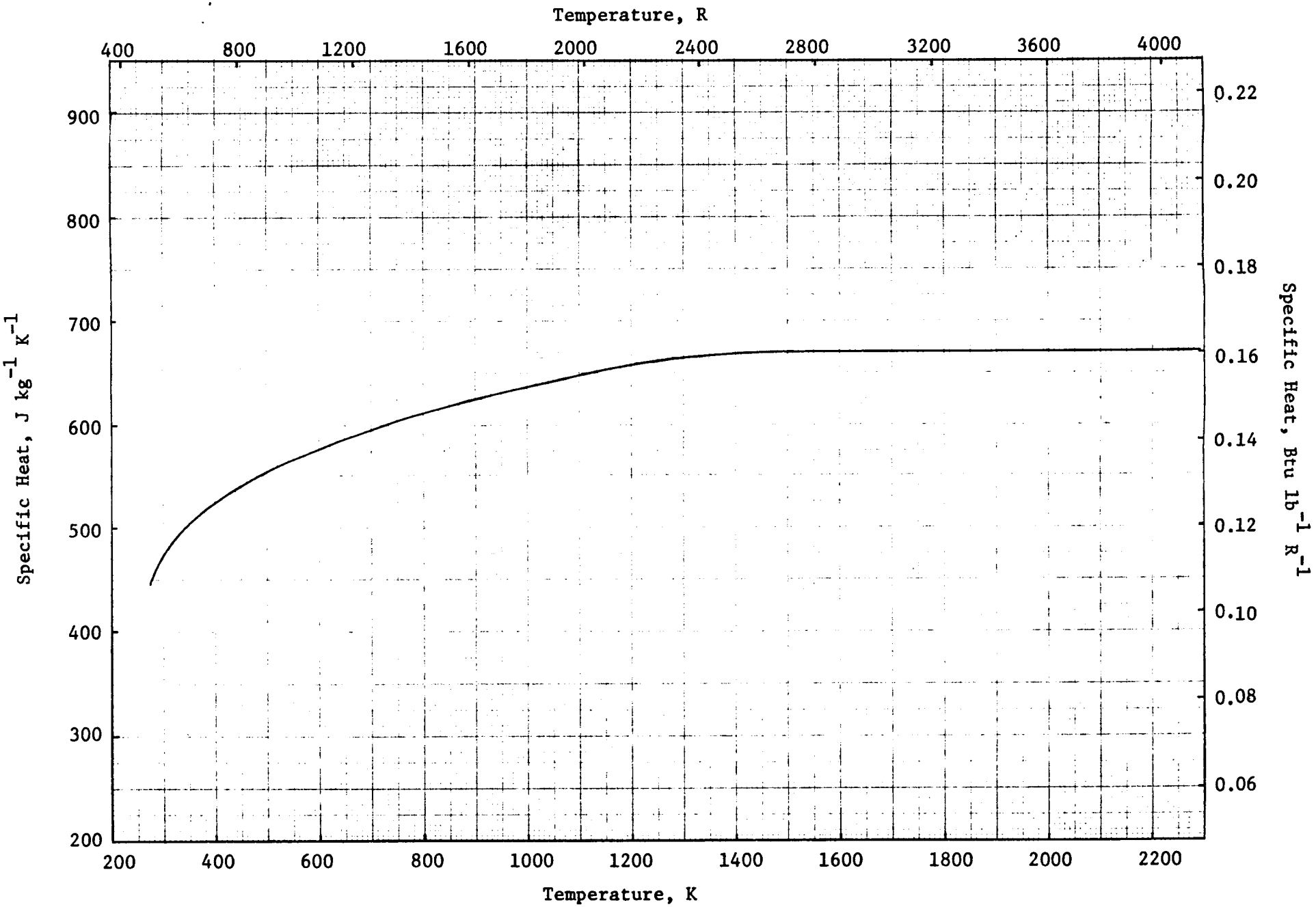

FIGURE 34. SPECIFIC HEAT OF PLASMA-SPRAYED Y_2O_3-STABILIZED ZrO_2

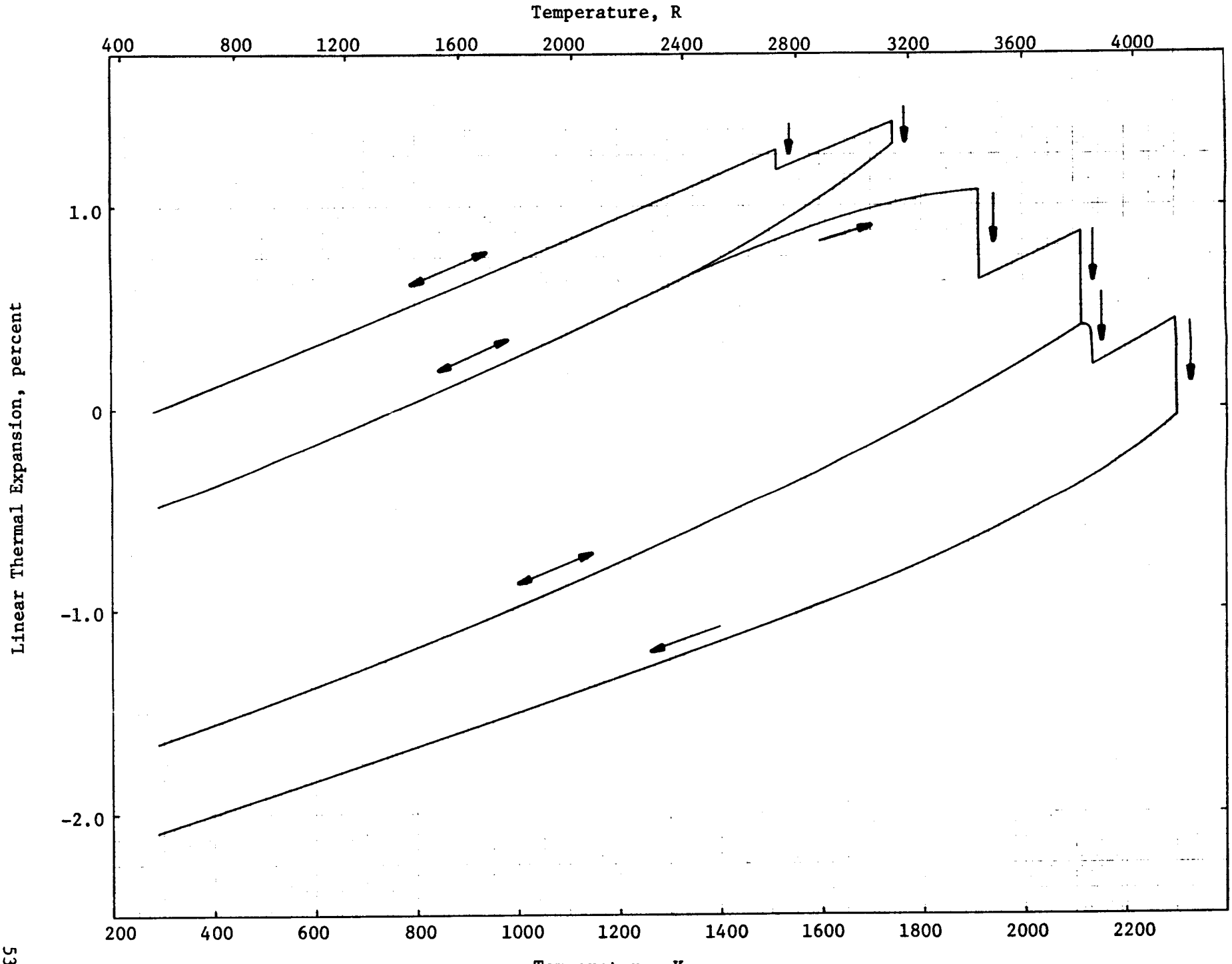

FIGURE 35. LINEAR THERMAL EXPANSION OF Y_2O_3-STABILIZED ZrO_2

TABLE 6. LINEAR THERMAL EXPANSION OF Y_2O_3-STABILIZED ZrO_2

Temperature, K	Expansion percent	Time at Temperature, min
295	0	
429	0.117	
580	0.270	
682	0.389	
821	0.519	0
821	0.528	25
974	0.688	0
974	0.688	35
1118	0.851	0
1118	0.852	40
737	0.433	0
737	0.433	12
292	-0.014	
673	0.366	
822	0.525	
852	0.557	
894	0.600	
917	0.631	
928	0.653	
966	0.682	
987	0.709	
1013	0.737	
1050	0.780	
1159	0.904	
1294	1.053	0
1294	1.052	45
829	0.518	
294	-0.021	
964	0.670	
1286	1.039	
1385	1.146	0
1382	1.132	35
1380	1.119	55
1520	1.236	0
1514	1.205	15
1516	1.194	31
1515	1.189	46
1516	1.182	61
1514	1.175	76
1743	1.396	0

TABLE 6 (Continued)

Temperature, K	Expansion percent	Time at Temperature, min
1744	1.350	15
1748	1.337	30
1748	1.334	45
1746	1.325	60
1743	1.313	80
1743	1.306	98
1506	0.828	
298	-0.476	
292	-0.480	
1323	0.619	
1911	1.068	0
1912	1.018	14
1915	0.957	30
1910	0.892	46
1914	0.831	73
1913	0.795	88
1914	0.764	104
1915	0.735	128
1913	0.702	153
1916	0.666	191
1916	0.632	231
2119	0.858	0
2115	0.760	21
2103	0.681	41
2113	0.529	99
2115	0.447	145
2113	0.401	181
1790	-0.080	
307	-1.630	
2126	0.398	0
2134	0.355	26
2135	0.334	49
2135	0.281	90
2130	0.251	120
2121	0.203	176
2304	0.423	0
2304	0.366	15
2304	0.318	27
2304	0.179	83
2304	0.082	150
2304	-0.010	218
2304	-0.040	240
2186	-0.276	
1973	-0.579	
1822	-0.766	
295	-2.082	

TABLE 7. CHEMICAL ANALYSES OF PLASMA-SPRAYED Al_2O_3 SAMPLES

Element	Weight percent		
	As-sprayed	Sample 1	Sample 2
Si	0.015	0.001	0.001
Fe	0.015	0.01	0.005
Mg	0.005	0.001	0.002
Ca	0.05	0.02	0.02
Mo	0.003	0.001	0.001
Ti	0.02	0.005	0.003
Ni	0.002	0.005	0.01
Cr	<0.001	0.001	0.001
Be	<0.0001		
Mn	0.0005		
V	<0.001		
Ga	0.005		
Cu	<0.0005		
Na	0.2		
Zr	0.01		

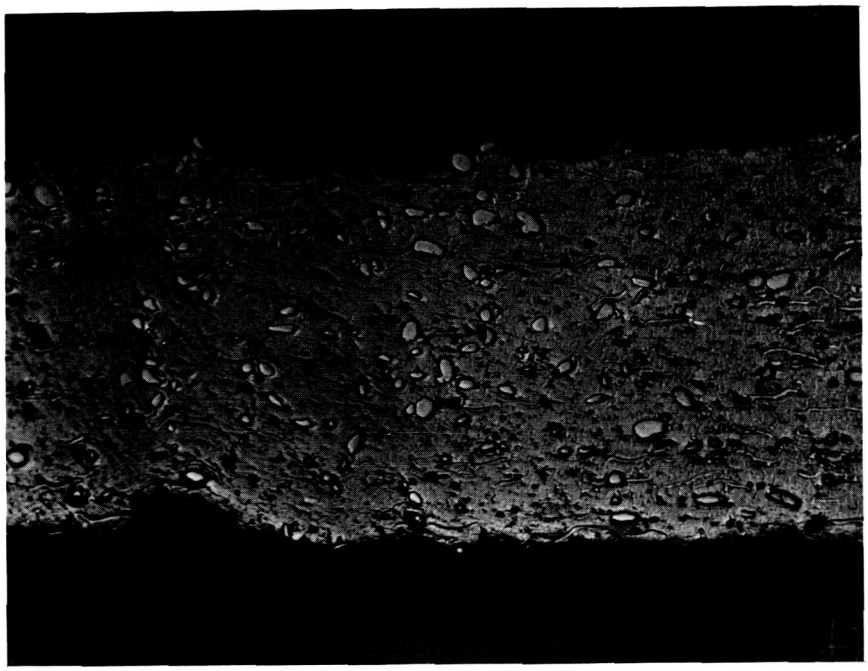

100X 2G271

FIGURE 36. MICROSTRUCTURE OF AS-SPRAYED Al_2O_3, LONGITUDINAL SECTION (AS-POLISHED)

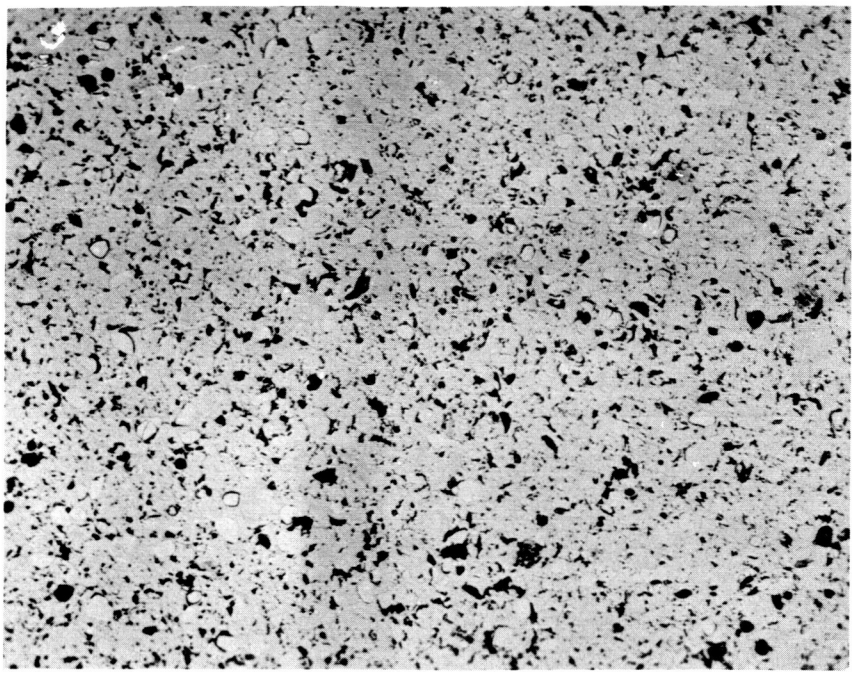

100X 2G272

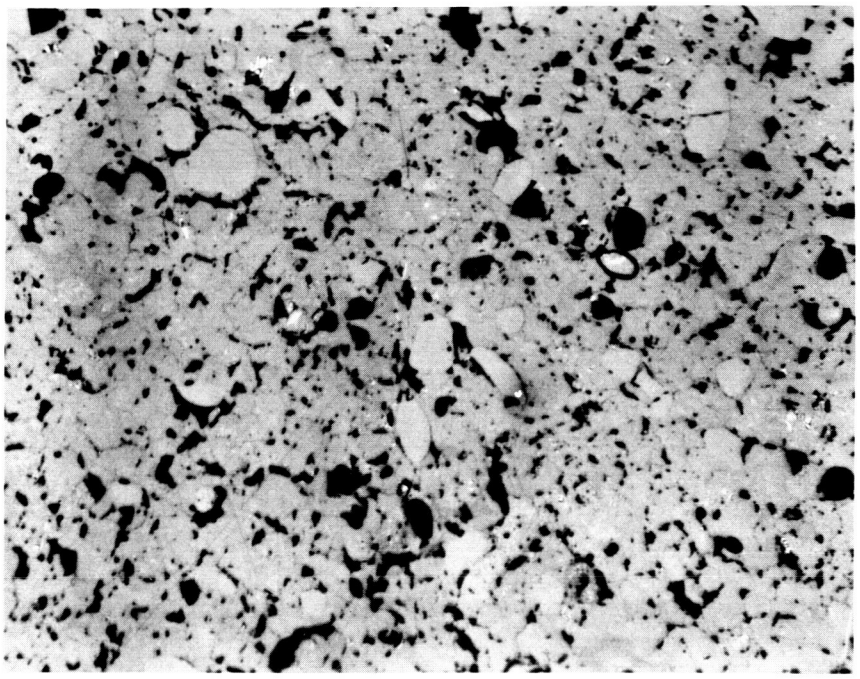

250X 2G273

FIGURE 37. MICROSTRUCTURE OF AS-SPRAYED Al_2O_3, TRANSVERSE SECTION (AS-POLISHED)

The thermal conductivity results for Al_2O_3 Sample 1 are given in Figure 38. The measurements were made in hydrogen at 515 psia. The sample was held at elevated temperatures for periods of approximately one-half hour during which diffusivity measurements were made. After each heat treatment measurements were made at lower temperatures to observe the effects of the heat treatment. As shown in Table 8, the density of this specimen increased from 3.35 g cm^{-3} before measurements to 3.62 g cm^{-3} following the measurements. The increases in conductivity associated with each heat treatment are apparently due to the increase in density along with a change in the distribution of porosity due to sintering. Photomicrographs of Sample 1 taken after the measurements are shown in Figures 39 and 40. Many of the lines shown in these two photomicrographs are not actually cracks but rather are grain boundaries delineated by relief caused by the polishing process. Bearing this in mind, the solid phase of Sample 1 is seen to be much more continuous than the as-sprayed material.

Also shown in Figure 38 is the TPRC recommended curve for 99.5 percent pure, 98 percent dense, polycrystalline Al_2O_3[10]. If the present data were corrected for porosity by the Maxwell-Eucken relation, the values after the final heat treatment would fall about 11 percent higher than they are plotted. These corrected values would then be at most 20 percent different from the recommended curve which is thought to be accurate to within 10 percent over the temperature range shown. Part of the discrepancy could be due to a combination of the following factors: (1) the present sample is of higher purity than that for which the TPRC curve is recommended, (2) transfer of heat by the high pressure gas may produce a small enhancing effect, (3) part of the opaque tungsten coating could have been lost by vaporization, allowing laser light to penetrate the sample and/or allowing the infrared detector to "view" the interior of the sample rather than the surface. However, the agreement between the present data and the recommended curve is actually fairly good considering the wide spread in literature data upon which the recommended curve is based.

The measurements on Sample 2 were performed to determine the effect of gas conduction and to determine whether long-time sintering effects are significant. The sample was first heated to 1323 K in vacuum ($\sim 6 \times 10^{-6}$ torr). After measuring the diffusivity under this condition, the furnace was pressurized to 515 psia hydrogen and the measurements were repeated. As shown in Figure 41, there is a significant difference between the data obtained in vacuum and that obtained in the gas. The large difference is probably due to an open porosity structure present before substantial sintering has occurred. The sample was then heated to 2073 K and a series of measurements was made. The sample was held at 2073 K for about 2 hours and another set of measurements was made. The values obtained at the end of the heat treatment were only slightly ($\sim$6 percent) higher than those obtained at the start, suggesting that long-time sintering effects are not significantly greater than the short-time effects. The sample was then cooled to 1333 K and measurements were made, first in 515 psia hydrogen and then in vacuum ($\sim 4 \times 10^{-4}$ torr). The difference between the data in gas and in vacuum is now much less than the difference before sintering. This is probably due to an initially open porosity changing to a more closed porosity as a result of the heat treatment, as borne out in the photomicrographs shown in Figure 42, where again most of the lines are grain boundaries rather than cracks.

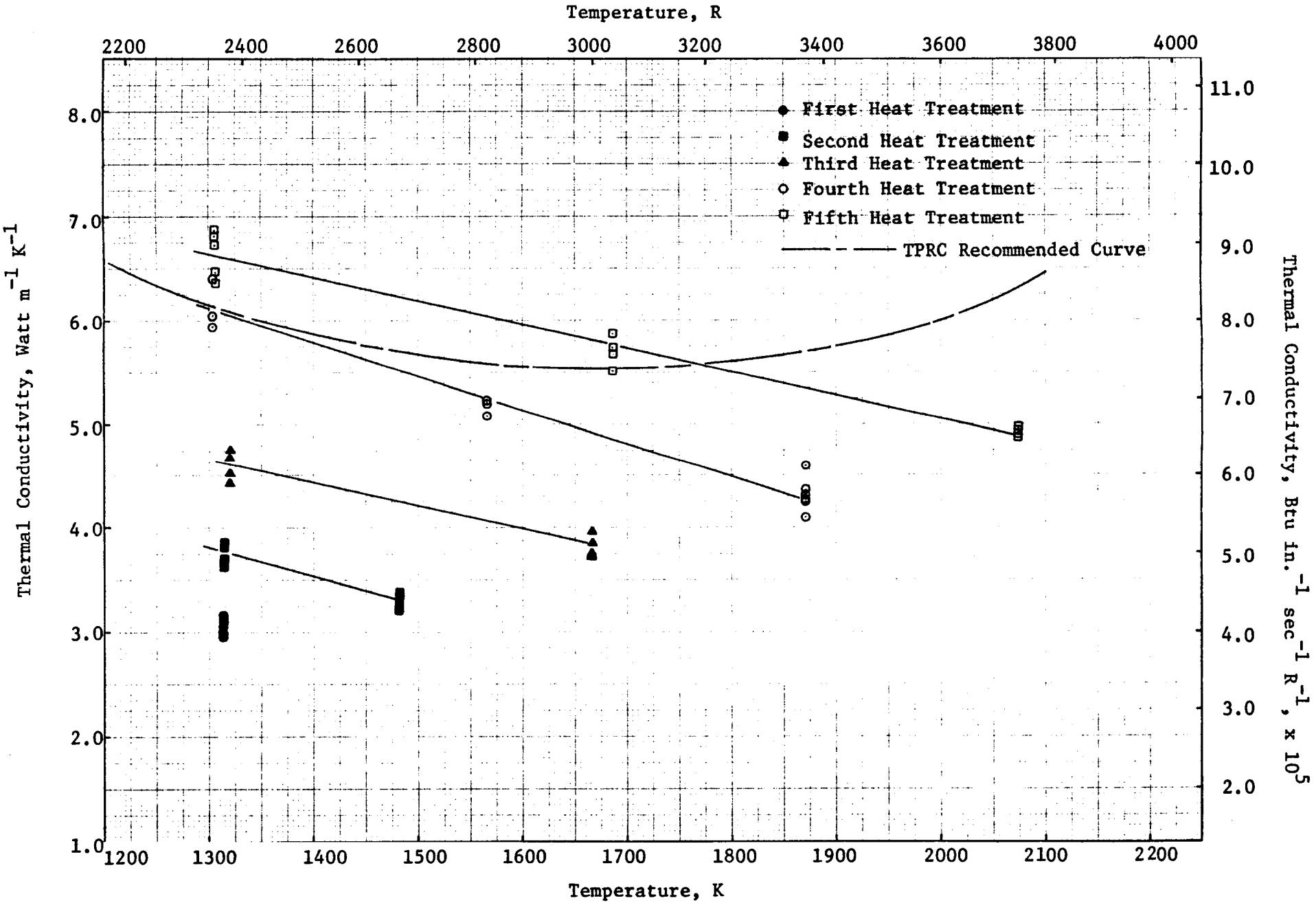

FIGURE 38. THERMAL CONDUCTIVITY OF PLASMA-SPRAYED Al_2O_3, SAMPLE 1

TABLE 8. PHYSICAL CHARACTERISTICS OF Al_2O_3 THERMAL DIFFUSIVITY SAMPLES

	Thickness, cm		Diameter, cm		Weight, g		Density, g cm^{-3}		Color
	Pretest	Posttest	Pretest	Posttest	Pretest	Posttest	Pretest	Posttest	
Sample 1	0.0683	0.0681	- -*	1.2260	0.2751	0.2734	3.35	3.62	Turned slightly gray in center section
Sample 2	0.0676	0.0711	- -*	1.2179	0.2758	0.2722	3.35	3.59	Center turned darker gray than Sample 1. Tungsten coating deteriorating.

*Too fragile to risk measurement

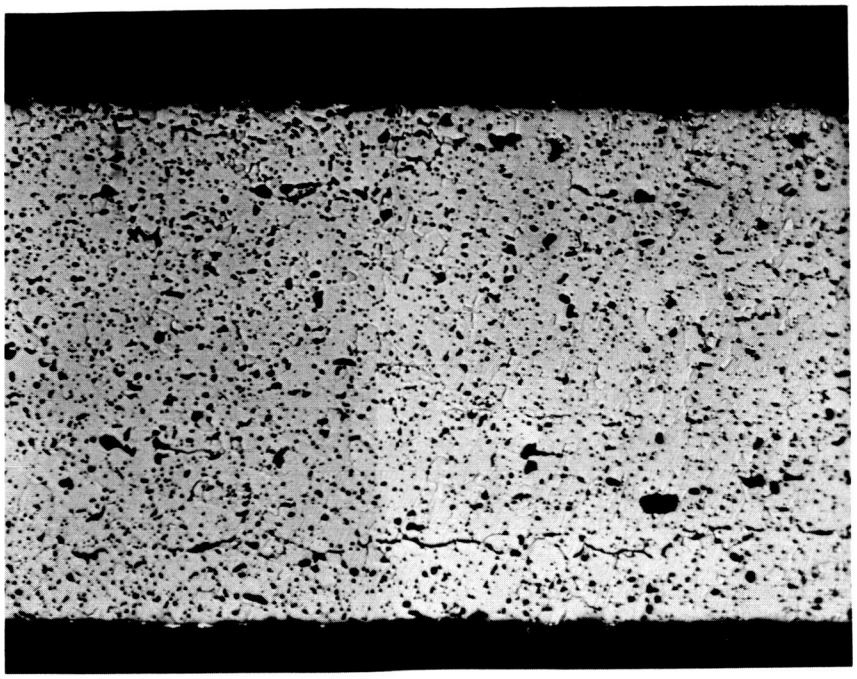

100X 2G274

FIGURE 39. POSTMEASUREMENT MICROSTRUCTURE OF Al_2O_3, SAMPLE 1, LONGITUDINAL SECTION (AS-POLISHED)

100X 2G275

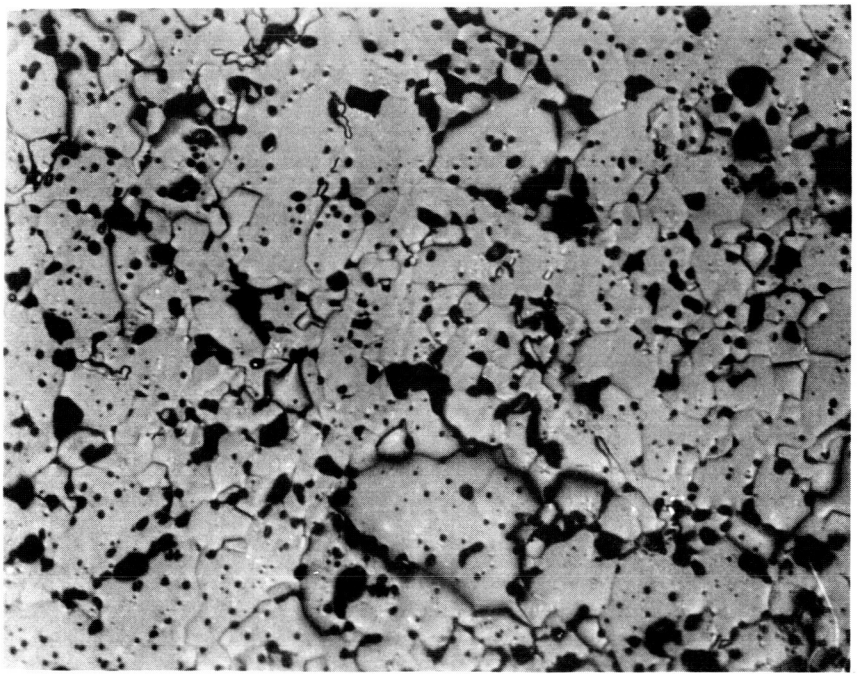

250X 2G276

FIGURE 40. POSTMEASUREMENT MICROSTRUCTURE OF Al_2O_3, SAMPLE 1, TRANSVERSE SECTION (AS-POLISHED)

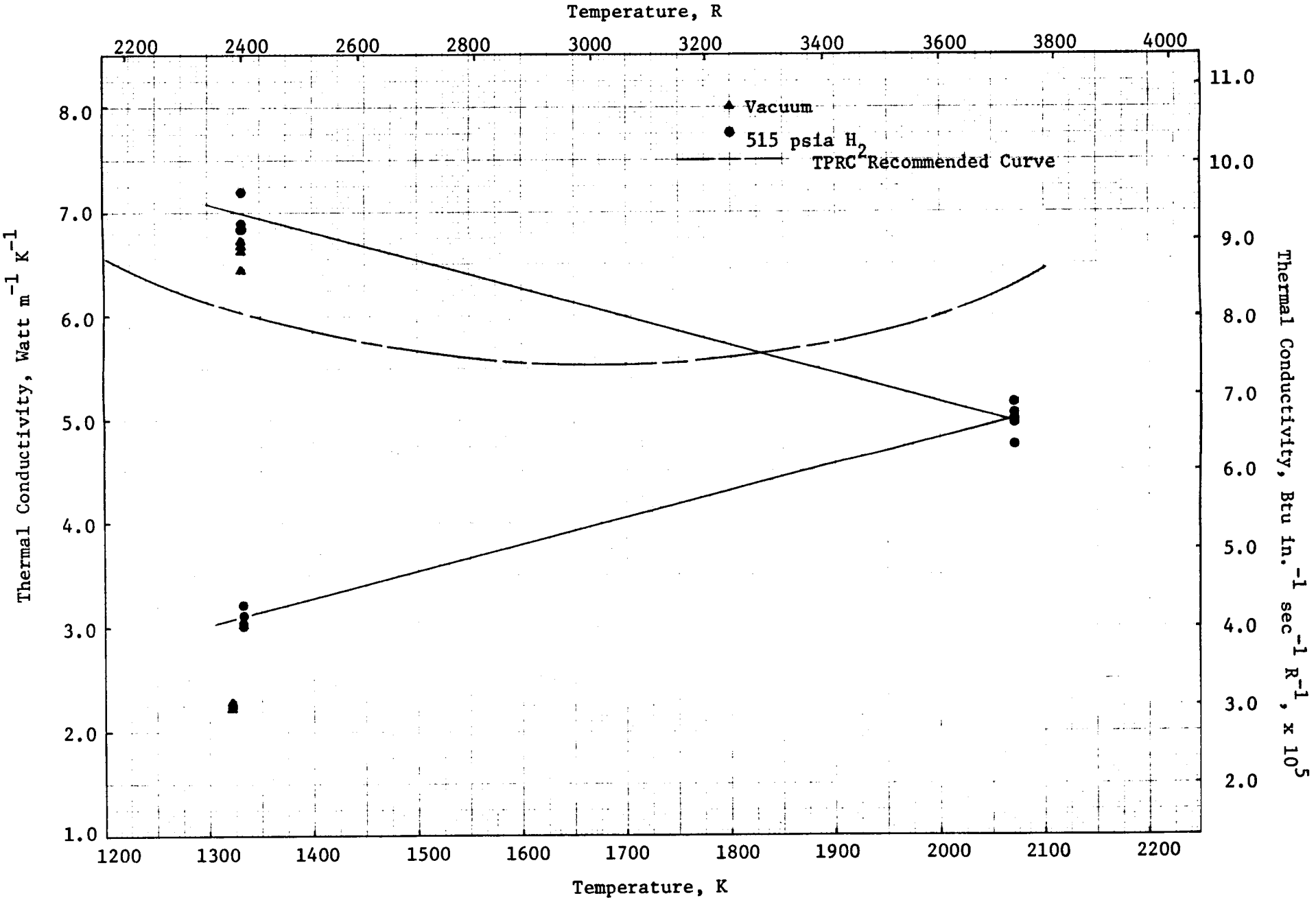

FIGURE 41. THERMAL CONDUCTIVITY OF PLASMA-SPRAYED Al_2O_3, SAMPLE 2

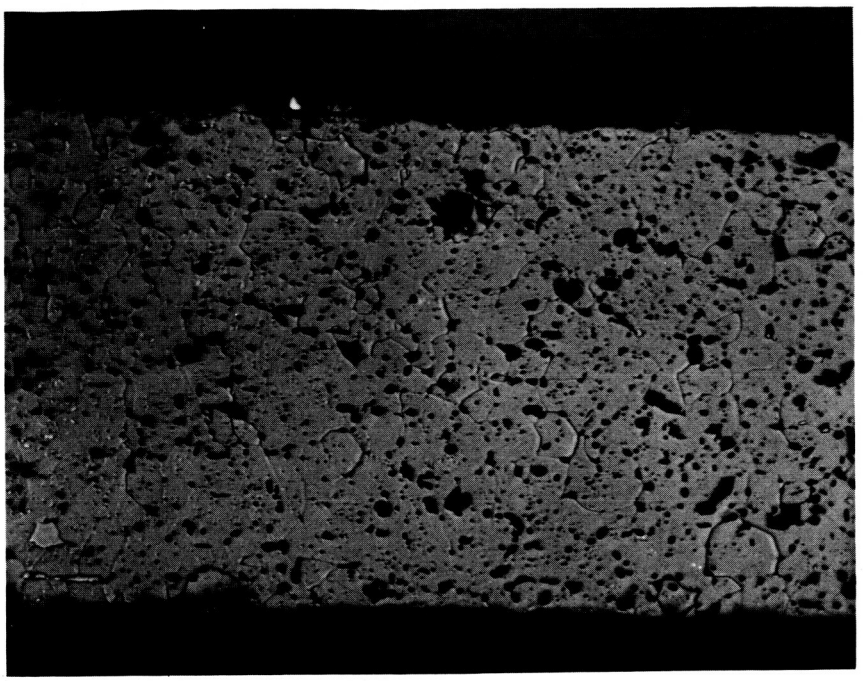

100X LONGITUDINAL SECTION 2G277

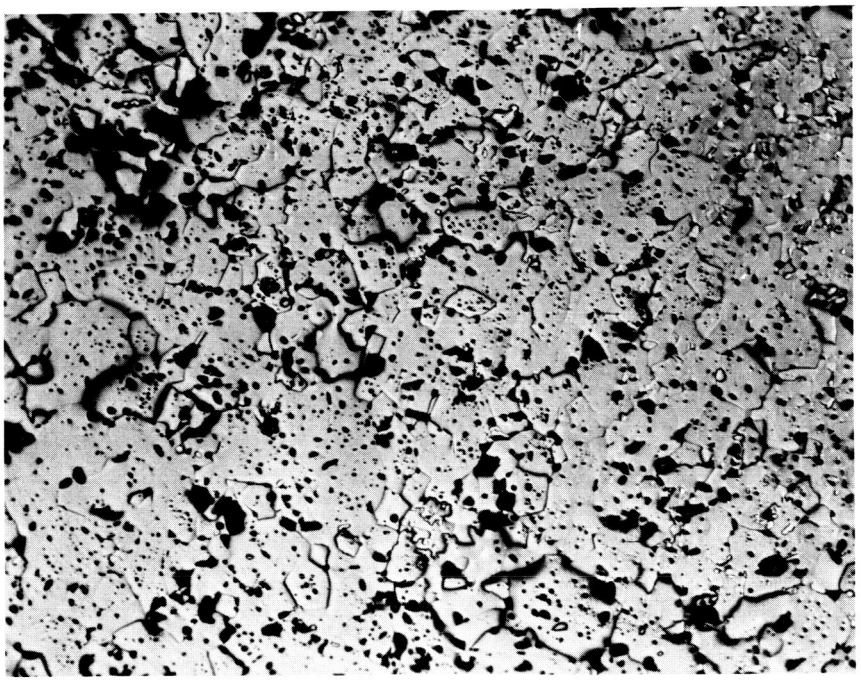

100X TRANSVERSE SECTION 2G278

FIGURE 42. POSTMEASUREMENT MICROSTRUCTURE OF Al_2O_3, SAMPLE 2, (AS-POLISHED)

The results of specific heat measurements on plasma-sprayed Al_2O_3 are shown in Figure 43. Between 373 and 1200 K, the present data are within about 1 to 1.5 percent of the data given by Furakawa et al for 99.98 percent pure Al_2O_3[11]. Also, between 1300 and 2000 K, the present data are within 1 to 1.5 percent of the data of Prophet and Stull.[12]

Linear thermal expansion measurements were made on one specimen of plasma-sprayed Al_2O_3 from room temperature to 2073 K. The measurements were made over several thermal cycles in an effort to determine the effects of time at temperature on the expansion characteristics of plasma-sprayed alumina. The results of these measurements are given in Table 9, where the data are given in chronological order. The results are also shown graphically in Figure 44, where for clarity, the individual data points have been omitted.

Upon initial heat-up, measurements were made at a number of temperatures with care being taken to insure that the specimen was not changing in length before proceeding to a higher temperature. No shrinkage was noted until the specimen was heated to the neighborhood of 1473 K. The sample was held at this temperature for approximately four hours during which time the specimen shrank continuously but at a decreasing rate. The specimen was then cooled and removed from the furnace. Visual inspection indicated no reaction between the specimen and its molybdenum holder. However, the color of the specimen had changed from white to light gray, probably due to a change in stoichiometry. Additional length measurements at room temperature confirmed the irreversible change in length. The specimen was then reinstalled in the apparatus and measurements were continued. The sample was held at higher temperature for various lengths of time during which further shrinkage was observed. During the hold at 1988 K, the windows of the apparatus became coated with a thin metallic film. The coating was removable with NaOH, but not with HNO_3, leading to a tentative identification as aluminum. Following cleaning of the windows, the specimen was heated to 2073 K. During a one hour hold at this temperature, the specimen shrank somewhat discontinuously. The discontinuities of shrinkage were accompanied by deposition of a metallic film, probably aluminum, on the windows of the apparatus.

The shrinkage at the lower temperatures is probably due to sintering since erosion of the sample ends due to reaction with the holders was not noted. At the higher temperatures, the shrinkage is probably due partly to sintering, but may also be due to loss of material, especially at the points of discontinuous shrinkage. The entire heating sequence caused a weight loss of about 5.4 percent.

HfO_2

HfO_2 was considered to be a possible alternative to ZrO_2 in the coating systems. A chemical analysis of the as-sprayed material is given in Table 10. Photomicrographs of the as-sprayed material are shown in Figures 45 and 46. In the photomicrographs, many of the large dark areas are not pores but are a second phase, or possibly regions of different composition or stoichiometry.

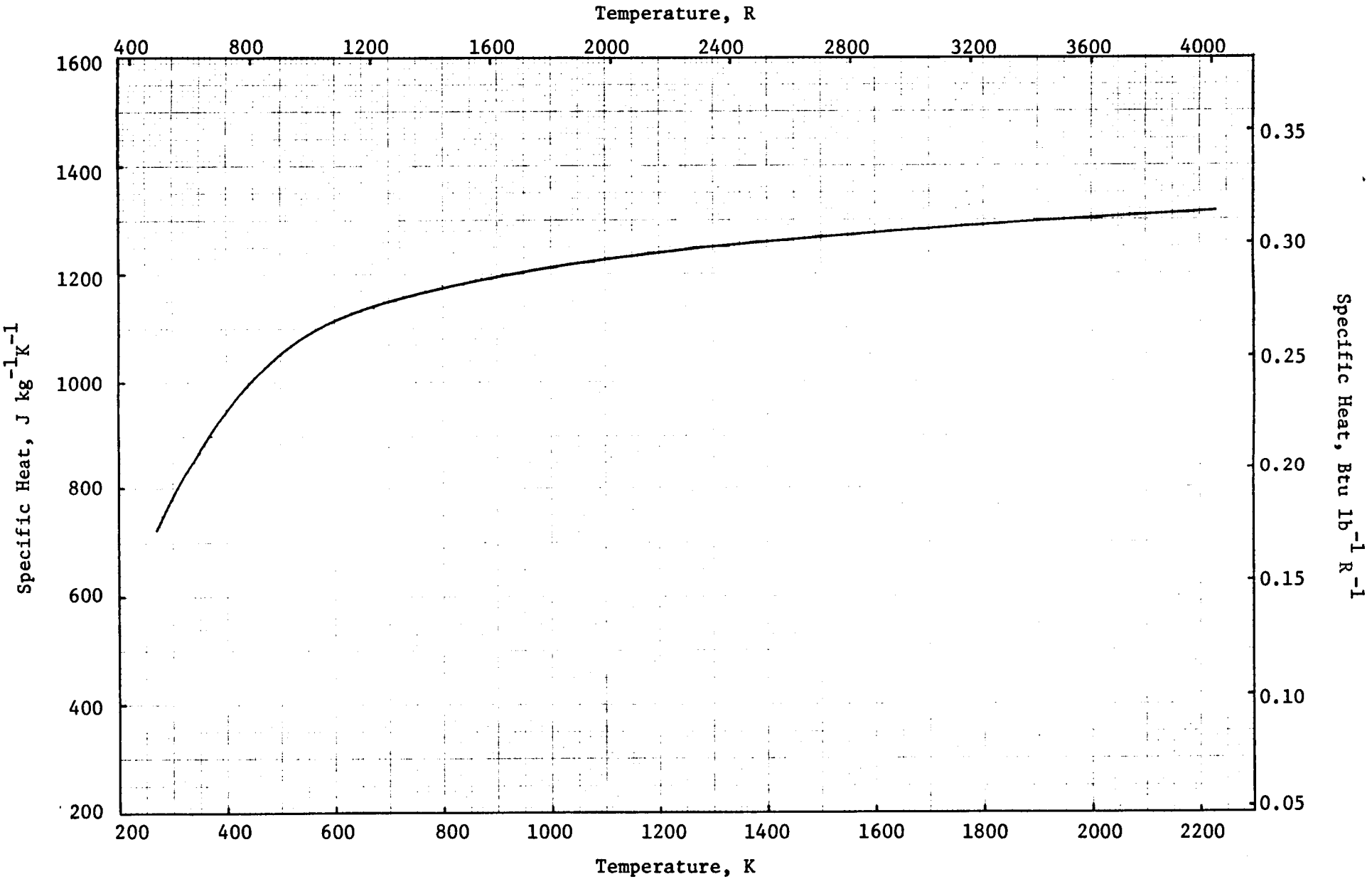

FIGURE 43. SPECIFIC HEAT OF PLASMA-SPRAYED Al_2O_3

TABLE 9. LINEAR THERMAL EXPANSION OF PLASMA-SPRAYED Al_2O_3

Temperature, K	Expansion,* percent	Time at Temperature, minutes	Temperature, K	Expansion,* percent	Time at Temperature, minutes
293	0	--	1483	0.228	200
459	0.091	--		0.218	205
632	0.206	--		0.207	210
741	0.283	--		0.200	215
859	0.368	--		0.190	220
967	0.463	--	1483	0.183	225
293	0	--		0.172	230
540	0.135	--		0.147	235
1055	0.542	0	1119	-0.209	--
1052	0.542	20	664	-0.593	--
1135	0.612	0	293	-0.840	--
1135	0.614	25	857	-0.426	--
1228	0.705	0	1327	-0.014	--
1227	0.705	25	1600	0.187	0
1369	0.797	0	1606	0.112	5
1369	0.796	25	1617	0.085	15
1481	0.971	0	1618	0.097	20
1483	0.957	20	1619	0.097	25
	0.885	35	1621	0.103	30
	0.866	50	1621	0.101	35
1483	0.722	65	1622	0.097	45
	0.710	70	1624	0.096	50
	0.693	75	1711	0.136	0
	0.671	80		0.109	5
	0.642	85		0.097	10
1483	0.611	90		0.077	15
	0.546	105		0.063	20
	0.524	110		0.041	25
	0.504	115		0.029	30
	0.483	120		0.014	35
1483	0.466	125	1711	0.006	40
	0.445	130		0	45
	0.429	135		-0.013	50
	0.410	140		-0.013	55
	0.394	145		-0.019	60
1483	0.377	150		-0.025	65
	0.349	155		-0.032	70
	0.335	160		-0.037	75
	0.315	165		-0.043	80
	0.305	170		-0.047	85
1483	0.289	175		-0.053	90
	0.276	180		-0.058	95
	0.266	185		-0.061	100
	0.252	190		-0.059	105
	0.240	195		-0.057	110

TABLE 9 (continued)

Temperature, K	Expansion,* percent	Time at Temperature, minutes	Temperature, K	Expansion,* percent	Time at Temperature, minutes
1711	-0.056	115	1868	-0.984	185
1853	-0.015	0		-1.003	200
	-0.083	5		-1.019	215
	-0.126	10		-1.035	230
	-0.177	15		-1.039	245
1853	-0.207	20	1988	-1.055	260
	-0.244	25		-1.022	0
	-0.262	30		-1.110	15
	-0.293	35		-1.143	30
	-0.316	40		-1.172	45
1853	-0.338	45	1988	-1.194	60
	-0.366	50		-1.207	75
	-0.383	55		-1.216	90
	-0.406	60		-1.219	105
	-0.422	65	293	-2.69	--
1853	-0.440	70	2073	-1.075	0
	-0.455	75		-1.088	5
	-0.469	80		-1.095	10
	-0.484	85		-1.098	15
	-0.497	90		-1.101	20
1853	-0.512	95	2073	-1.106	25
	-0.528	100		-1.115	30
	-0.541	105		-1.117	35
	-0.552	110		-1.127	40
	-0.567	115		-1.151	45
1853	-0.580	120	2073	-1.151	50
1347	-1.110	--		-1.156	55
902	-1.490	--		-1.170	60
293	-1.968	--	1848	-1.42	--
1122	-1.310	--	1728	-1.57	--
1353	-1.090	--	1543	-1.75	--
1868	-0.638	0	1448	-1.89	--
	-0.661	10	293	-2.842	--
	-0.696	20			
	-0.722	30			
1868	-0.758	40			
	-0.776	50			
	-0.820	65			
	-0.844	80			
	-0.871	95			
1868	-0.895	110			
	-0.912	125			
	-0.936	140			
	-0.953	155			
	-0.969	170			

*Figures are based on the initial length at room temperature.

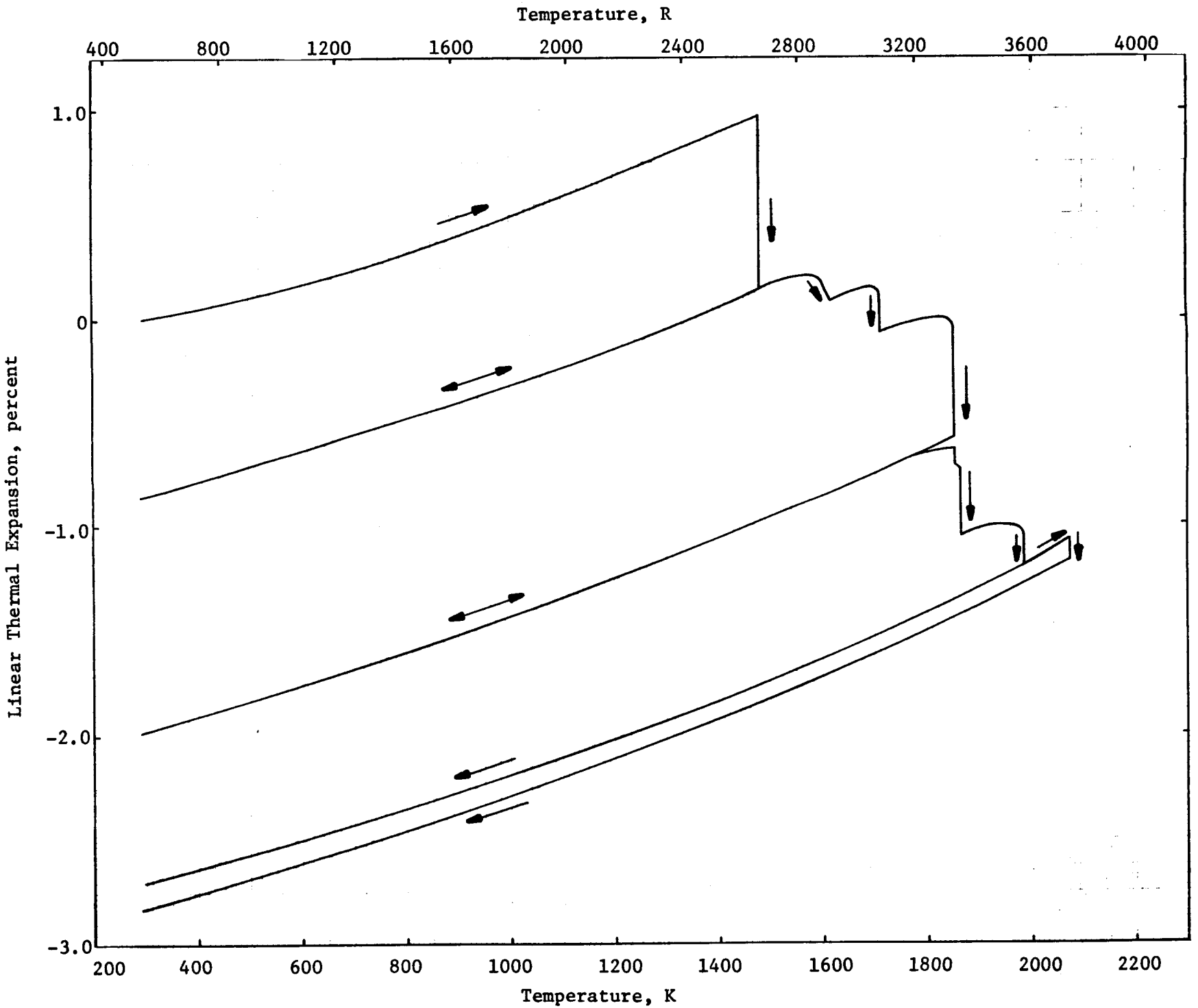

FIGURE 44. LINEAR THERMAL EXPANSION OF PLASMA-SPRAYED Al_2O_3

TABLE 10. CHEMICAL ANALYSES OF HfO_2 SAMPLES

Element	Weight percent	
	As-sprayed	Sample 1
Y_2O_3	4.35	4.6
Ba	0.002	
Si	0.07	0.01
Mn	0.03	
Fe	0.03	0.3
Mg	0.02	<0.005
Cr	0.02	
W	<0.01	
Al	0.1	0.1
Mo	0.001	
V	0.003	
Cu	0.001	
Ti	0.1	0.4
Ni	0.01	
Co	<0.001	
Ca	0.2	0.2
Zr		0.5

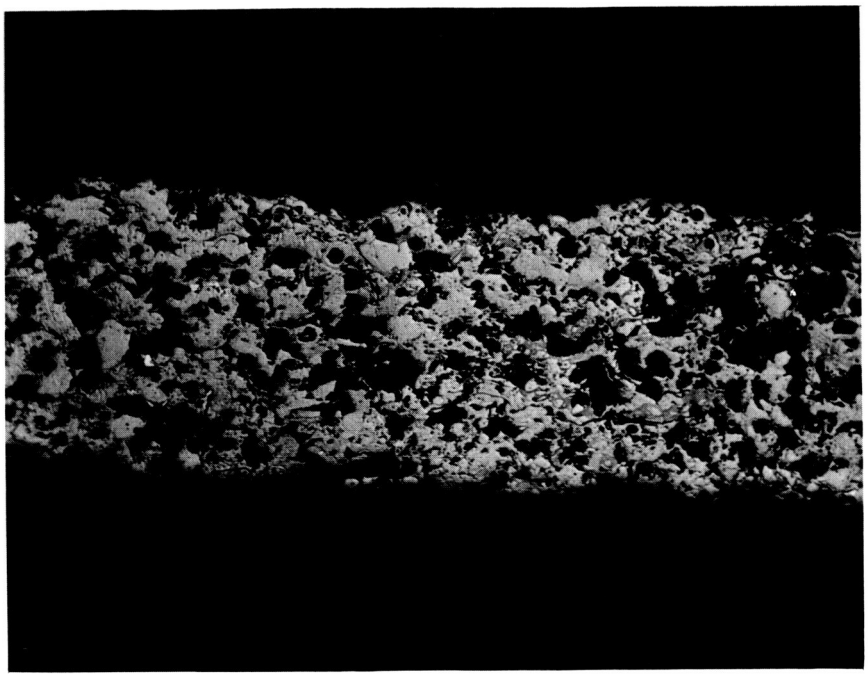

100X 2G280

FIGURE 45. MICROSTRUCTURE OF AS-SPRAYED HfO_2, LONGITUDINAL SECTION (AS-POLISHED)

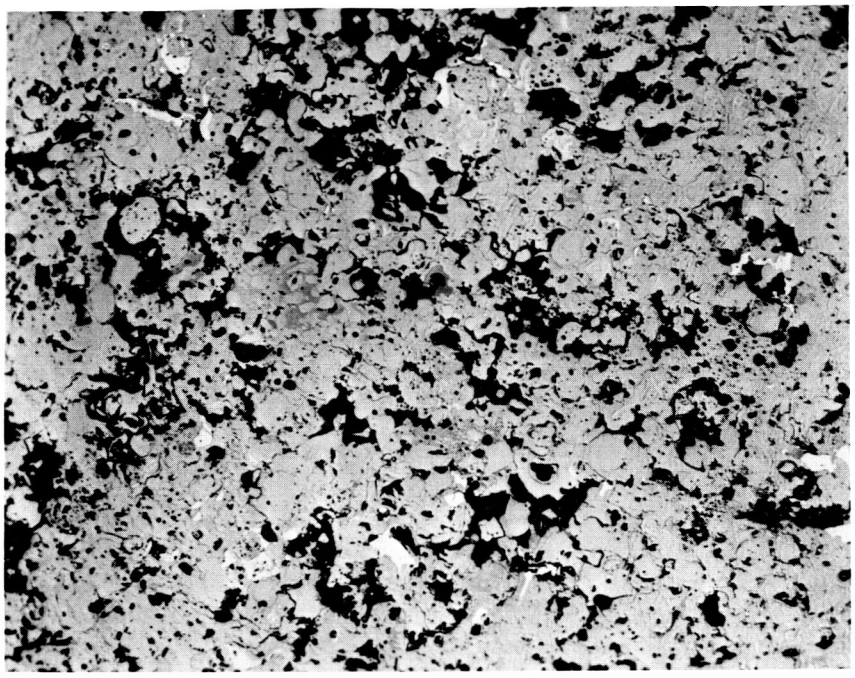

100X 2G282

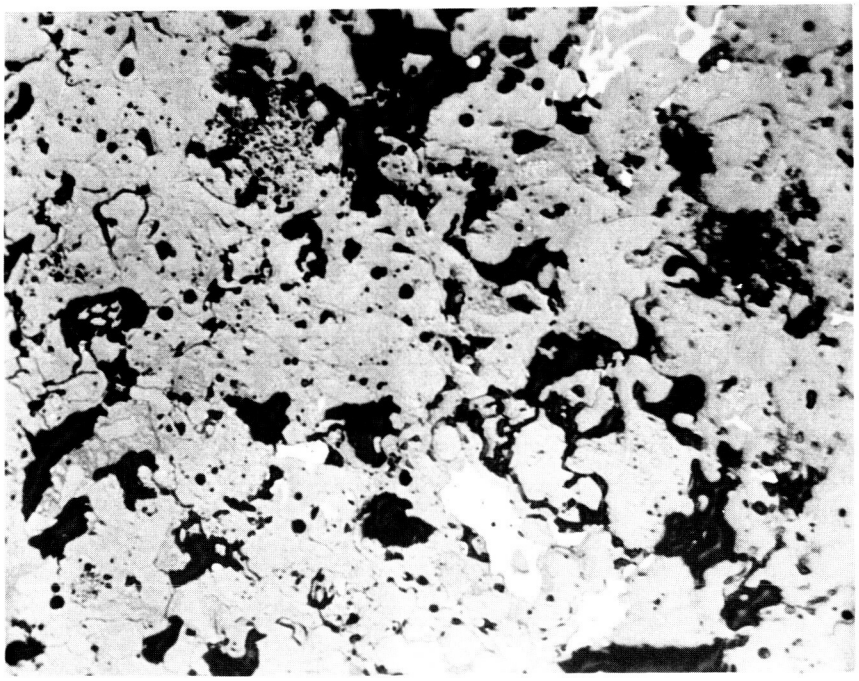

100X 2G281

FIGURE 46. MICROSTRUCTURE OF AS-SPRAYED HfO_2, TRANSVERSE SECTION (AS-POLISHED)

Thermal diffusivity measurements were performed on one specimen of HfO_2 under 515 psia hydrogen. The sample was held at elevated temperatures for periods of approximately one-half hour during which diffusivity measurements were made. The results of the measurements, shown in Figure 47, showed a general tendency to increase following each heat treatment. This is probably due to sintering as evidenced in the photomicrographs of this sample, shown in Figures 48 and 49. After the heat treatment near 2273 K, however, the low temperature conductivity is seen to be lowered. This may be due to an unstable behavior of the material other than sintering effects. Physical characteristics of this sample are given in Table 11.

TABLE 11. PHYSICAL CHARACTERISTICS OF HfO_2, SAMPLE 1

	Pretest	Posttest
Thickness, cm	0.0419	0.0406
Weight, g	0.3372	0.3246
Density, g cm^{-3}	6.80	7.45

The results of specific heat measurements on HfO_2 are given in Figure 50. The results are seen to be in fairly good agreement with those of previous investigations[6,13]. According to Brown and Mazdiyasni[14], the Y_2O_3 content of approximately 4 mole percent may not be sufficient to fully stabilize HfO_2. The anomalous behavior of the specific heat is thus probably related to the monoclinic-to-tetragonal phase transformation. X-ray diffraction work performed at NASA Lewis has confirmed that the material is not fully stabilized in the cubic structure.

Thermal Conductivity Phase II

The materials studied in this phase were those which would be used to form intermediate layers between the cooled substrate and the outer layer. These materials are plasma-sprayed molybdenum, mixtures of molybdenum with Al_2O_3 and CaO-stabilized ZrO_2, and nichrome and NiAl.

Molybdenum

Molybdenum specimens were prepared from Metco No. 63 powder. Chemical analyses are given in Table 12. Photomicrographs of the as-sprayed specimen

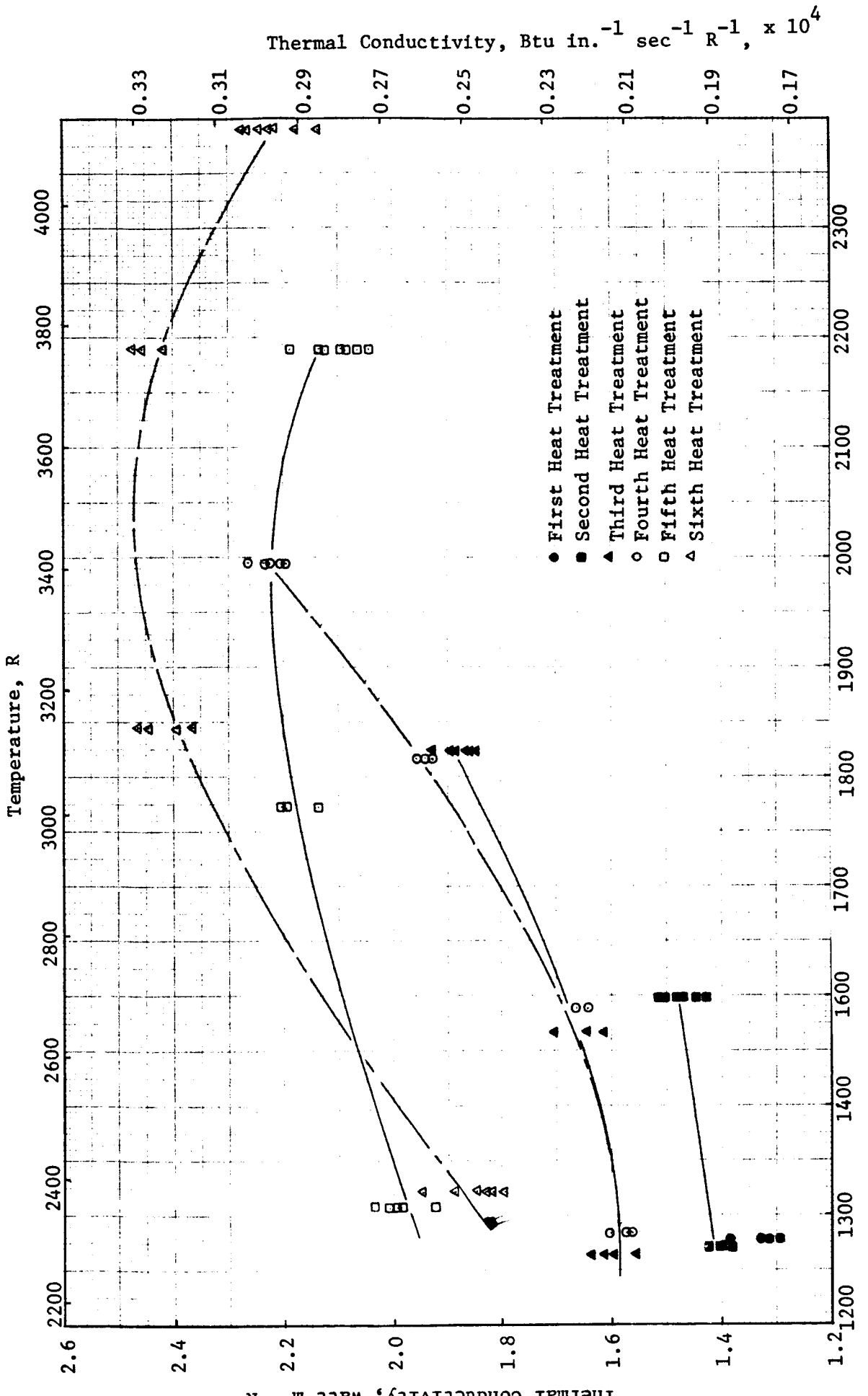

FIGURE 47. THERMAL CONDUCTIVITY OF HfO_2 IN 515 PSIA HYDROGEN

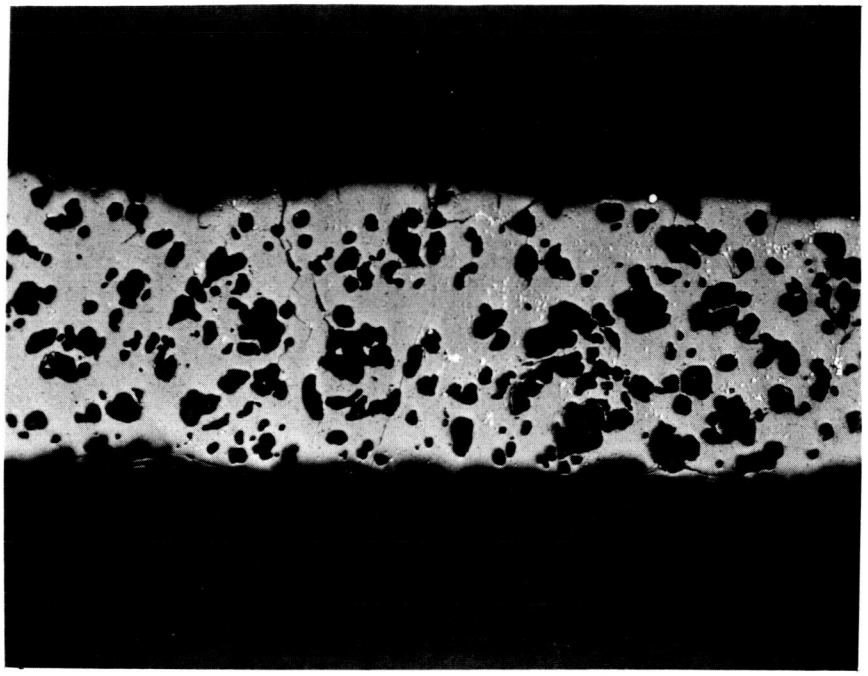

100X 2G283

FIGURE 48. POSTMEASUREMENT MICROSTRUCTURE OF HfO_2, SAMPLE 1, LONGITUDINAL SECTION (AS-POLISHED)

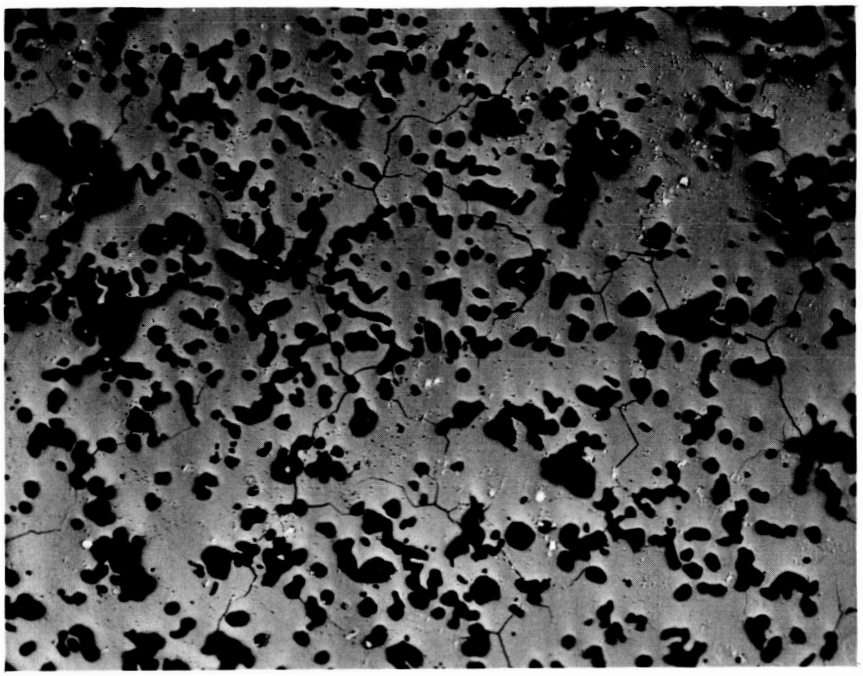

100X 2G285

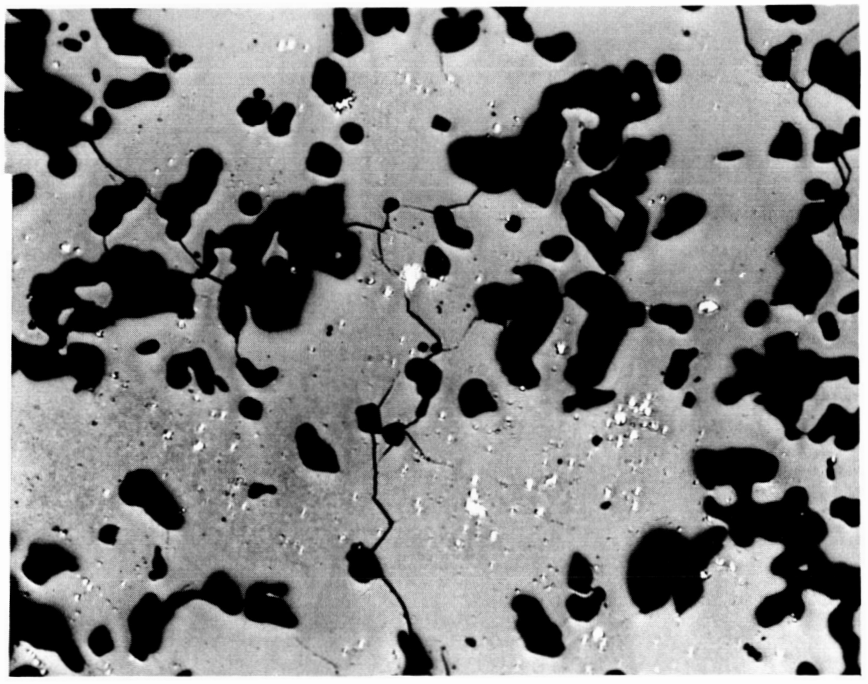

100X 2G284

FIGURE 49. POSTMEASUREMENT MICROSTRUCTURE OF HfO_2, SAMPLE 1, TRANSVERSE SECTION (AS--POLISHED)

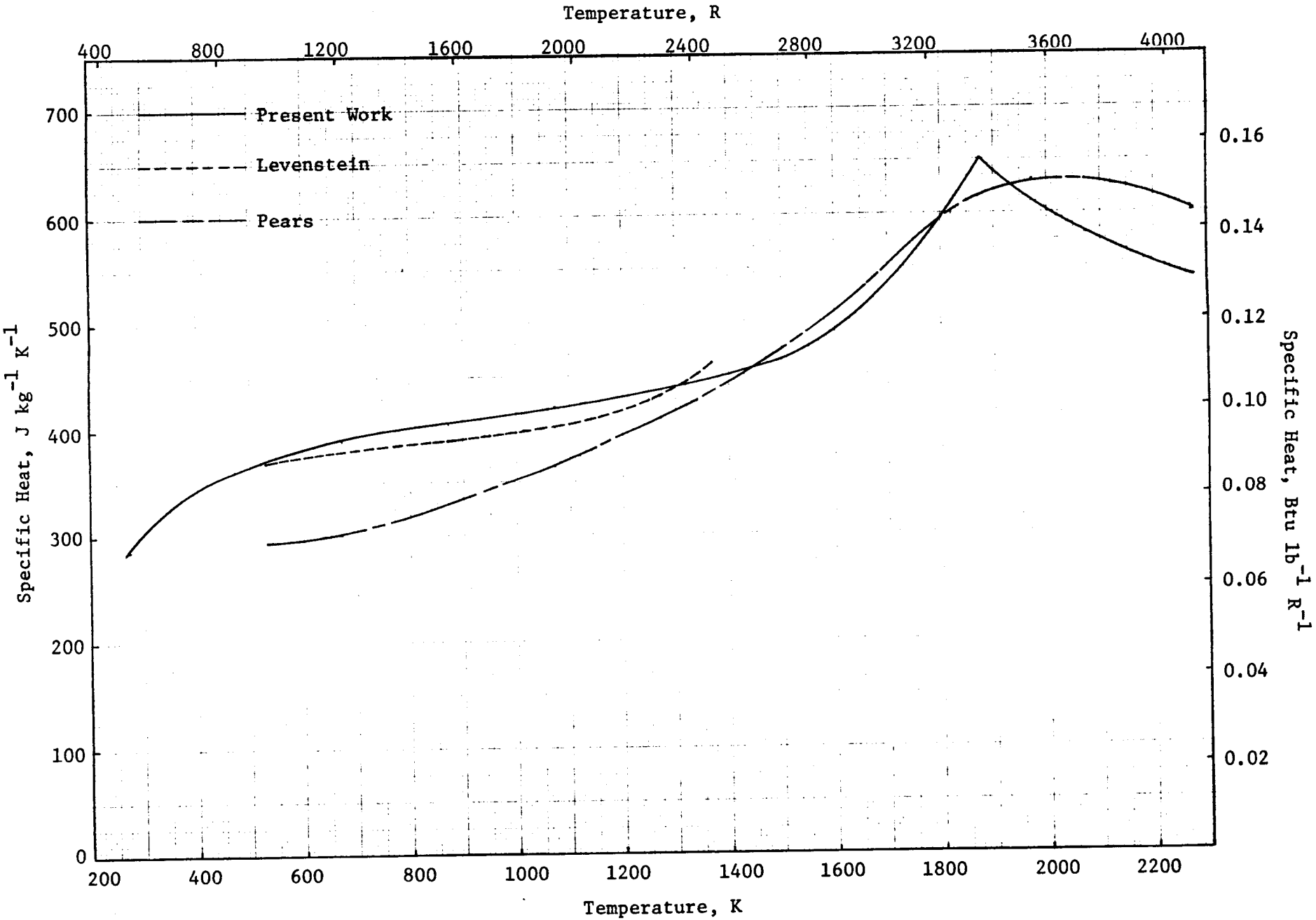

FIGURE 50. SPECIFIC HEAT OF PLASMA-SPRAYED Y_2O_3-STABILIZED HfO_2

are shown in Figures 51 and 52. Physical characteristics of the diffusivity specimens are given in Table 13.

TABLE 12. CHEMICAL ANALYSES OF Mo SAMPLES

	Weight percent	
Element	As-sprayed	Sample 1
Fe	0.01	0.01
Si	<0.001	<0.001
Ni	0.01	0.01
Ti	<0.001	<0.001
O	2.83	

The first set of measurements on Sample 1 was made in the low-pressure apparatus, with the atmosphere being alternated between vacuum and helium at atmospheric pressure. The results of these measurements are shown in Figure 53, and represent two heating cycles between about 473 and 1073 K. As noted from this figure, the conductivity in vacuum is essentially the same as that in helium. Also, it is seen that the conductivity during the second heating cycle is significantly higher than during the initial heating.

Following these measurements, the specimen was transferred to the high-pressure hydrogen furnace. At the initiation of measurements in hydrogen, condensation of a liquid on the upper window of the furnace chamber was observed when the specimen was at about 1173 K. Following this treatment, it was found that the specimen had incurred a weight loss of about 2.89 percent. This weight loss is very close to the oxygen content of the as-sprayed sample. According to Shunk[15], the solid solubility of oxygen in Mo at 1922 K is about 0.003 w/o, and would be expected to be even less at lower temperatures. The oxygen is thus assumed to be present as MoO_2, since MoO_3 is more volatile. The reaction of the oxide with the hydrogen environment would probably not be deleterious to nozzle coating performances unless the water vapor formed by the reaction could not escape.

Following this initial heat treatment in hydrogen, diffusivity measurements were made in hydrogen at pressures ranging from 315 to 515 psia and in the temperature range 1273 to 2273 K. The sample was held at elevated temperatures for periods of approximately one-half hour during which thermal diffusivity measurements were made. After each heat treatment, measurements were made at lower temperatures in order to observe the effects of the heat treatment. The results of these measurements are given in Figure 54.

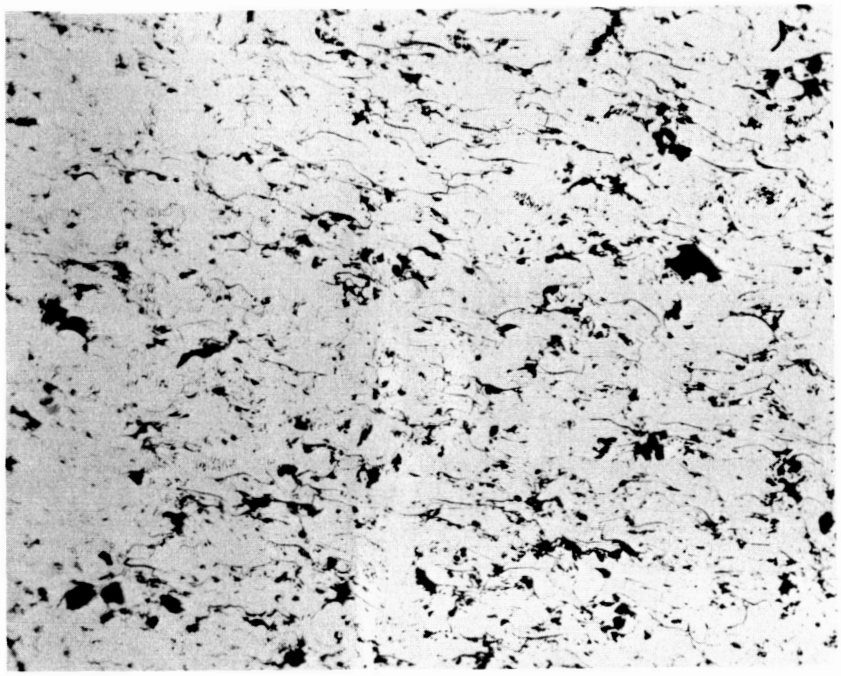

100X 2G319

FIGURE 51. MICROSTRUCTURE OF AS-SPRAYED MOLYBDENUM, LONGITUDINAL SECTION (AS-POLISHED)

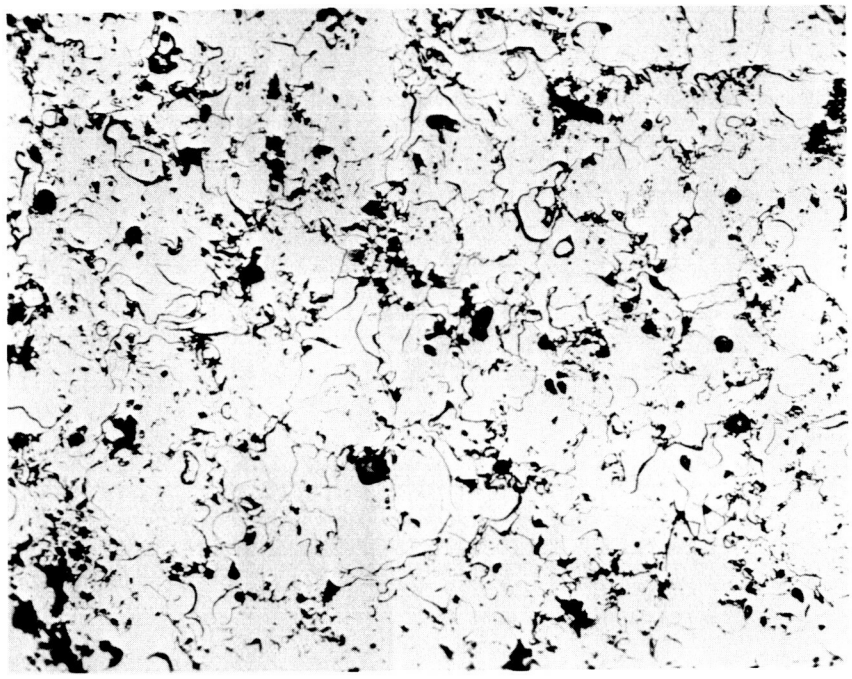

100X 2G320

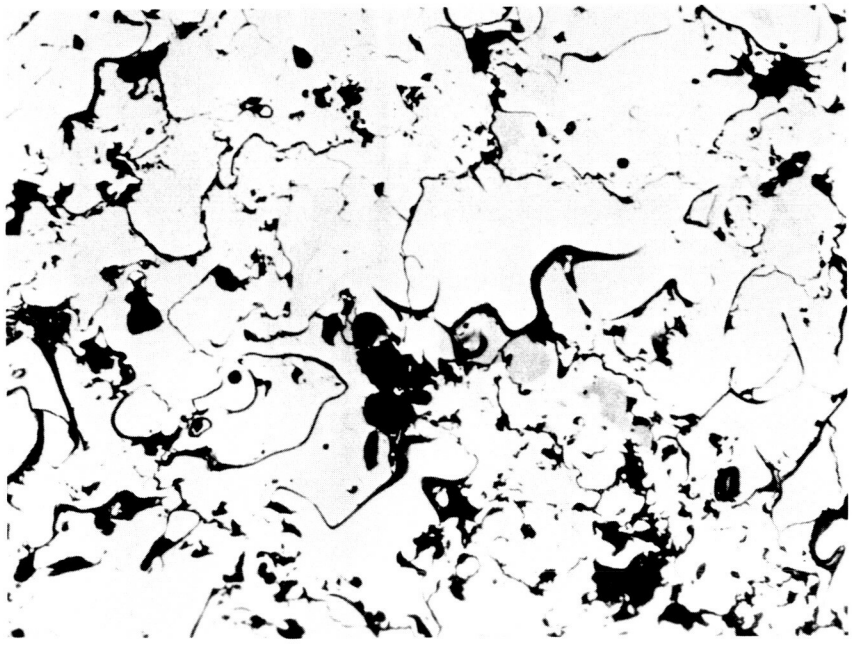

250X 2G321

FIGURE 52. MICROSTRUCTURE OF AS-SPRAYED MOLYBDENUM, TRANSVERSE SECTION (AS-POLISHED)

TABLE 13. PHYSICAL CHARACTERISTICS OF PLASMA-SPRAYED MOLYBDENUM SAMPLES

	Thickness, cm	Diameter, cm	Weight, g	Density, g cm^{-3}
Sample 1:				
Pretest	0.3269	1.2692	3.1487	7.71
After first heating in vacuum and He	0.3294	1.2715	3.1451	- -
After second heating in vacuum and He	0.3287	1.2697	3.1451	- -
After second heat treatment in H_2	0.3231	1.2476	3.0540	~7.86
After sixth heat treatment in H_2	0.3160	1.2194	3.0536	8.40
Sample 2:				
Pretest	0.2789	1.2667	2.7042	7.73
After first heat treatment in H_2	0.2766	1.2548	2.6238	7.78
After second heat treatment in H_2	0.2746	1.2517	2.6231	7.89
Posttest	0.2748	1.2507	2.6233	7.90

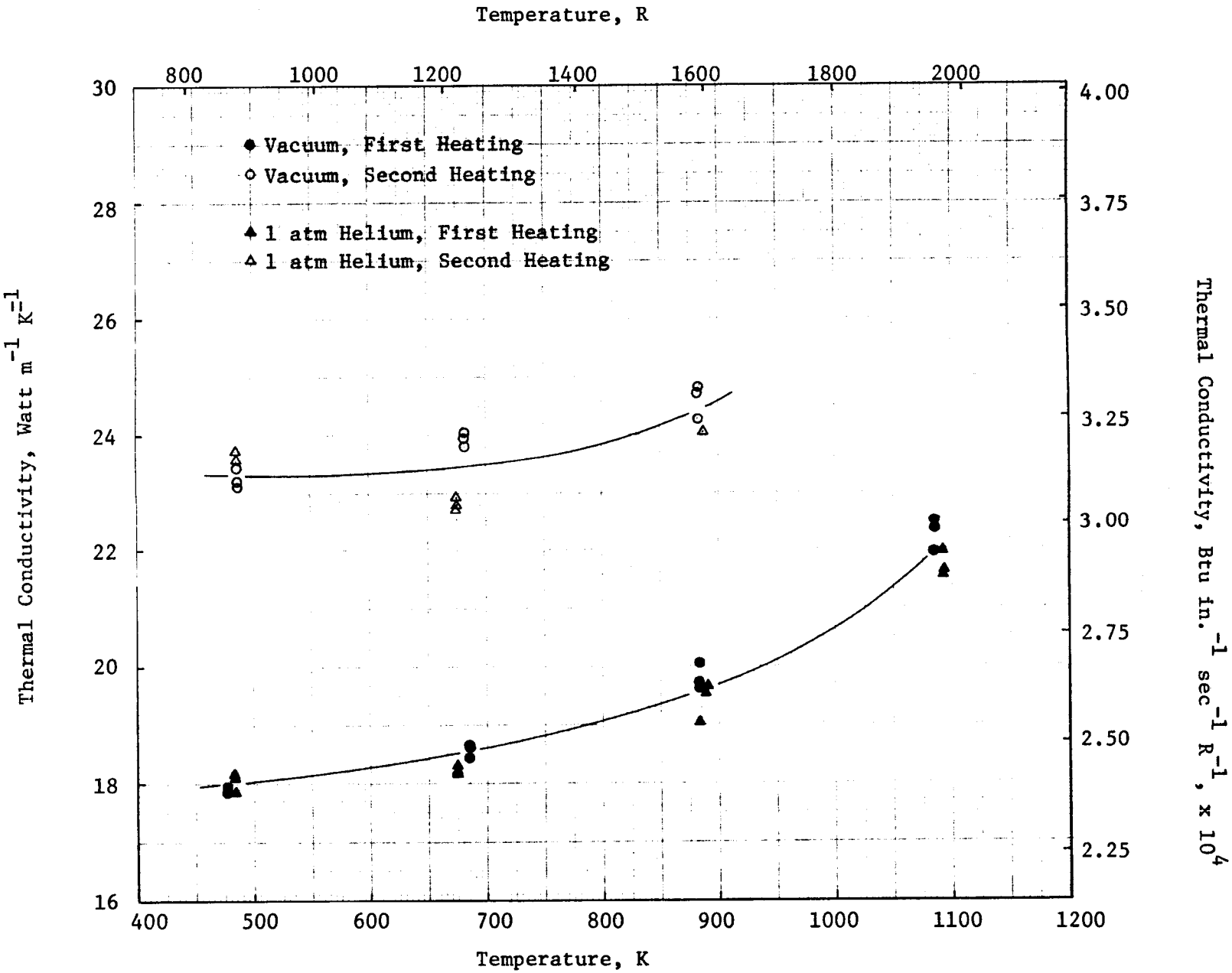

FIGURE 53. THERMAL CONDUCTIVITY OF PLASMA-SPRAYED MOLYBDENUM, SAMPLE 1

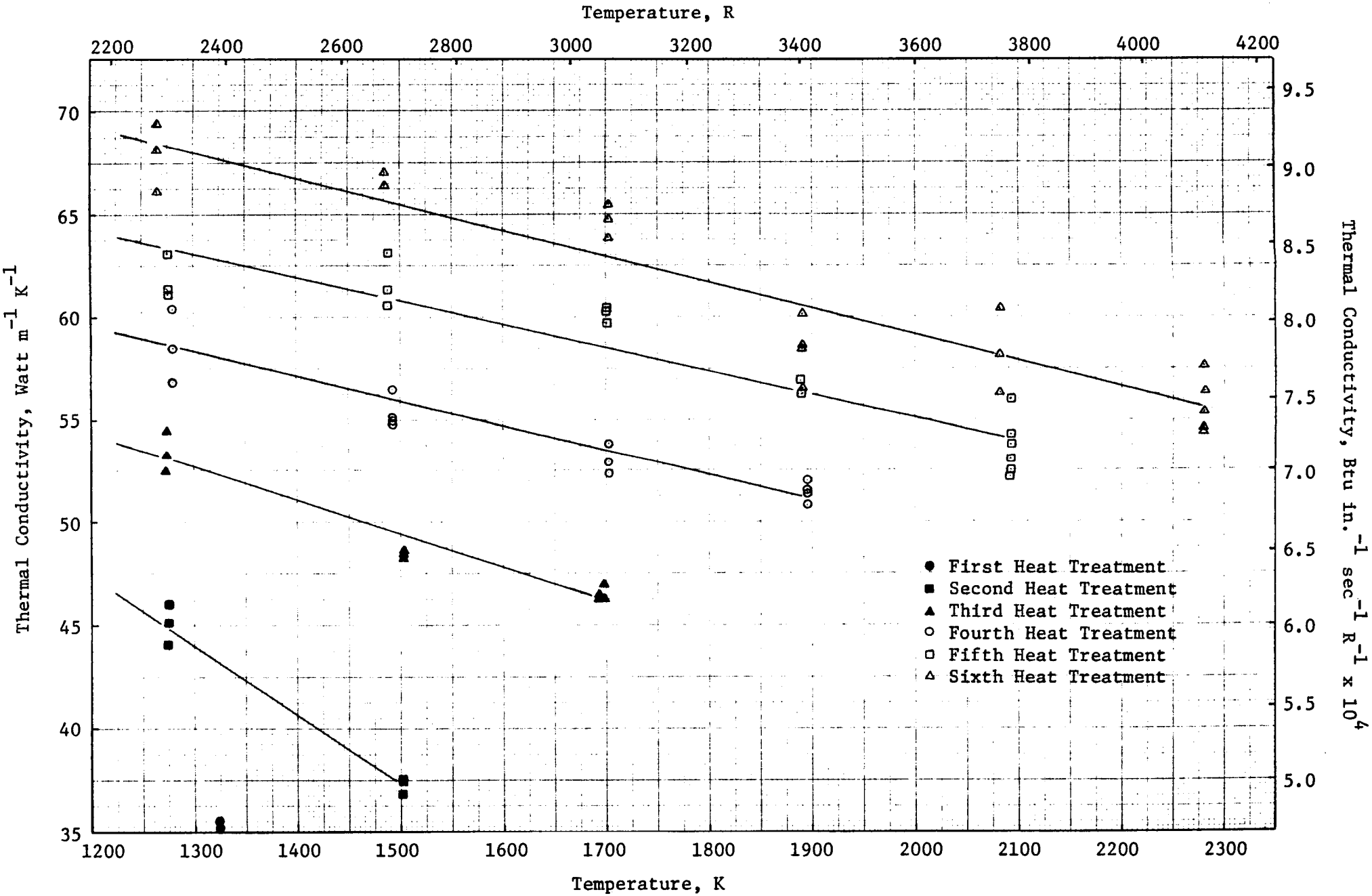

FIGURE 54. THERMAL CONDUCTIVITY OF PLASMA-SPRAYED MOLYBDENUM IN HIGH PRESSURE HYDROGEN

As noted on previous specimens, the general trend in the conductivity is an increase following each heat treatment. The microstructure of this sample, shown in Figures 55 and 56 shows that most of the fine hairline porosity has disappeared, which probably accounts for the increase in conductivity. The conductivity values after the final heat treatment are approximately 32 to 35 percent lower than the TPRC-recommended curve for 99.95 percent pure molybdenum[16]. A correction for porosity using the Maxwell-Eucken relation brings the values within 10 to 15 percent below the recommended curve.

Diffusivity measurements were made on Sample 2 in order to observe the low temperature conductivity after heat treatment at a moderate temperature. The sample was first heat treated near 1250 K in 515 psia hydrogen for about 30 minutes. Following this heat treatment, the thickness was found to be shrunken by 0.87 percent and the weight was decreased by about 2.97 percent. These effects are presumably due to reduction of molybdenum oxides. Further heat treatment in hydrogen resulted in negligible weight changes.

The specimen was then reheated in hydrogen and diffusivity measurements were made up to 1373 K. The specimen was then installed in the low temperature furnace and a series of measurements was made in helium at 29 psia. The results of these measurements are given in Figure 57.

Specific heat measurements were made on plasma-sprayed molybdenum samples in both the as-sprayed and the hydrogen-heat treated conditions. The results of these measurements are shown in Figure 58. As noted above, samples of as-sprayed Mo were found to contain about 2.8 to 2.9 w/o oxygen. The second specific heat sample was heat treated for about 20 minutes near 1273 K in hydrogen at 515 psia. Condensation of moisture on the top furnace window appeared almost immediately. Following this treatment, the sample was found to be reduced in weight by about 3.1 percent. Since the solid solubility of oxygen in Mo is very low, this oxygen is presumably present as an oxide. If the oxide is present as MoO_2, then the oxide content of the as-sprayed sample is about 12.4 w/o. Since the specific heat of MoO_2 is roughly twice as great as that of Mo, the presence of this amount of oxide could acoount for a substantial part of the difference between the two sets of data. The Mo data of Taylor and Finch[17] are also shown in Figure 58. (The reported accuracy of this data is ±4 percent.) Taylor and Finch's data are seen to be in good agreement with the present data for plasma-sprayed Mo following heat treatment in hydrogen. The data of Kirillin, et al[18] (reported to be accurate to ±1.2 percent) are almost identical with the present data over the temperature range 973 to 2273 K, and are thus not shown on the graph.

The results of linear thermal expansion measurements are given in Figure 59 and Table 14. The results are given in chronological order in the table. The sample was held at a number of elevated temperatures for long periods of time, during which steady shrinkage was observed. The final shrinkage at room temperature was found to be 2.351 percent.

Mo-Oxide Mixtures

Thermal diffusivity and specific heat measurements were performed on specimens of nominal compositions 75 w/o Mo-25 w/o ZrO_2, 25 w/o Mo-75 w/o ZrO_2,

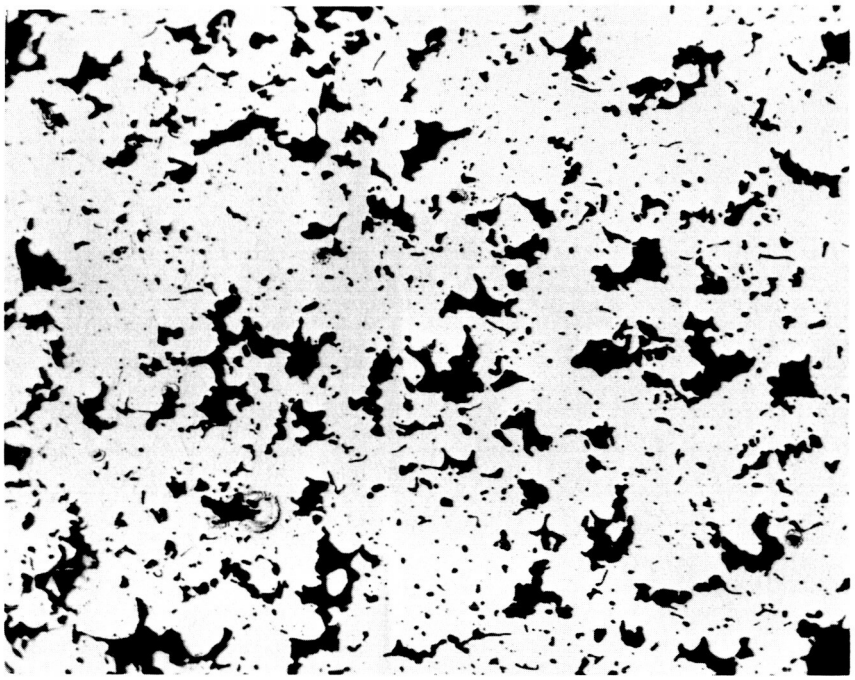

100X 2G328

FIGURE 55. POSTMEASUREMENT MICROSTRUCTURE OF MOLYBDENUM, SAMPLE 1, LONGITUDINAL SECTION (AS-POLISHED)

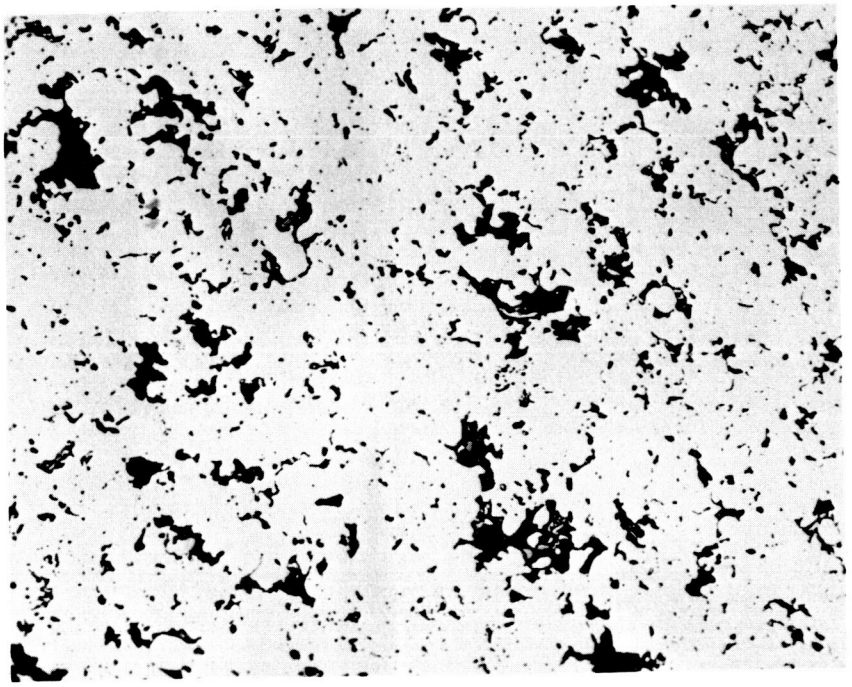

100X 2G330

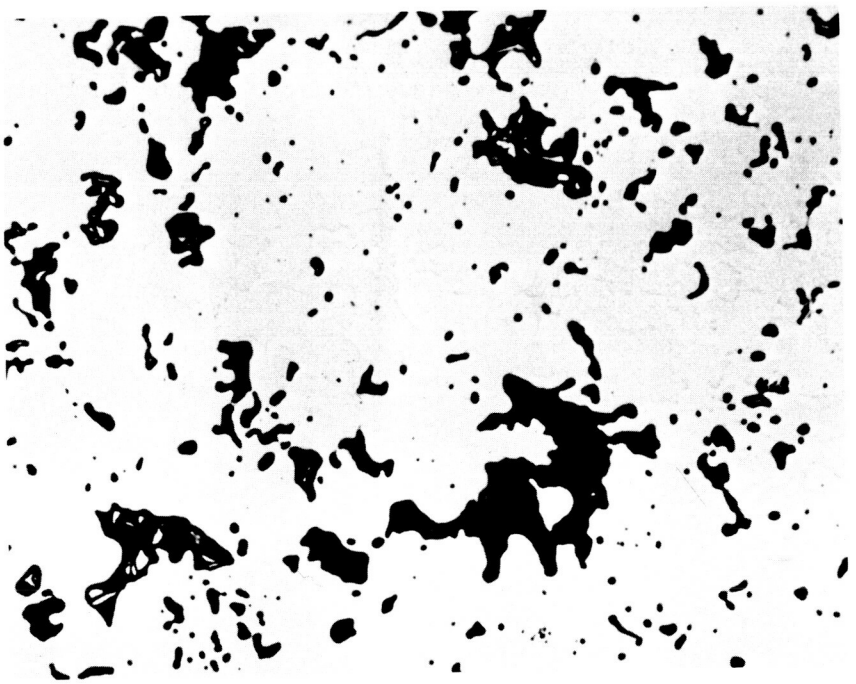

250X 2G329

FIGURE 56. POSTMEASUREMENT MICROSTRUCTURE OF MOLYBDENUM, SAMPLE 1, TRANSVERSE SECTION (AS-POLISHED)

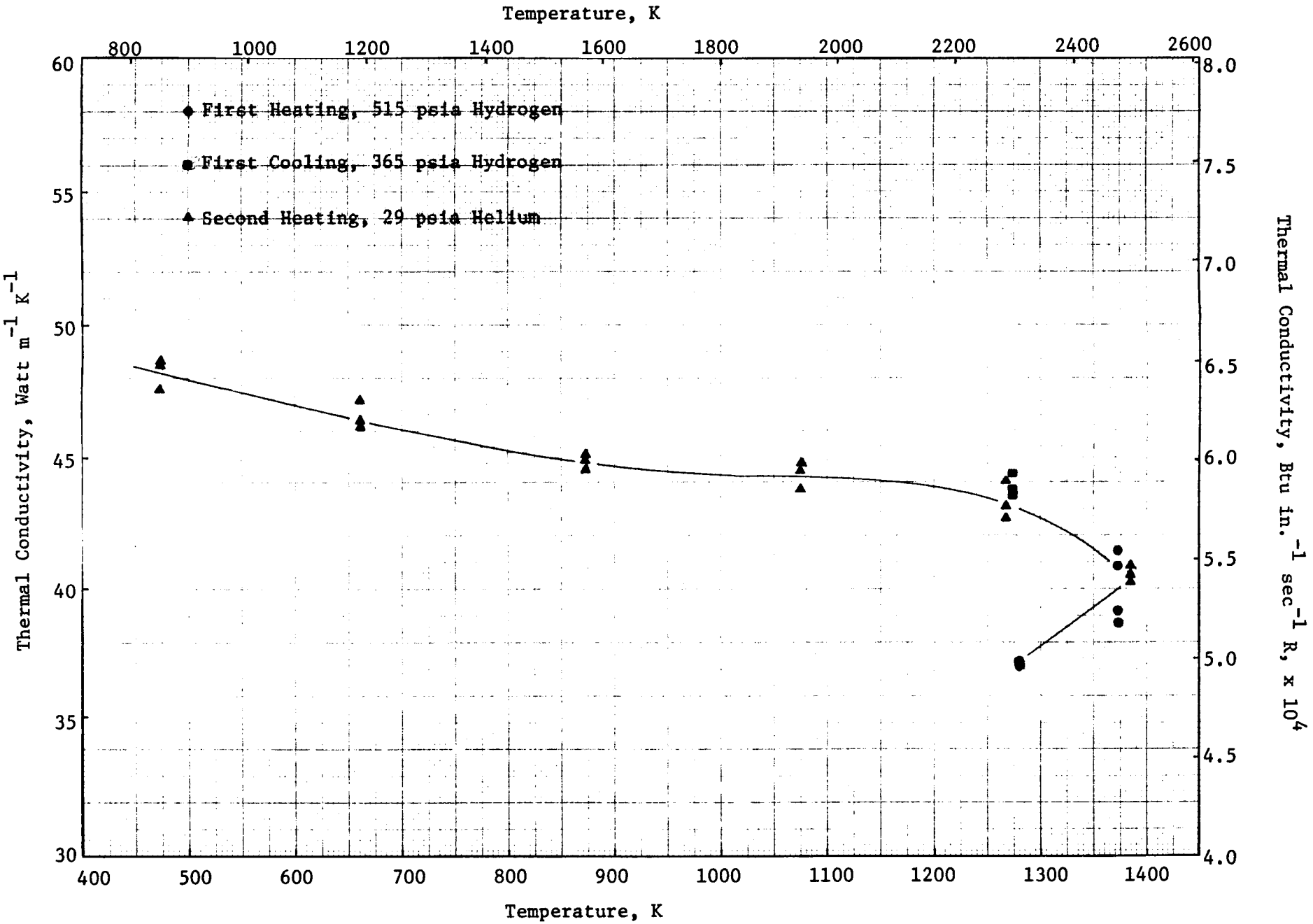

FIGURE 57. THERMAL CONDUCTIVITY OF PLASMA-SPRAYED MOLYBDENUM, SAMPLE 2

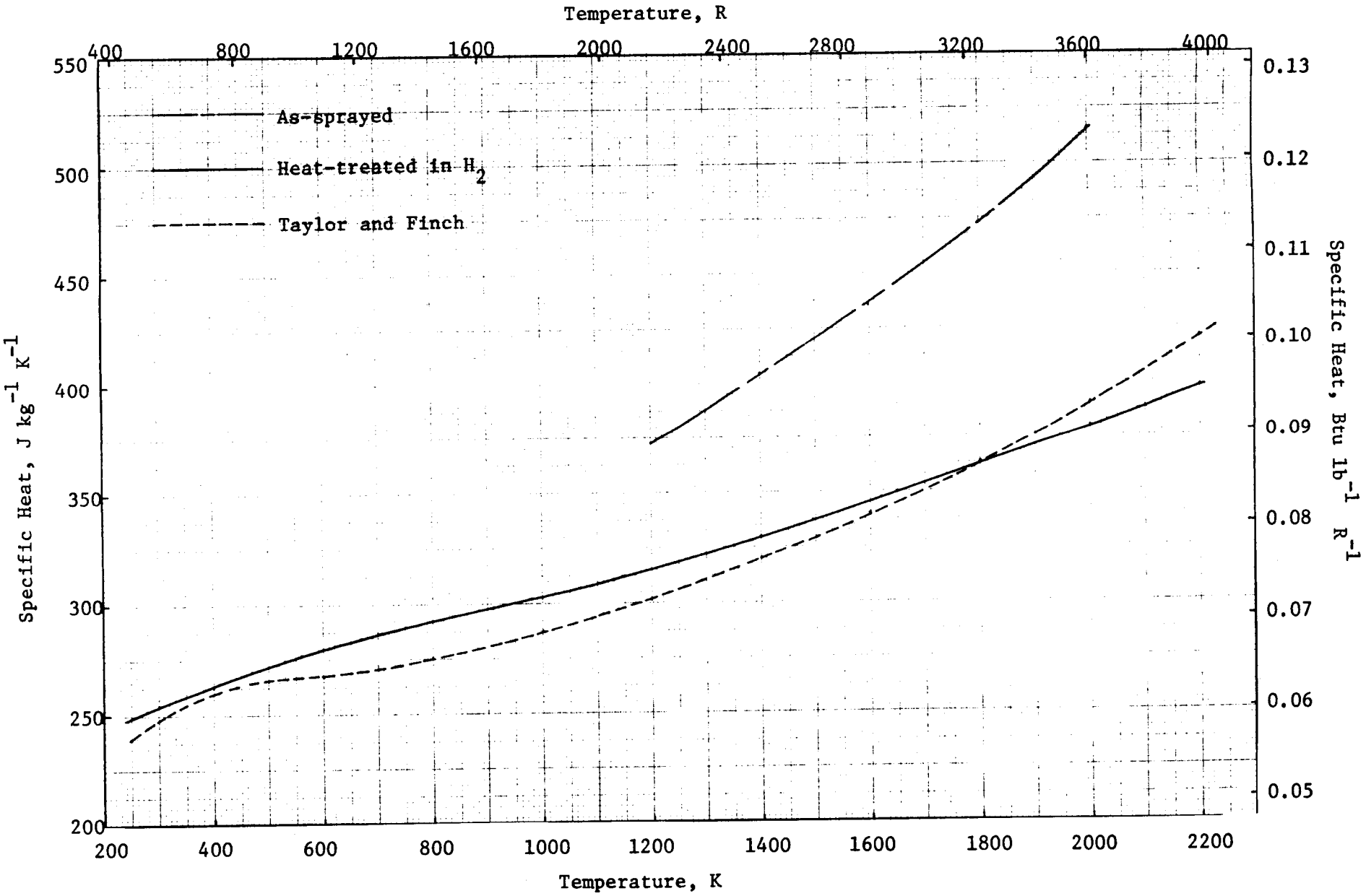

FIGURE 58. SPECIFIC HEAT OF PLASMA-SPRAYED MOLYBDENUM

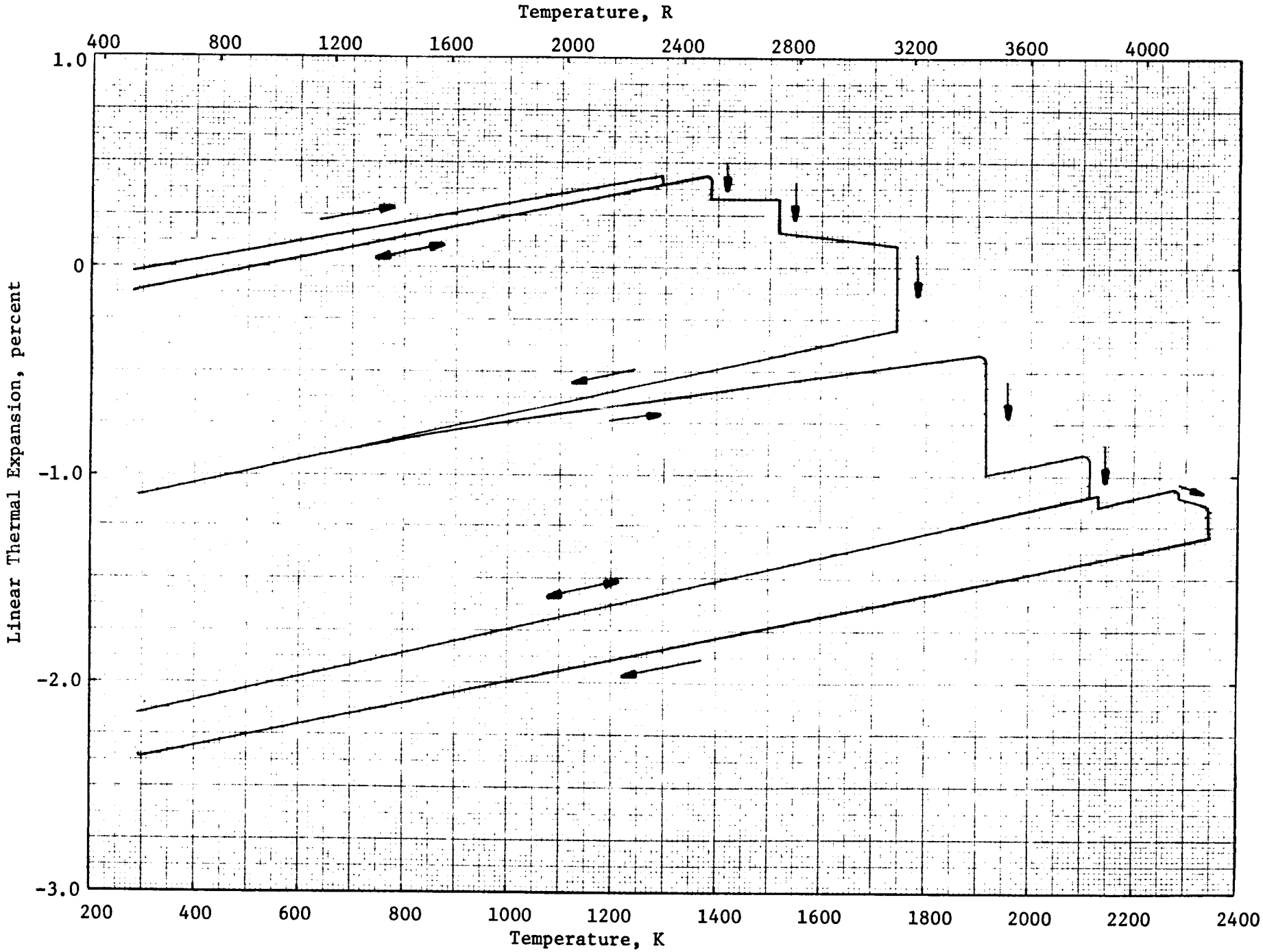

FIGURE 59. LINEAR THERMAL EXPANSION OF PLASMA-SPRAYED MOLYBDENUM

TABLE 14. LINEAR THERMAL EXPANSION OF PLASMA-SPRAYED MOLYBDENUM

Temperature, K	Expansion, percent	Time at Temperature, minutes	Temperature, K	Expansion, percent	Time at Temperature, minutes
295	0		1745	-0.282	81
428	0.053		1745	-0.311	98
581	0.121		1505	-0.431	
682	0.169		295	-1.107	
821	0.235	0	1323	-0.621	
821	0.232	22	1907	-0.451	0
974	0.308	0	1912	-0.514	4
974	0.304	37	1915	-0.575	20
1118	0.376	0	1910	-0.688	45
1118	0.371	33	1913	-0.736	62
740	0.168		1913	-0.784	85
740	0.165		1914	-0.824	105
292	-0.039		1915	-0.868	125
673	0.135		1914	-0.897	142
821	0.208		1917	-0.954	190
851	0.219		1917	-0.985	221
939	0.269		2116	-0.889	0
1012	0.308		2114	-0.932	9
1159	0.391		2102	-0.987	44
1294	0.439	0	2112	-1.036	92
1294	0.418	10	2114	-1.075	147
1294	0.410	20	2114	-1.091	176
1294	0.403	30	1790	-1.339	
1294	0.398	40	307	-2.110	
829	0.140		2127	-1.097	0
293	-0.111		2131	-1.098	19
964	0.211		2133	-1.117	50
1284	0.383		2133	-1.131	81
1387	0.418	0	2135	-1.150	120
1384	0.378	17	2122	-1.161	169
1385	0.363	32	2295	-1.048	0
1381	0.339	52	2287	-1.052	8
1520	0.322	0	2279	-1.073	26
1515	0.264	15	2260	-1.105	76
1516	0.233	30	2338	-1.148	150
1517	0.208	45	2351	-1.169	209
1516	0.191	60	2341	-1.192	239
1514	0.163	85	2183	-1.323	
1744	0.110	0	1968	-1.491	
1743	0	16	1818	-1.581	
1748	-0.046	31	295	-2.351	
1748	-0.197	46			
1746	-0.251	61			

TABLE 15. PHYSICAL CHARACTERISTICS OF PLASMA-SPRAYED Mo-OXIDE MIXTURES

	Thickness, cm	Diameter, cm	Weight, g	Density, g cm^{-3}
25 Mo-75 Al_2O_3				
Pretest	0.1039	1.2560	0.6519	5.17
First Heating in Hydrogen	0.1036	1.2530	0.6468	- -
Posttest	0.0965	1.2139	0.6436	5.93
75 Mo-25 Al_2O_3				
Pretest	0.2050	1.2664	2.2099	8.46
First Heating in Hydrogen	0.2050	1.2591	2.1732	8.47
Posttest	0.1981	1.2332	2.1645	9.24
25 Mo-75 ZrO_2				
Pretest	0.0764	1.2616	0.6510	7.36
First Heating in Hydrogen	- -	- -	0.6396	- -
Posttest	0.0732	1.2207	0.6361	7.94
75 Mo-25 ZrO_2				
Pretest	- -	- -	1.9906	- -
First Heating in Hydrogen	- -	- -	1.9328	- -
Before Diffusivity Measurement	0.1786	1.2583	1.8122*	8.31
Posttest	0.1687	1.2128	1.7934	9.37

*Note: Weight decrease at this point is due to machining of specimen.

75 w/o Mo-25 w/o Al_2O_3, and 25 w/o Mo-75 w/o Al_2O_3. The starting powders were the same as used for preparing the Mo, Al_2O_3, and CaO-stabilized ZrO_2 specimens described above. Photomicrographs of diffusivity specimens in both the as-sprayed and postmeasurement conditions are shown in Figures 60 through 67. In these figures the white phase is Mo, the gray phase is the oxide, and the black phase is porosity. A layering effect is obvious in most of the longitudinal sections. Physical characteristics of the diffusivity samples are given in Table 15.

Thermal conductivity results on the four Mo-oxide mixtures are given in Figures 68 through 71. All measurements on the Mo-ZrO_2 mixtures were made under 515 psia hydrogen, while measurements on the Mo-Al_2O_3 mixtures were made under either 415 or 515 psia hydrogen with most of the heat treatments being made under 515 psia. The samples were held at elevated temperatures for periods of approximately one-half hour during which diffusivity measurements were made. After each heat treatment, measurements were made at lower temperatures in order to observe the effects of the heat treatment. In common with the other plasma-sprayed coatings, there is a tendency for the conductivity to increase following each heat treatment at successively higher temperatures. These increases are apparently related to sintering effects as reflected in the photomicrographs.

In each case, significant weight losses were observed upon initial heat treatment in hydrogen, accompanied by formation of moisture on the window of the furnace chamber. Again, these weight losses are apparently due to the reduction of molybdenum oxides.

Quantitative metallographic determinations of the volume percents of the Mo phase were made on the thermal diffusivity specimens in the postmeasurement condition. This information, along with a knowledge of the specimen density and the theoretical densities of the oxides and metal, was used to determine the volume percent of the oxide and the porosity. These quantities are summarized in Table 16. These relationships may be used in correlating the thermal conductivity results on the mixtures.

TABLE 16. PHASE PERCENTAGES IN Mo-OXIDE MIXTURES

Material	Volume percent			Weight percent	
	Mo	Oxide	Porosity	Mo	Oxide
25 Mo-75 ZrO_2	70.5	13.3	16.2	90.5	9.5
75 Mo-25 ZrO_2	95.9	~0	4.1	~100	~0
25 Mo-75 Al_2O_3	40.9	44.2	14.9	70.3	29.7
75 Mo-25 Al_2O_3	87.6	7.7	4.7	96.7	3.3

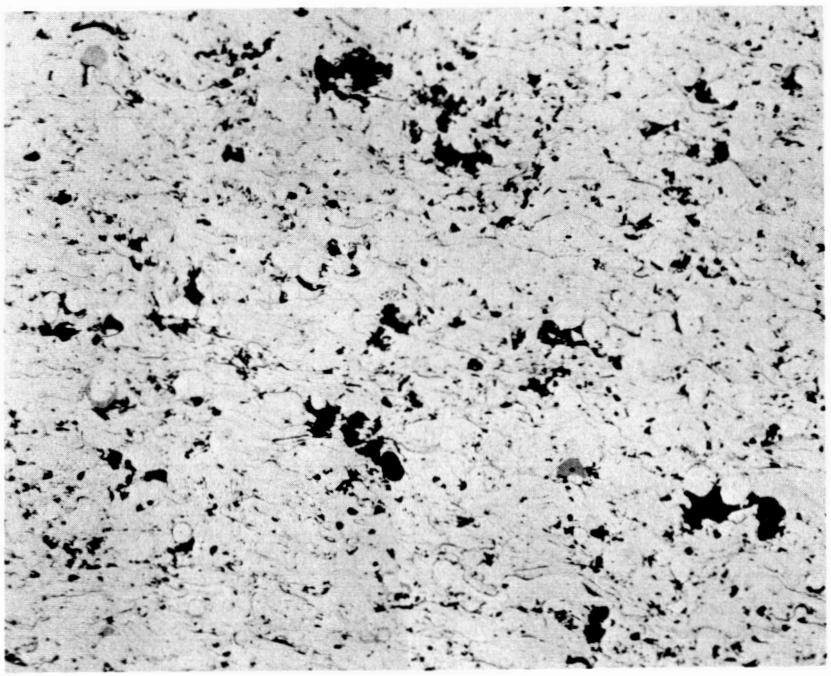

100X LONGITUDINAL SECTION 2G301

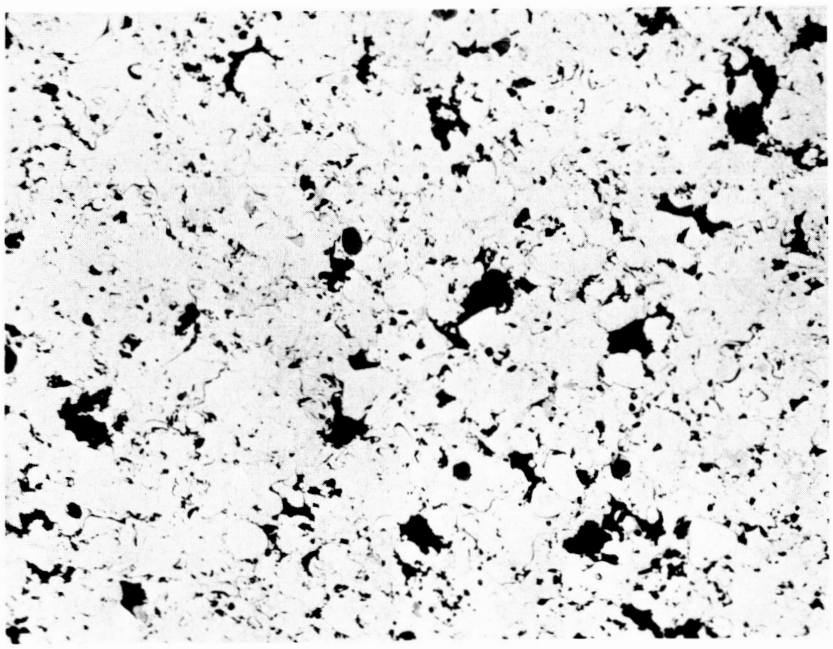

100X TRANSVERSE SECTION 2G299

FIGURE 60. MICROSTRUCTURE OF AS-SPRAYED 75 w/o Mo-25 w/o ZrO_2 (AS-POLISHED)

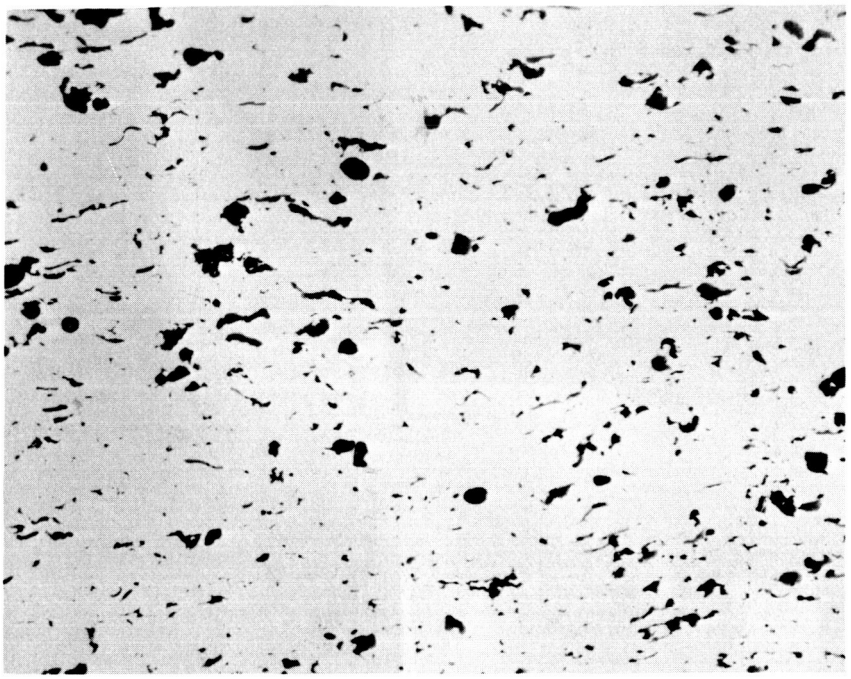

100X LONGITUDINAL SECTION 2G298

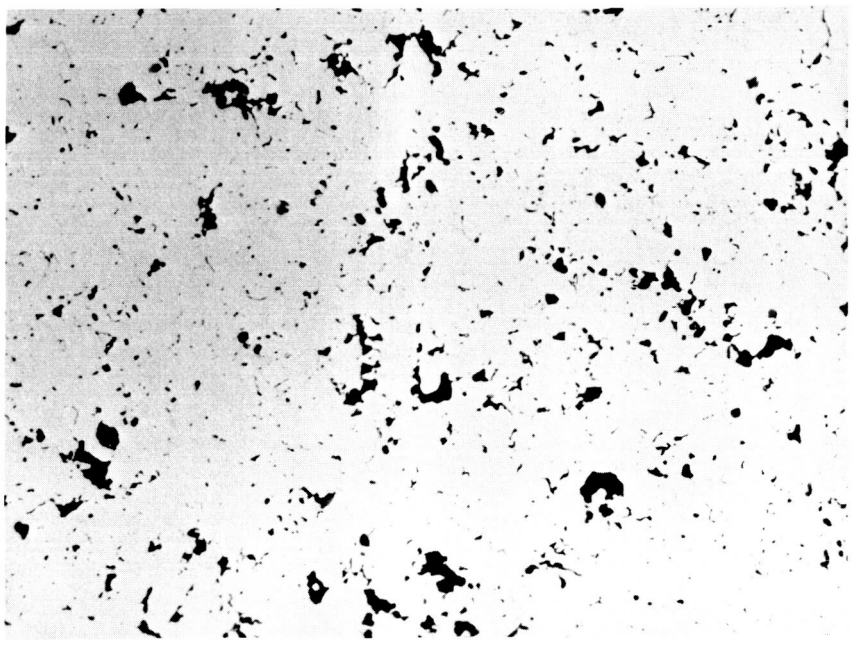

100X TRANSVERSE SECTION 2G302

FIGURE 61. POSTMEASUREMENT MICROSTRUCTURE OF 75 w/o Mo-25 w/o ZrO_2-CaO, SAMPLE 1 (AS-POLISHED)

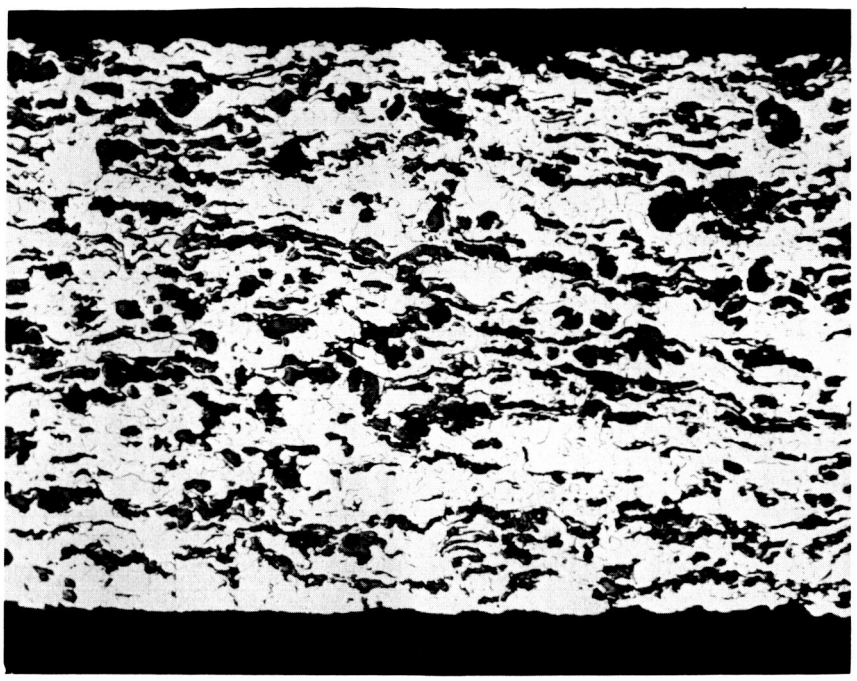

100X LONGITUDINAL SECTION 2G307

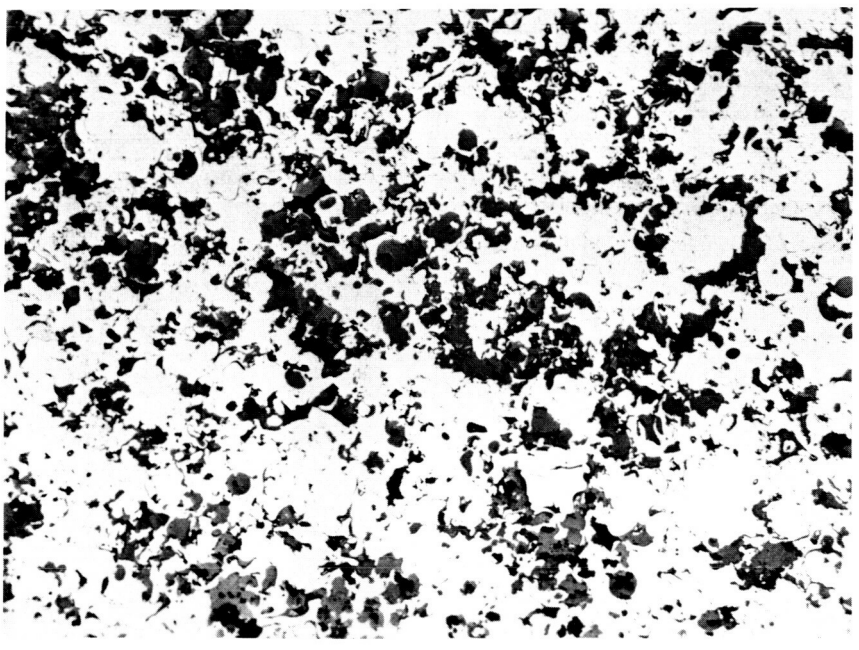

100X TRANSVERSE SECTION 2G305

FIGURE 62. MICROSTRUCTURE OF AS-SPRAYED 25 w/o Mo-75 w/o ZrO_2-CaO (AS-POLISHED)

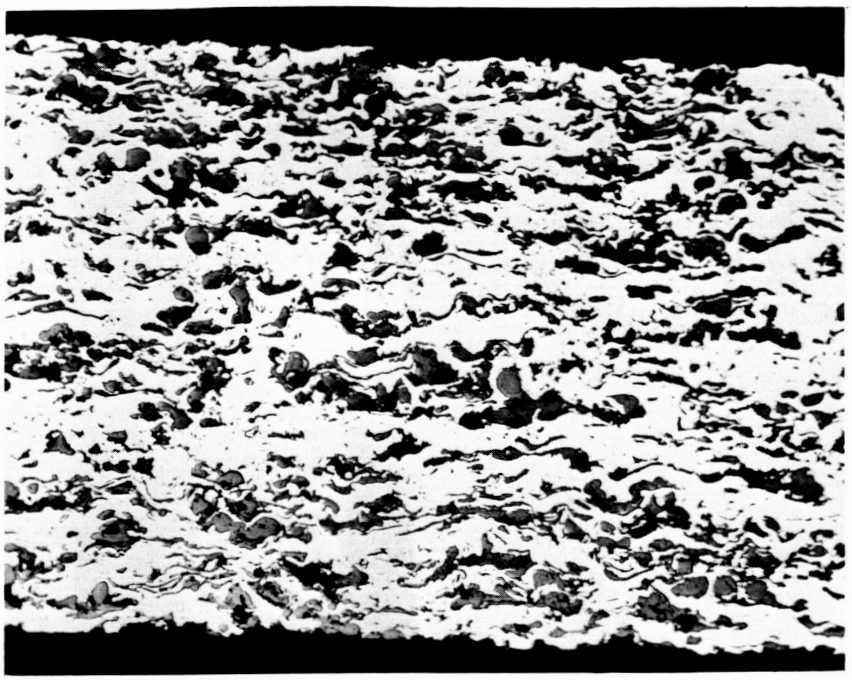

100X LONGITUDINAL SECTION 2G304

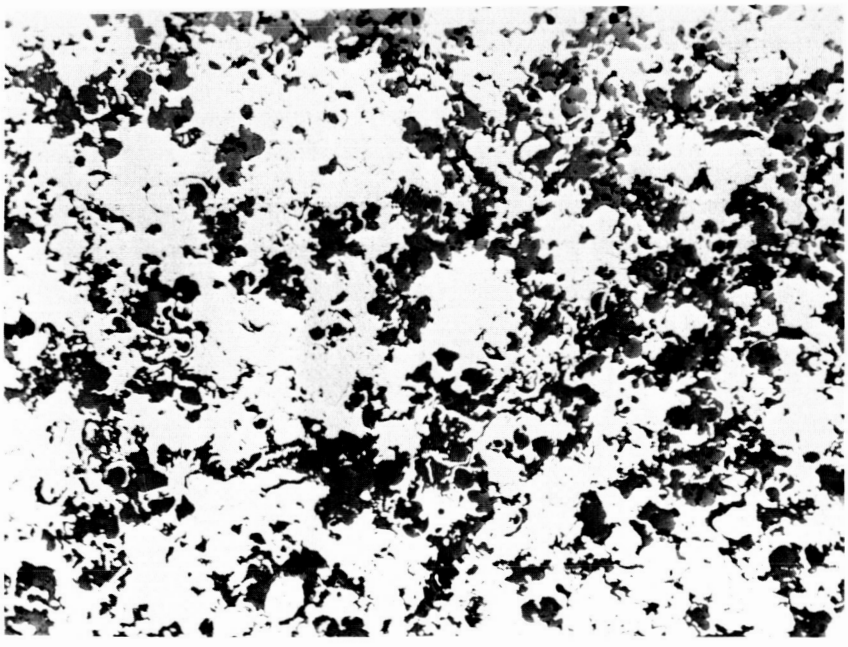

100X TRANSVERSE SECTION 2G308

FIGURE 63. POSTMEASUREMENT MICROSTRUCTURE OF 25 w/o Mo-75 w/o ZrO_2- CaO, SAMPLE 1 (AS-POLISHED)

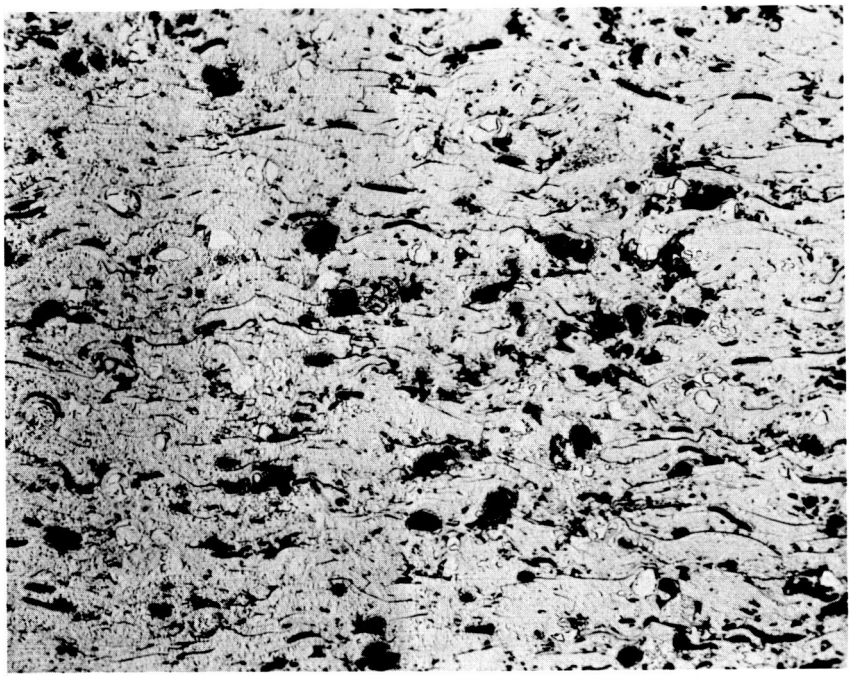

100X LONGITUDINAL SECTION 2G292

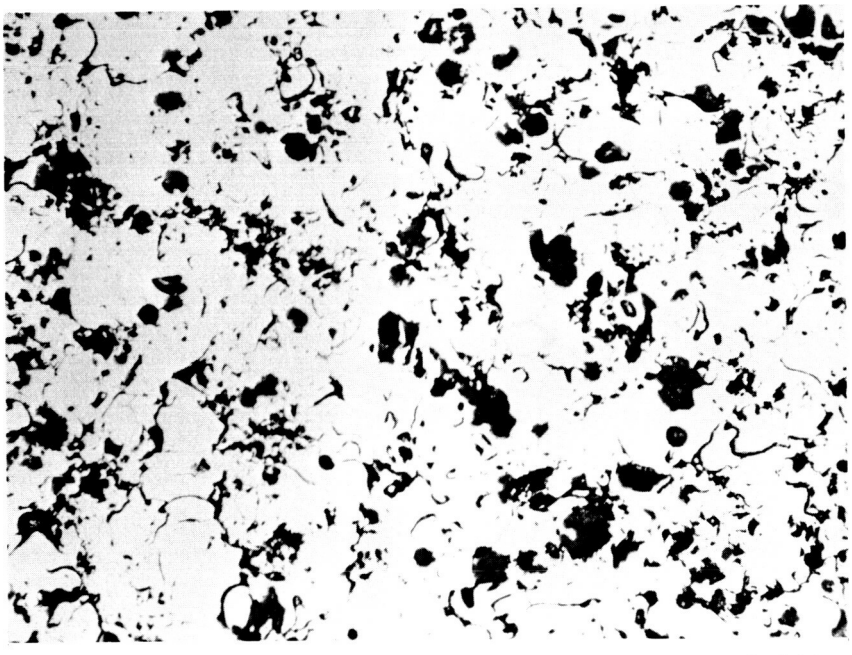

100X TRANSVERSE SECTION 2G293

FIGURE 64. MICROSTRUCTURE OF AS SPRAYED 75 w/o MoO-25 w/o Al_2O_3 (AS-POLISHED)

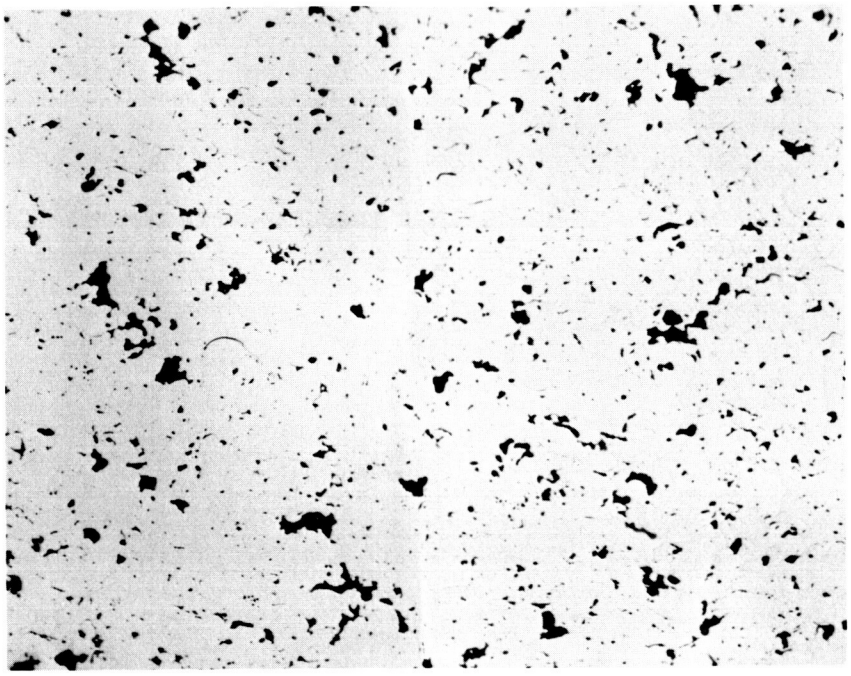

100X LONGITUDINAL SECTION 2G295

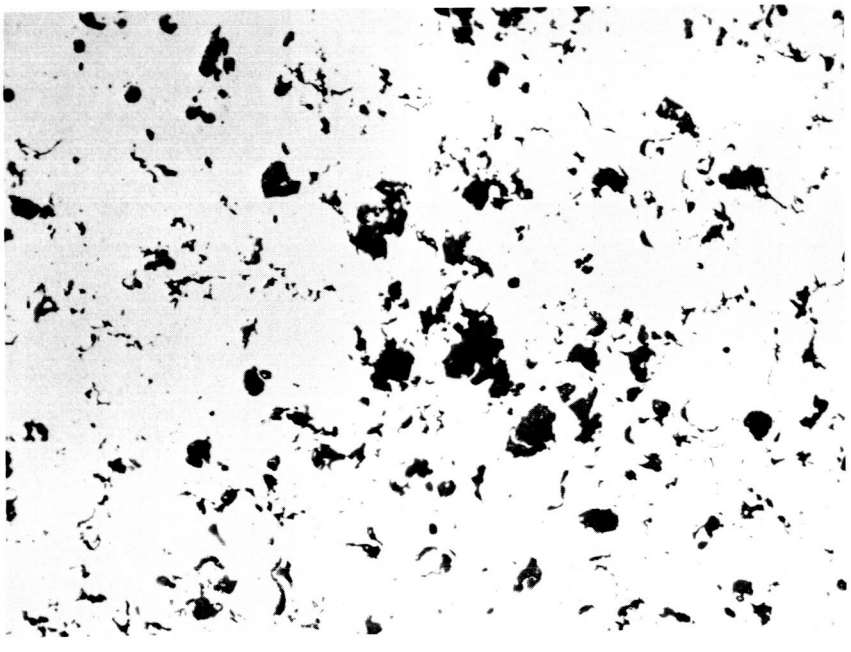

100X TRANSVERSE SECTION 2G296

FIGURE 65. POSTMEASUREMENT MICROSTRUCTURE OF 75 w/o Mo-25 w/o Al_2O_3, SAMPLE 1 (AS-POLISHED)

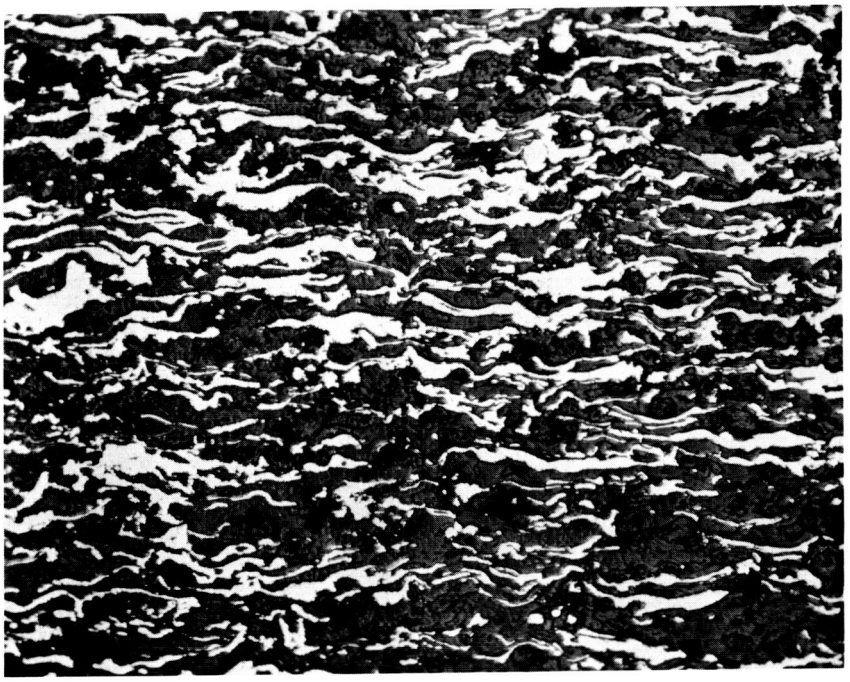

100X LONGITUDINAL SECTION 2G286

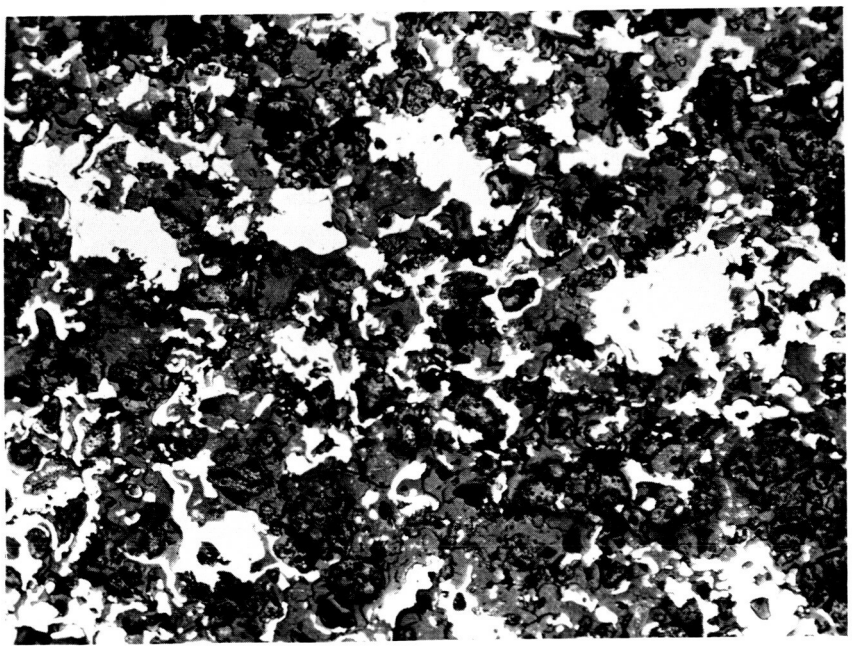

100X TRANSVERSE SECTION 2G288

FIGURE 66. MICROSTRUCTURE OF AS-SPRAYED 25 w/o Mo-75 w/o Al_2O_3 (AS-POLISHED)

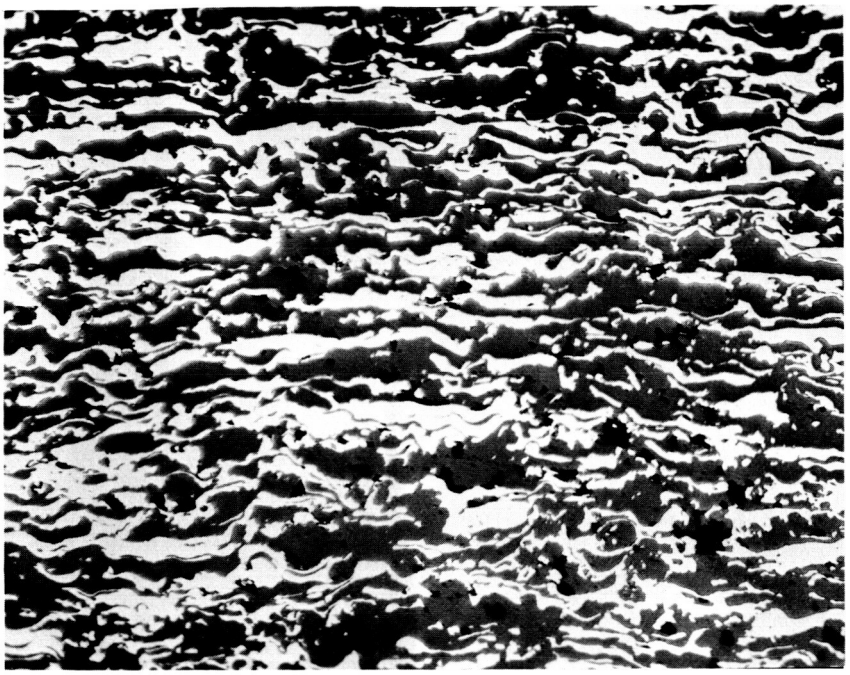

100X LONGITUDINAL SECTION 2G289

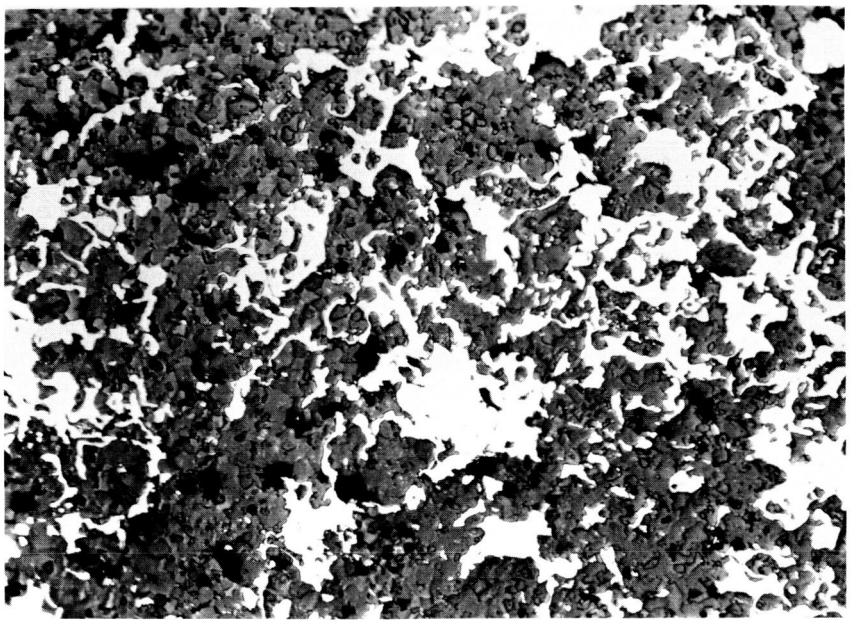

100X TRANSVERSE SECTION 2G290

FIGURE 67. POSTMEASUREMENT MICROSTRUCTURE OF 25 w/o Mo-75 w/o Al_2O_3, SAMPLE 1 (AS-POLISHED)

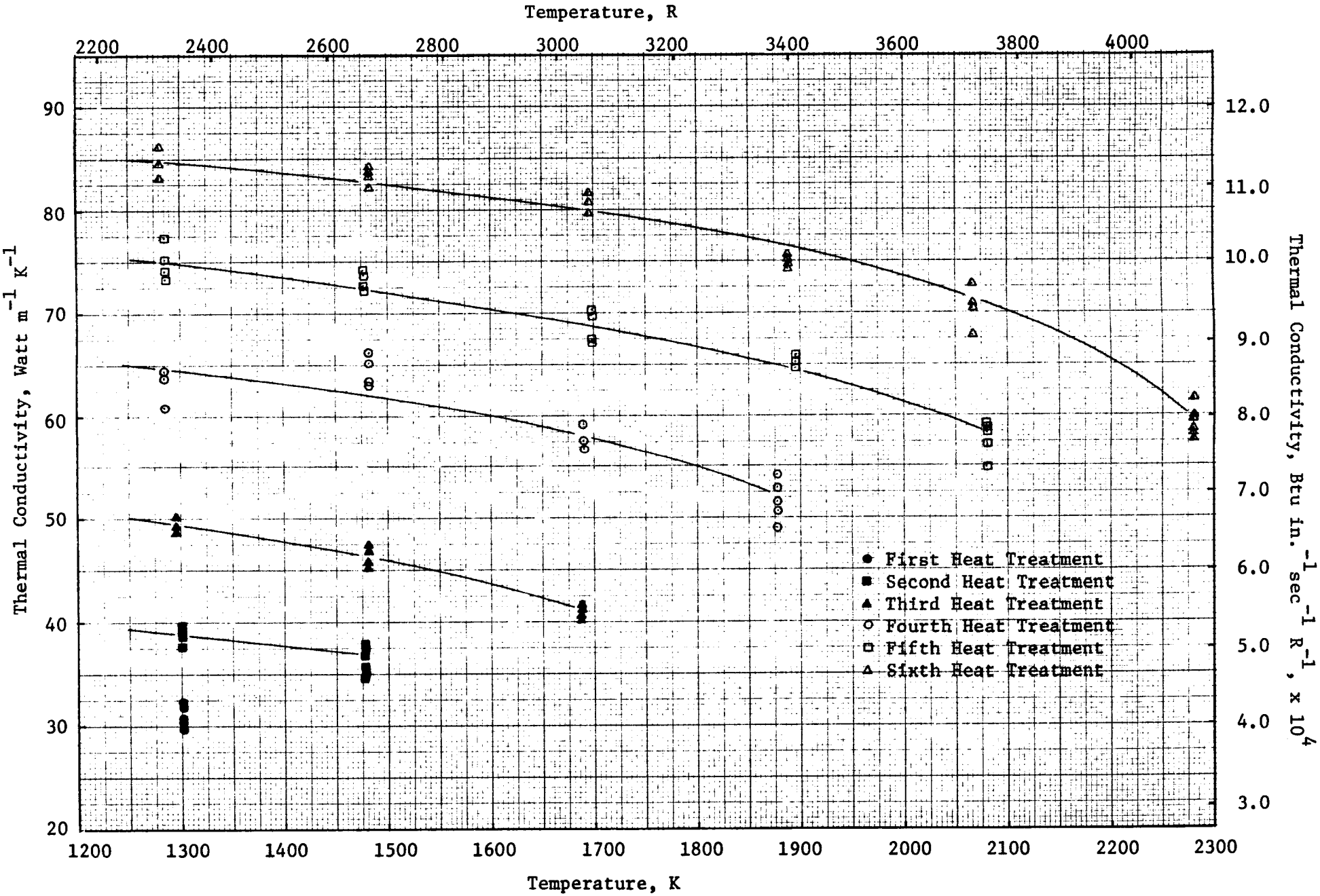

FIGURE 68. THERMAL CONDUCTIVITY OF PLASMA-SPRAYED 75 w/o Mo-25 w/o ZrO_2 IN HYDROGEN AT 515 PSIA

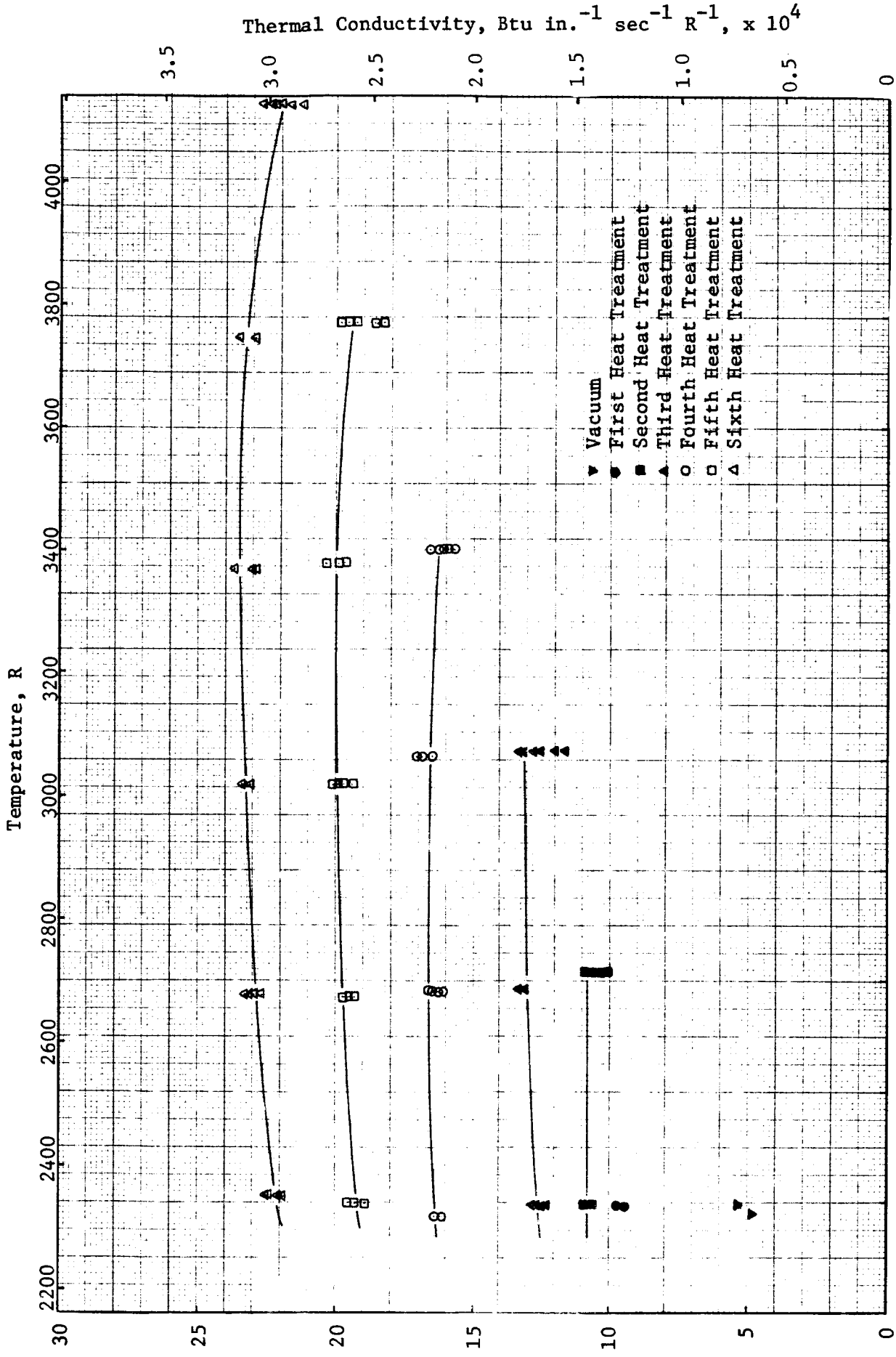

FIGURE 69. THERMAL CONDUCTIVITY OF PLASMA-SPRAYED 25 w/o Mo-75 w/o ZrO_2 IN HYDROGEN AT 515 PSIA

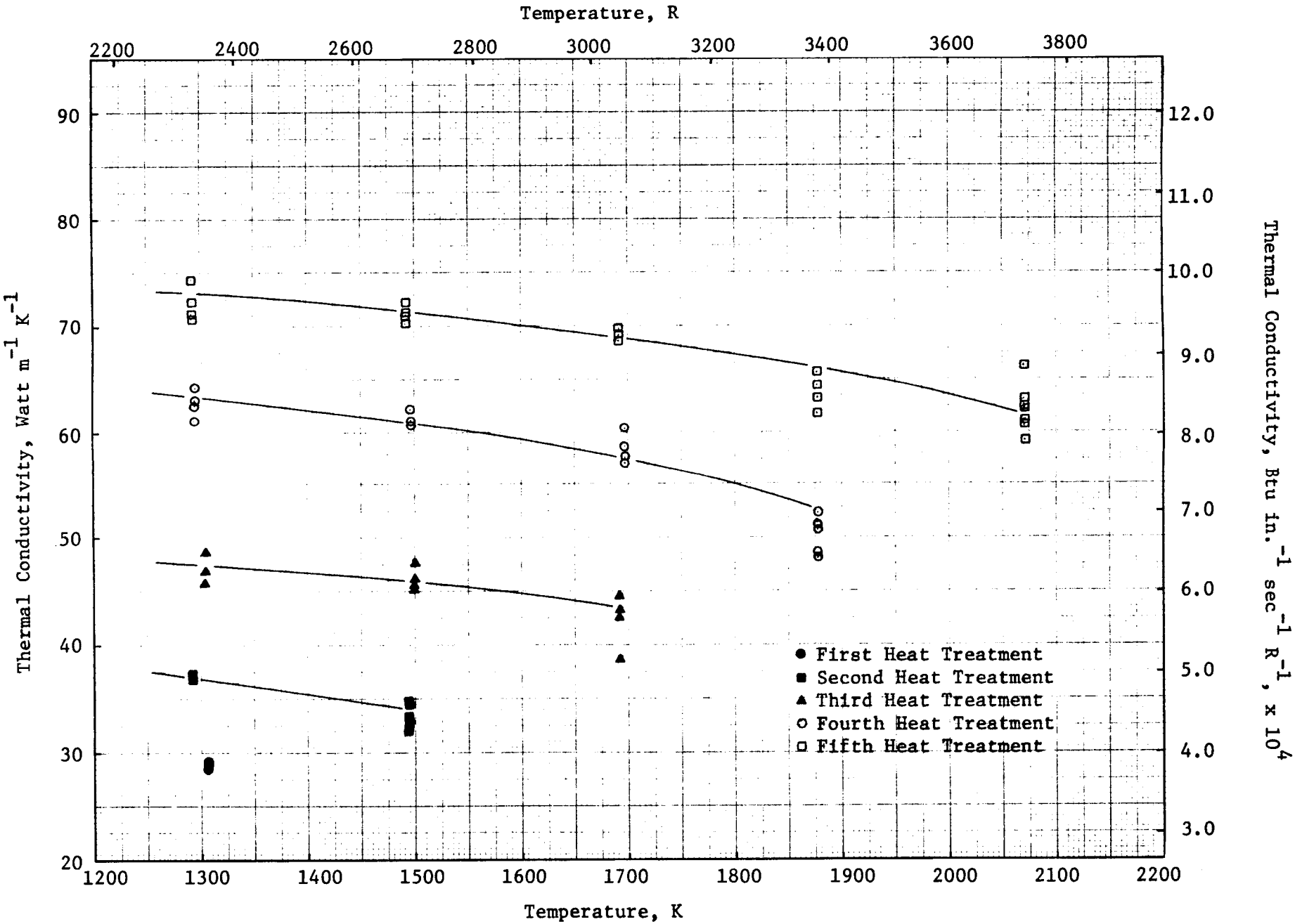

FIGURE 70. THERMAL CONDUCTIVITY OF PLASMA-SPRAYED 75 w/o Mo-25 w/o Al_2O_3 IN HIGH PRESSURE HYDROGEN

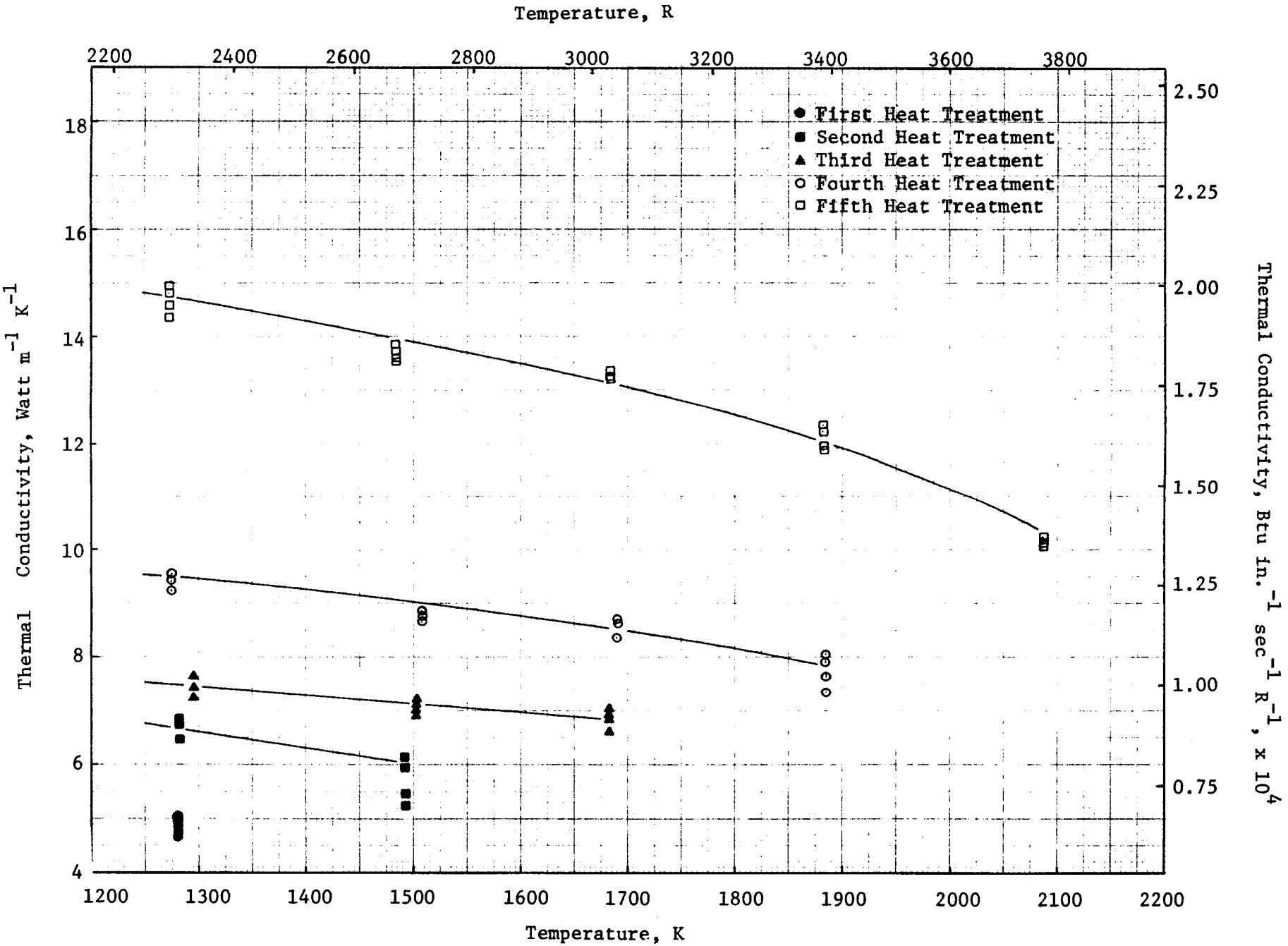

FIGURE 71. THERMAL CONDUCTIVITY OF PLASMA-SPRAYED 25 w/o Mo-75 w/o Al_2O_3 IN HIGH PRESSURE HYDROGEN

Measured conductivity values may be corrected approximately for porosity by the Maxwell-Eucken relation

$$\lambda_o = \lambda \frac{1 + 1/2\ P}{1 - P} \quad , \tag{5}$$

where

λ = measured thermal conductivity

λ_o = thermal conductivity at zero porosity

P = fraction porosity.

The corrected values of thermal conductivity at 1300 K and 2000 K after final heat treatment are shown in Figures 72 and 73 for Mo-ZrO_2 mixtures and in Figures 74 and 75 for the Mo-Al_2O_3 mixtures. The abscissae in these figures are the volume percent oxide of the total amount of solid phase. The end points of the curves are the corrected values of the thermal conductivity as measured on the single materials after the appropriate heat treatment. The four curves in the figures correspond to the calculated conductivity as a function of composition for four idealized cases. Curve 1 corresponds to the conductivity of a composite made up of flat slabs of the two materials with heat flow parallel to the slabs. Curve 2 represents the Maxwell-Eucken relationship for dilute mixtures of low conductivity noninteracting spheres in a high conductivity matrix, while Curve 3 represents the same relationship but with high conductivity spheres in a low conductivity matrix. Curve 4 represents the conductivity of a composite made up of slabs of the two materials with heat flow normal to the slabs. The mathematical relationships for these four curves are[19]:

$$\text{Curve 1: } \lambda = V_1 \lambda_1 + V_2 \lambda_2 \quad , \tag{6}$$

$$\text{Curves 2 and 3: } \lambda = \lambda_c \left[\frac{1 + 2V_d \left(\frac{1 - \lambda_c/\lambda_d}{2\lambda_c/\lambda_d + 1} \right)}{1 - V_d \left(\frac{1 - \lambda_c/\lambda_d}{2\lambda_c/\lambda_d + 1} \right)} \right] , \tag{7}$$

$$\text{Curve 4: } \lambda = \frac{\lambda_1 \lambda_2}{V_1 \lambda_2 + V_2 \lambda_1} \quad , \tag{8}$$

where

λ = thermal conductivity of mixture

λ_1 = thermal conductivity of Phase 1

λ_2 = thermal conductivity of Phase 2

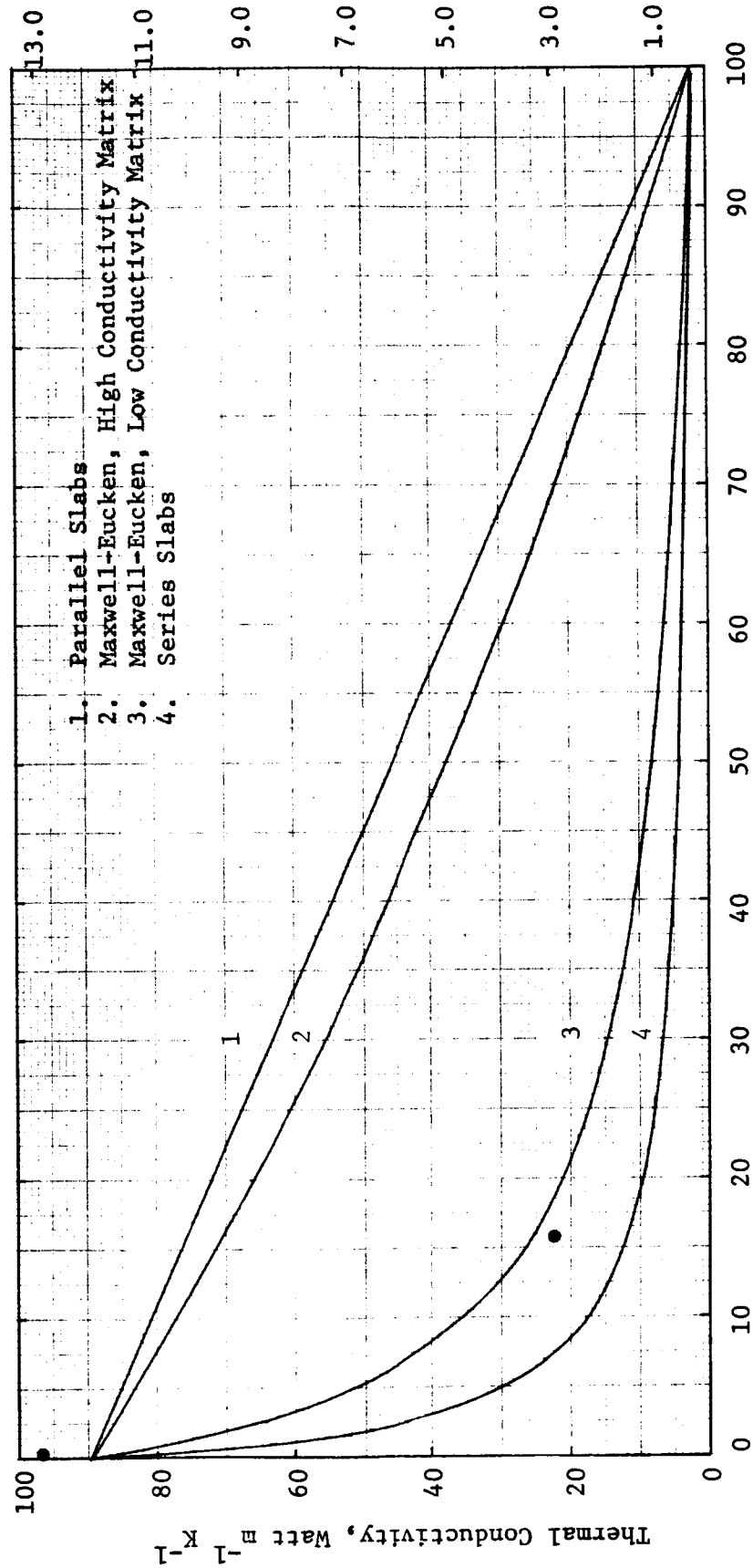

FIGURE 72. THERMAL CONDUCTIVITY OF Mo-ZrO_2-CaO MIXTURES AT 1300 K FOLLOWING FINAL HEAT TREATMENT

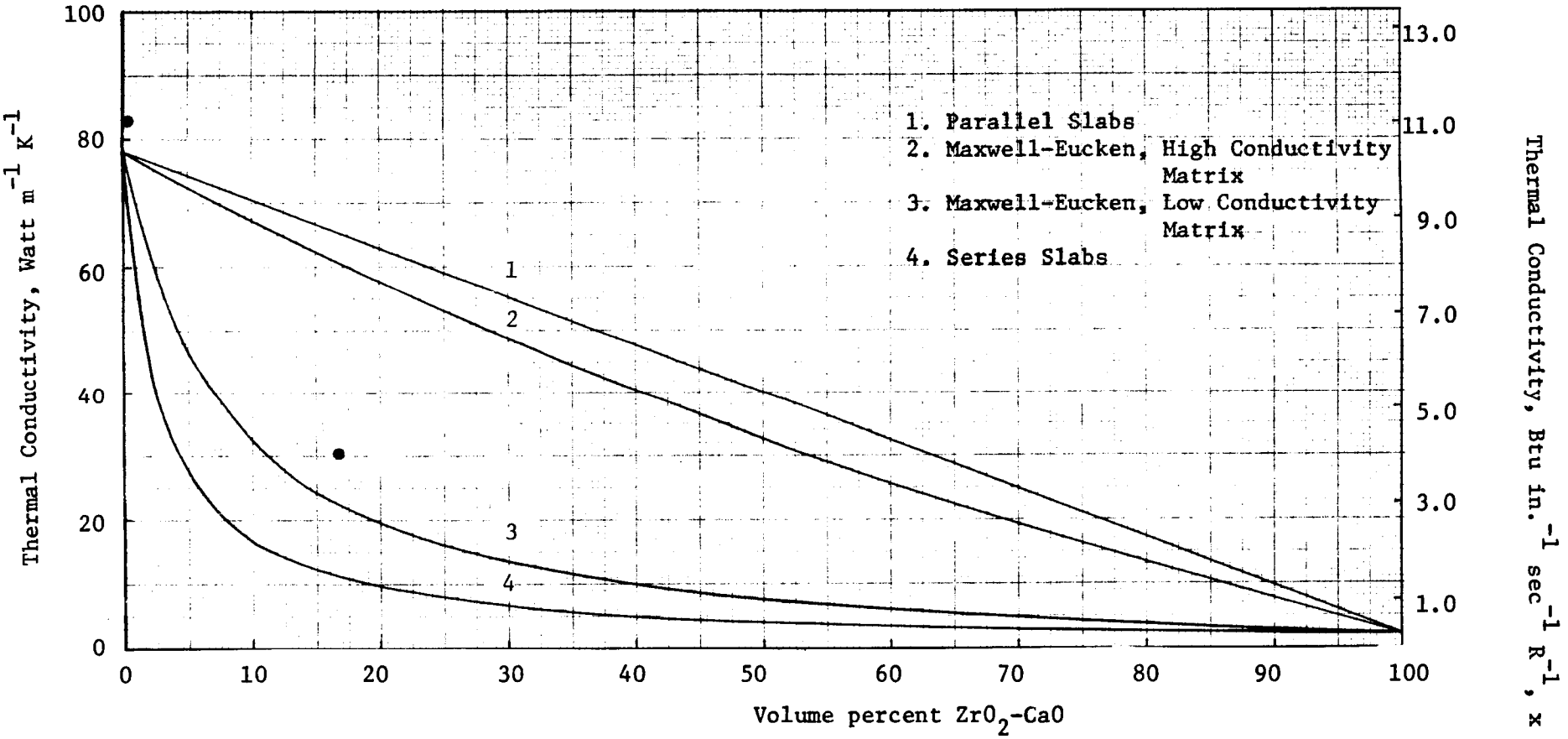

FIGURE 73. THERMAL CONDUCTIVITY OF Mo-ZrO_2-CaO MIXTURES AT 2000 K FOLLOWING FINAL HEATTREATMENT

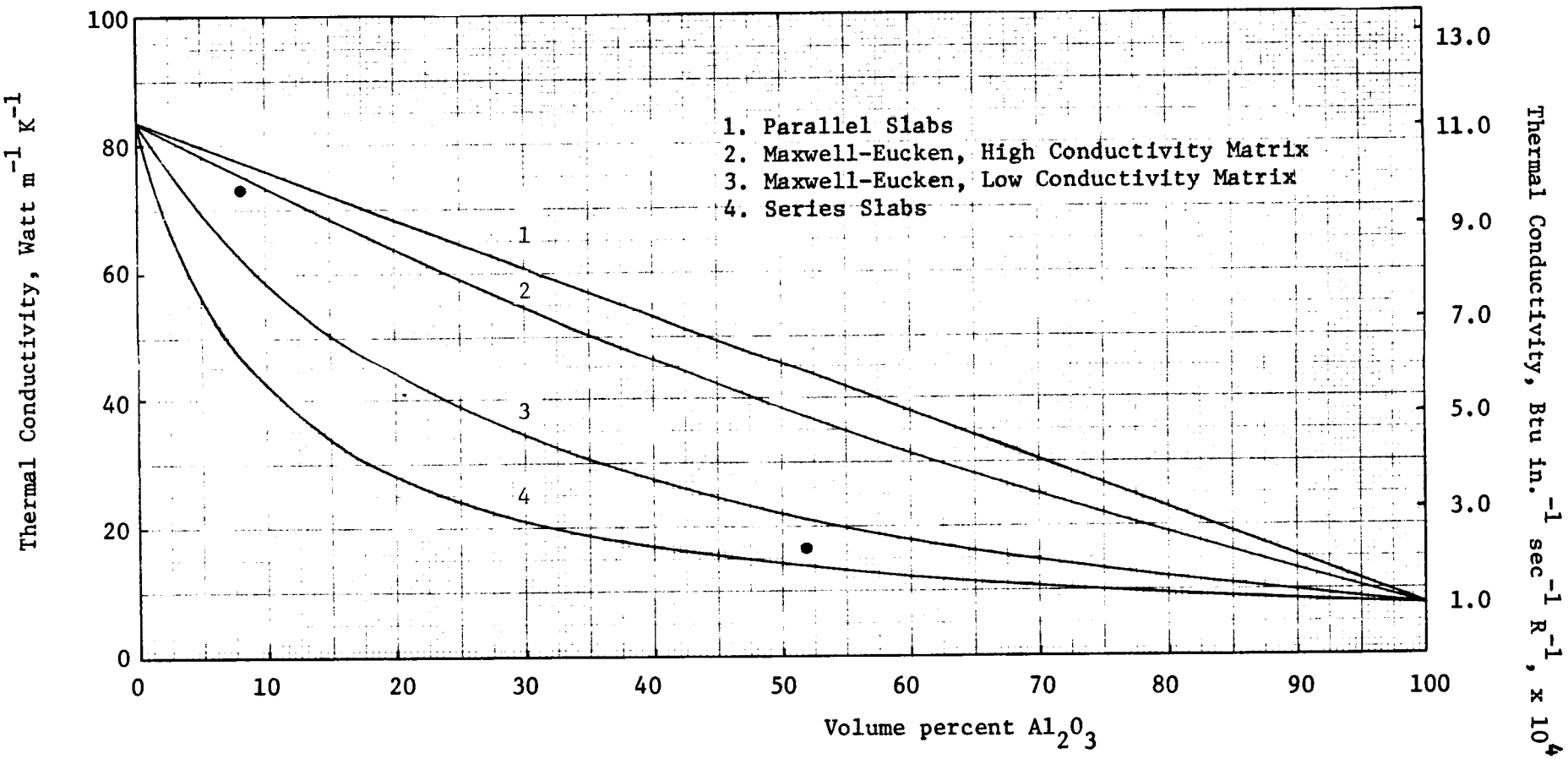

FIGURE 74. THERMAL CONDUCTIVITY OF Mo-Al_2O_3 MIXTURES AT 1300 K FOLLOWING FINAL HEAT TREATMENT

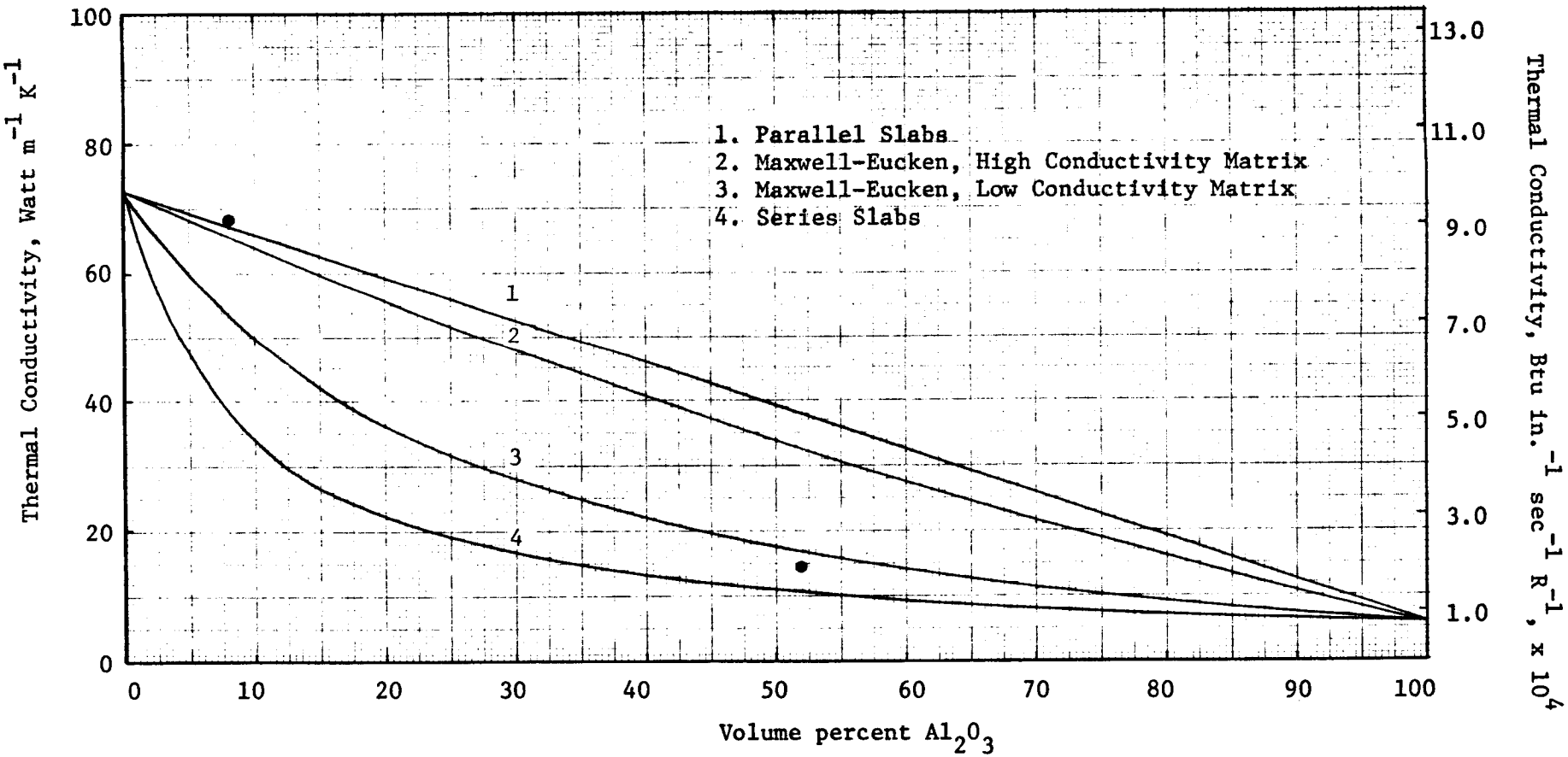

FIGURE 75. THERMAL CONDUCTIVITY OF Mo-Al_2O_3 MIXTURES AT 2000 K FOLLOWING FINAL HEATTREATMENT

V_1 = volume fraction of Phase 1

V_2 = volume fraction of Phase 2

λ_c = thermal conductivity of continuous (matrix) phase

λ_d = thermal conductivity of dispersed phase

V_c = volume fraction of continuous phase

V_d = volume fraction of dispersed phase.

As seen from Figures 72 through 75, the conductivities of the 25 Mo-75 ZrO_2 and 25 Mo-75 Al_2O_3 mixtures are closest to Curves 3 and 4, as might be expected from their layered microstructures. The conductivity of the 75 Mo-25 ZrO_2 is close to that of Mo, as expected due to the almost negligible ZrO_2 content. The conductivity of the 75 Mo-25 Al_2O_3 is closest to Curves 1 and 2, as might be expected from the continuous nature of the Mo in the microstructure. These curves should be useful in predicting the thermal conductivities of coatings of other compositions.

The volume phase relationships in Table 16 were used to calculate weight fractions which are also given in this table. It is evident that the actual compositions are much different than the nominal values. This is apparently due to a decrease in oxide content during the plasma spraying process. Similar oxide losses have been observed at NASA Lewis. These weight fractions and measured values of the specific heat of the components were used to calculate the specific heat of the mixtures by the relation

$$Cp = \sum_i M_i \; Cp_i \quad , \tag{9}$$

where

Cp = specific heat of mixture
Cp_i = specific heat of i^{th} phase
M_i = mass fraction of i^{th} phase.

The calculated values are compared with the experimentally determined values for the specific heat of the mixtures in Figures 76 through 79. Except for the 25 Mo-75 Al_2O_3, the calculated values agree fairly well with the measured values. The observed discrepancies could be due to compositional differences between the specific heat and diffusivity specimens or to errors in the determination of the compositions.

Nichrome and NiAl

Plasma sprayed nichrome and NiAl are potentially useful in coating systems, since both are fairly refractory materials and have a thermal conductivity substantially lower than that of Mo. Chemical analyses and photomicrographs of diffusivity specimens in both the as-sprayed and postmeasurement conditions are given in Tables 17 and 18 and in Figures 80 through 83. Physical characteristics of the diffusivity specimens are given in Table 19.

Thermal diffusivity measurements were made on a sample of plasma-sprayed nichrome over the temperature range 473 to 1373 K. The results of these measurements are shown in Figure 84. Initial measurements at 473 K were conducted in four atmospheres: vacuum ($<10^{-5}$ torr), 1 atm argon, 1 atm helium, 2 atm helium. Since these results showed very little dependence upon atmosphere, the remaining measurements were made alternating between vacuum and 2 atm helium. Following the first heating cycle to 1373 K, the sample was cooled to room temperature and the measurements were repeated during a second heating cycle. In common with other plasma-sprayed materials, the data obtained during the second heating cycle are substantially higher than those of the first heating, presumably due to sintering effects. The sample was then placed in the hydrogen furnace and was heat treated near 1250 K in 515 psia hydrogen for about 30 minutes. Following this initial heat treatment, diffusivity measurements were made in 315 psia hydrogen at temperatures between about 1275 and 1370 K. Following this, the sample was reinstalled in the low pressure furnace and diffusivity measurements in 29 psia helium were repeated between 475 and 1390 K. As seen in Figure 84, the effect of the hydrogen heat treatment is an increase of less than 12 percent.

Similar thermal diffusivity measurements were made on a sample of plasma-sprayed NiAl over the same temperature range. These data are shown in Figures 85 and 86. Again, a substantial permanent increase in conductivity is observed after heating to near 1373 K, with a much smaller permanent increase resulting from the hydrogen heat treatment. The effect of the atmosphere is again relatively unimportant. It is obvious from the chemical analyses that the samples are not entirely composed of the β' or NiAl phase.

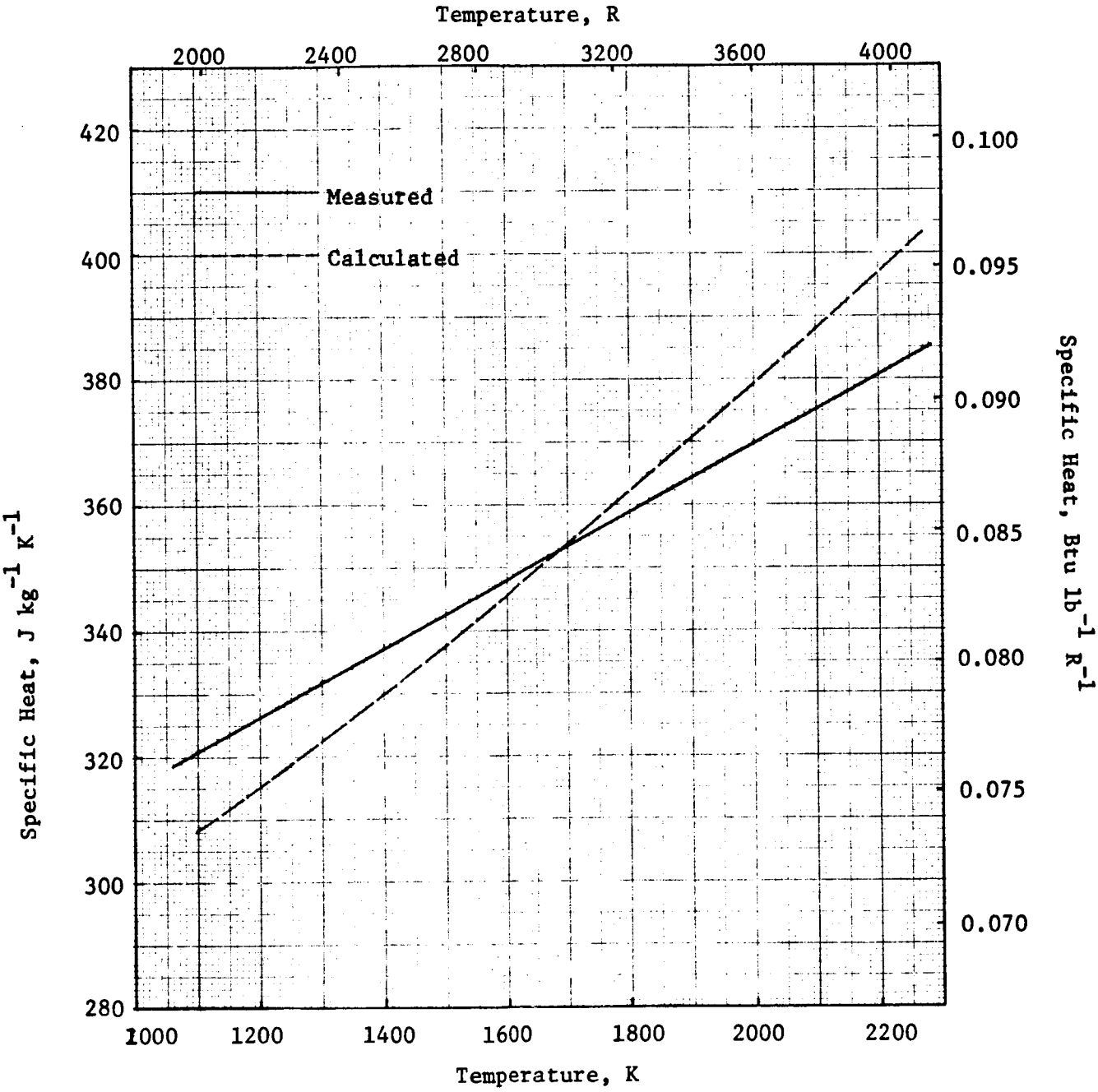

FIGURE 76. SPECIFIC HEAT OF 75 w/o Mo-25 w/o ZrO_2-CaO

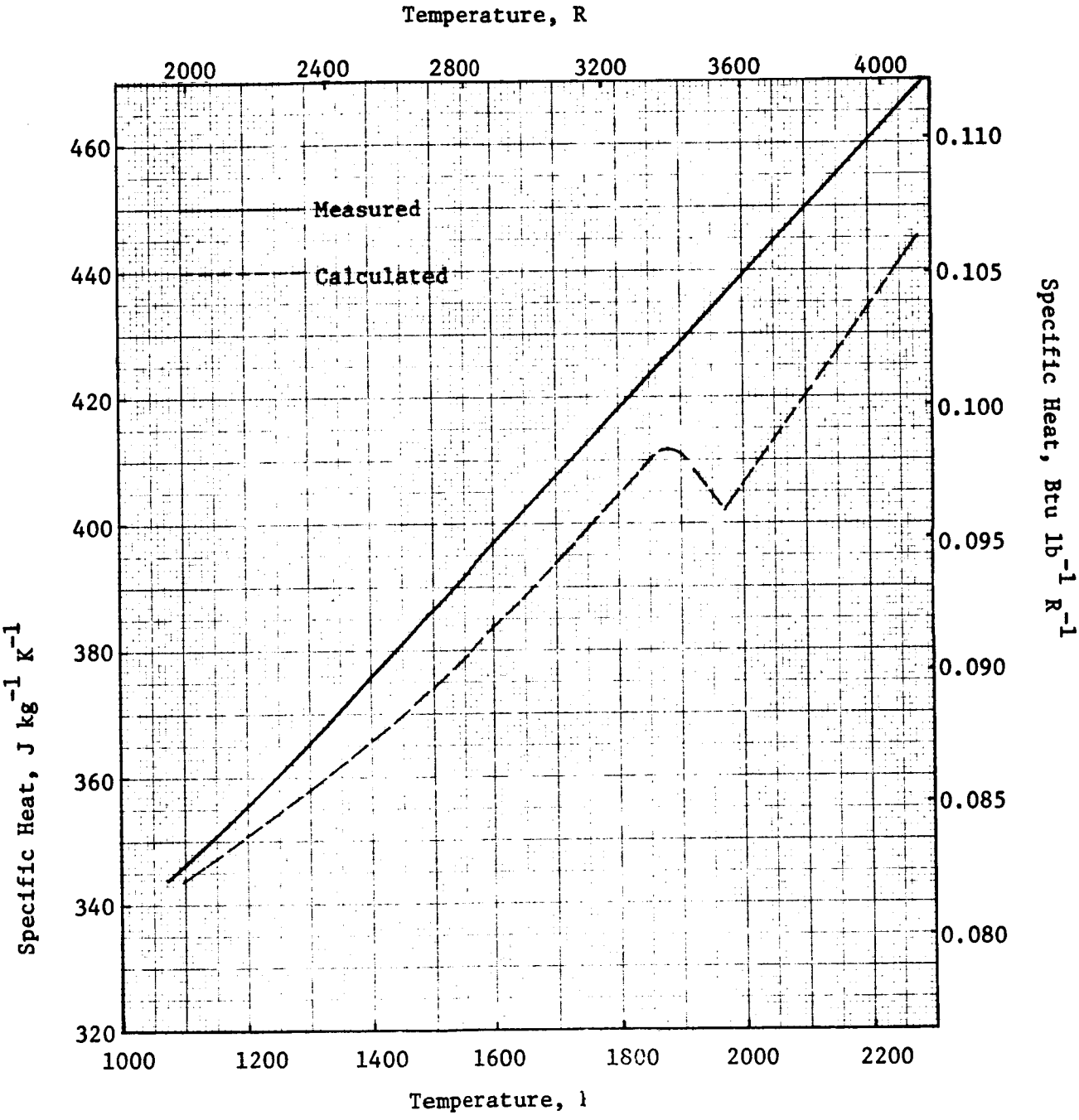

FIGURE 77. SPECIFIC HEAT OF 25 w/o Mo-75 w/o ZrO_2-CaO

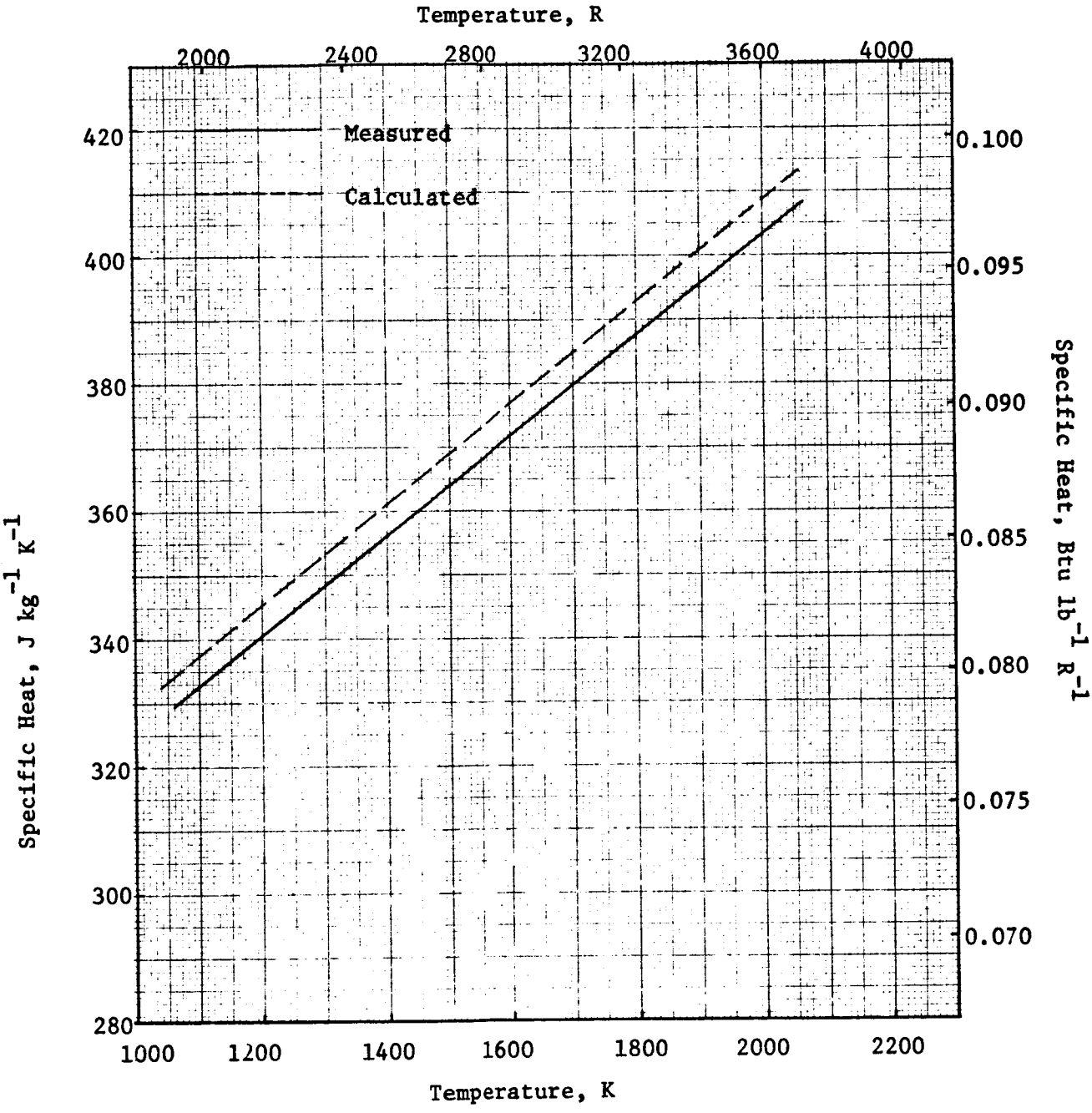

FIGURE 78. SPECIFIC HEAT OF 75 w/o Mo-25 w/o Al_2O_3

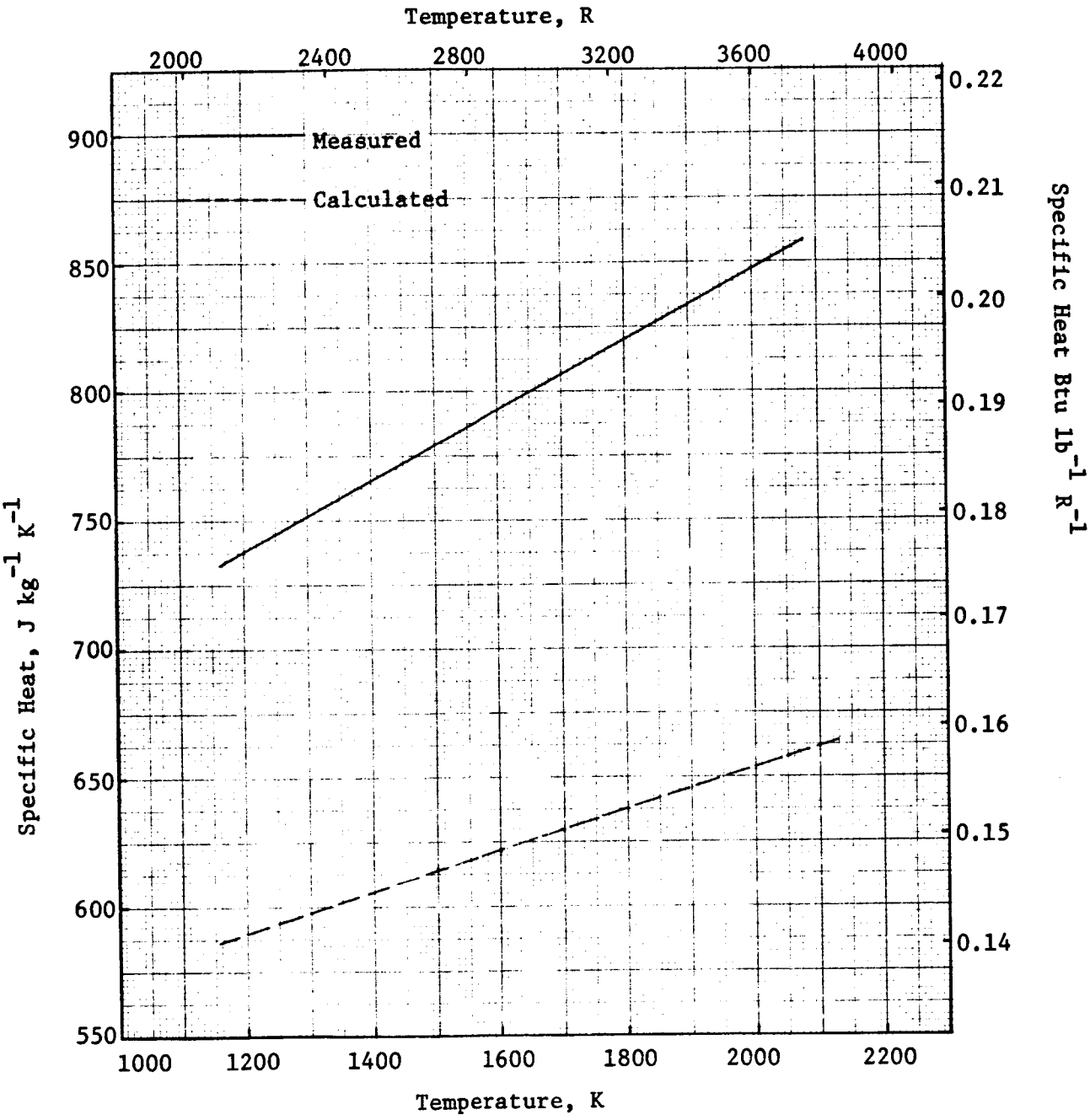

FIGURE 79. SPECIFIC HEAT OF 25 w/o Mo-75 w/o Al_2O_3

TABLE 17. CHEMICAL ANALYSES OF NICHROME SAMPLES

Element	Weight percent	
	As-Sprayed	Sample 1
Ni	75.0	75.5
Cr	23.6*	22.8*
Si	0.6	0.9
Mn	0.3	0.3
Fe	0.4	0.4
Al	<0.001	<0.001
Mo	0.002	0.002
Cu	0.05	0.005
Co	0.05	0.05
Ca	0.01	0.005

*By difference

TABLE 18. CHEMICAL ANALYSES OF NiAl SAMPLES

Element	Weight percent	
	As-Sprayed	Sample 1
Ni	94.8	94.4
Al	5.0*	5.4*
Si	0.003	0.005
Mn	<0.001	<0.001
Fe	0.003	0.003
Cr	<0.003	<0.003
Mo	0.05	0.05
Cu	0.005	0.005
Co	0.1	0.1
Ca	0.003	0.003

*By difference

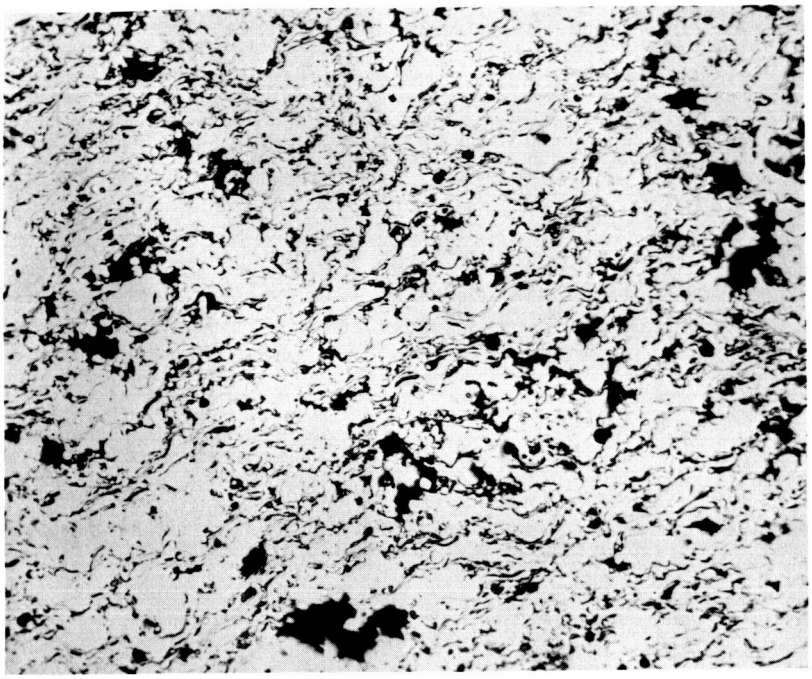

100X LONGITUDINAL SECTION 2G325

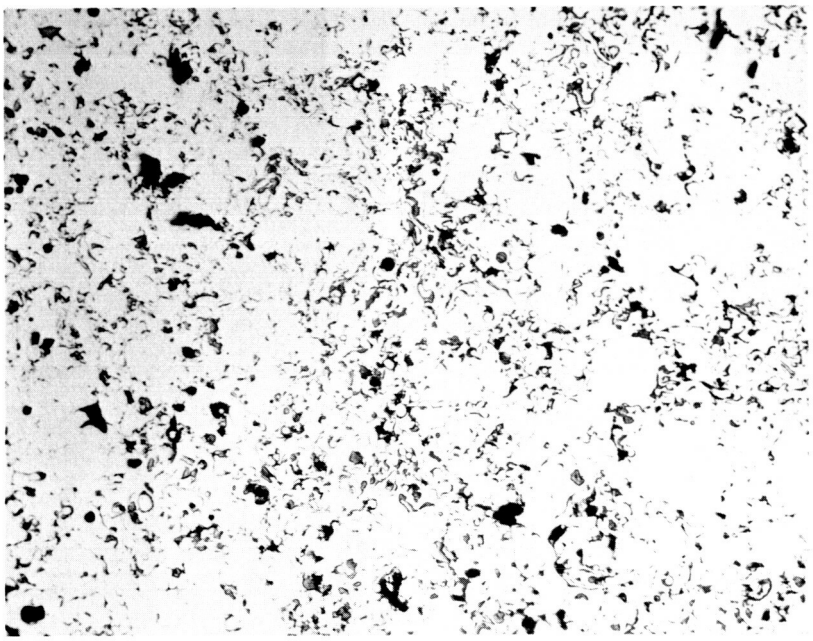

100X TRANSVERSE SECTION 2G326

FIGURE 80. MICROSTRUCTURE OF AS SPRAYED NICHROME (AS-POLISHED)

100X LONGITUDINAL SECTION 2G464

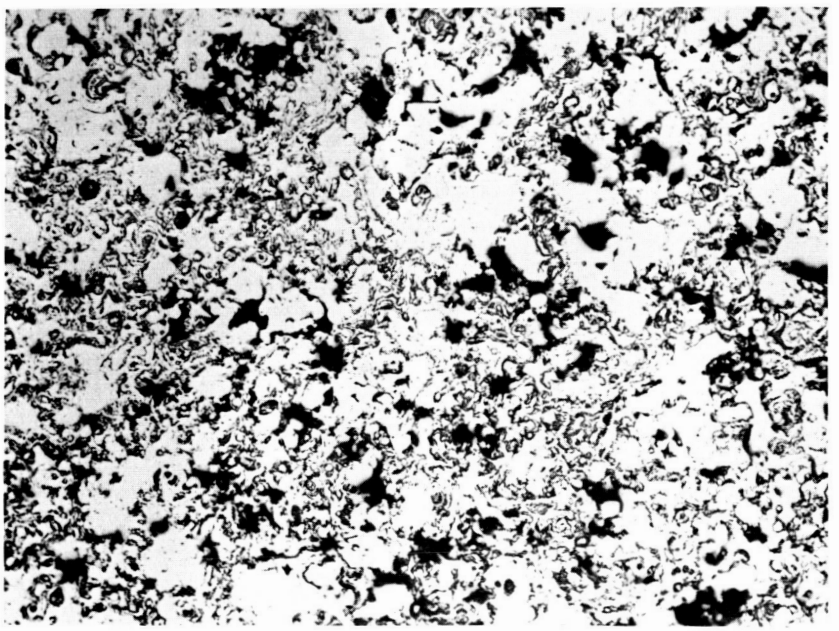

100X TRANSVERSE SECTION 2G462

FIGURE 81. POSTMEASUREMENT MICROSTRUCTURE OF NICHROME, SAMPLE 1 (AS-POLISHED)

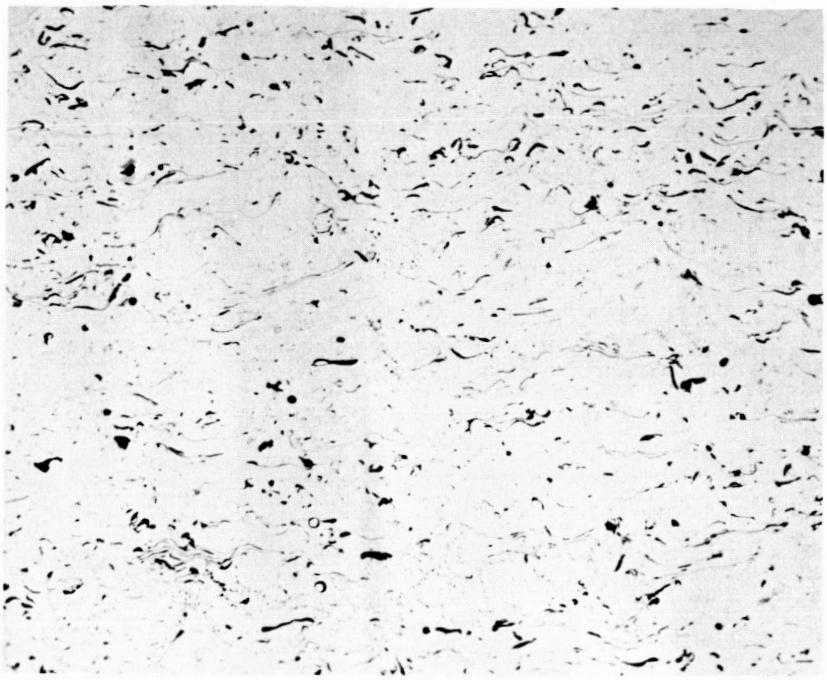

100X LONGITUDINAL SECTION 2G322

100X TRANSVERSE SECTION 2G323

FIGURE 82. MICROSTRUCTURE OF AS-SPRAYED NiAl (AS-POLISHED)

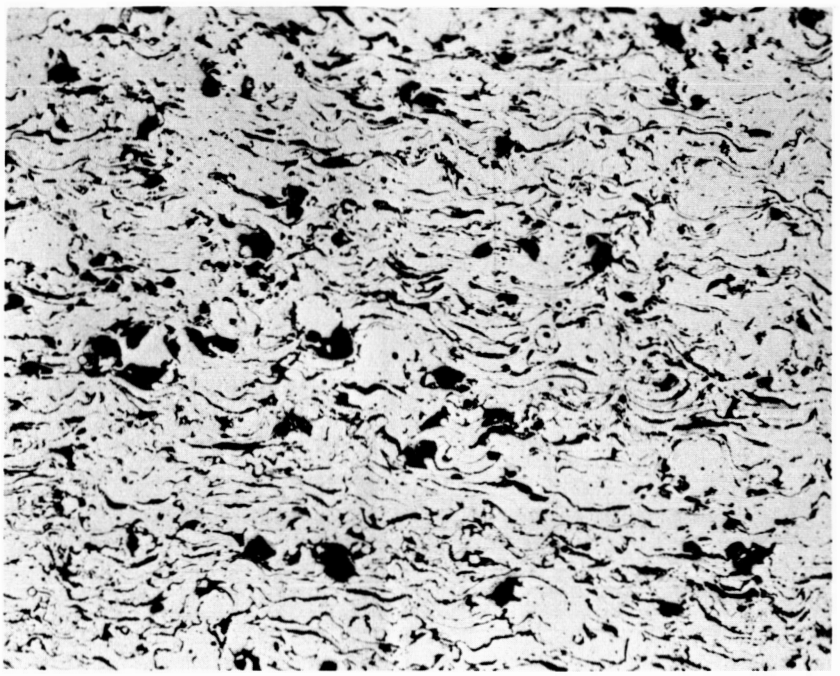

100X LONGITUDINAL SECTION 2G460

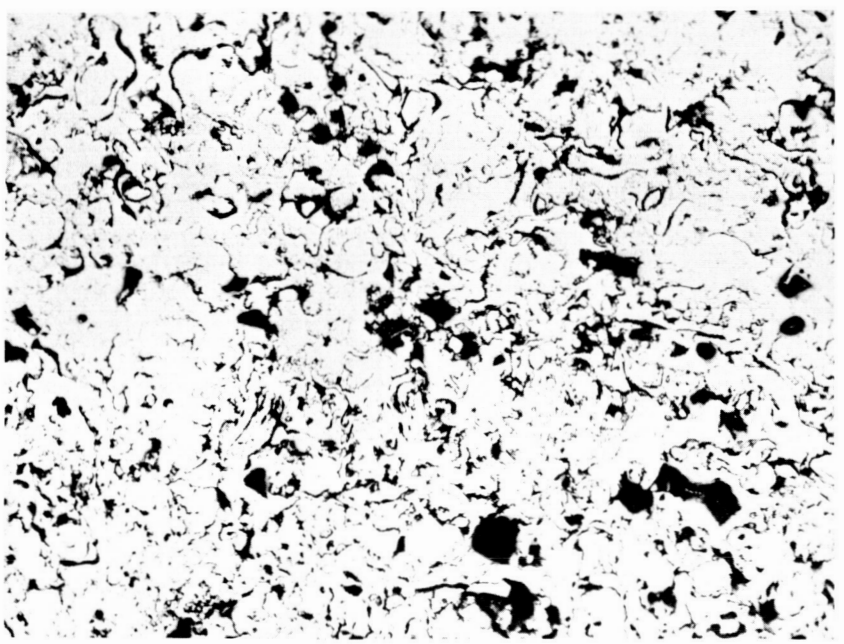

100X TRANSVERSE SECTION 2G458

FIGURE 83. POSTMEASUREMENT MICROSTRUCTURE OF NiAl, SAMPLE 1, (AS-POLISHED)

TABLE 19. PHYSICAL CHARACTERISTICS OF NICHROME AND NiAl THERMAL DIFFUSIVITY SPECIMENS

	Thickness, cm	Diameter, cm	Weight, g	Density, g cm^{-3}
Nichrome				
Pretest	0.2012	1.2664	1.6980	6.80
After First Heating	0.2012	- -	1.6963	- -
After Second Heating	0.2007	1.2639	1.6958	6.82
After First Heat Treatment in Hydrogen	0.2002	1.2649	1.6976	6.82
Posttest	0.2002	1.2621	1.6898	6.79
NiAl				
Pretest	0.2535	1.2659	2.3254	7.40
After First Thermal Cycle	0.2664	1.2700	2.3222	6.99
After First Heat Treatment in Hydrogen	0.2690	1.2845	2.3394	- -
Posttest	0.2690	1.2489*	2.2149*	6.80

*These values differ from those directly above due to additional machining of specimen.

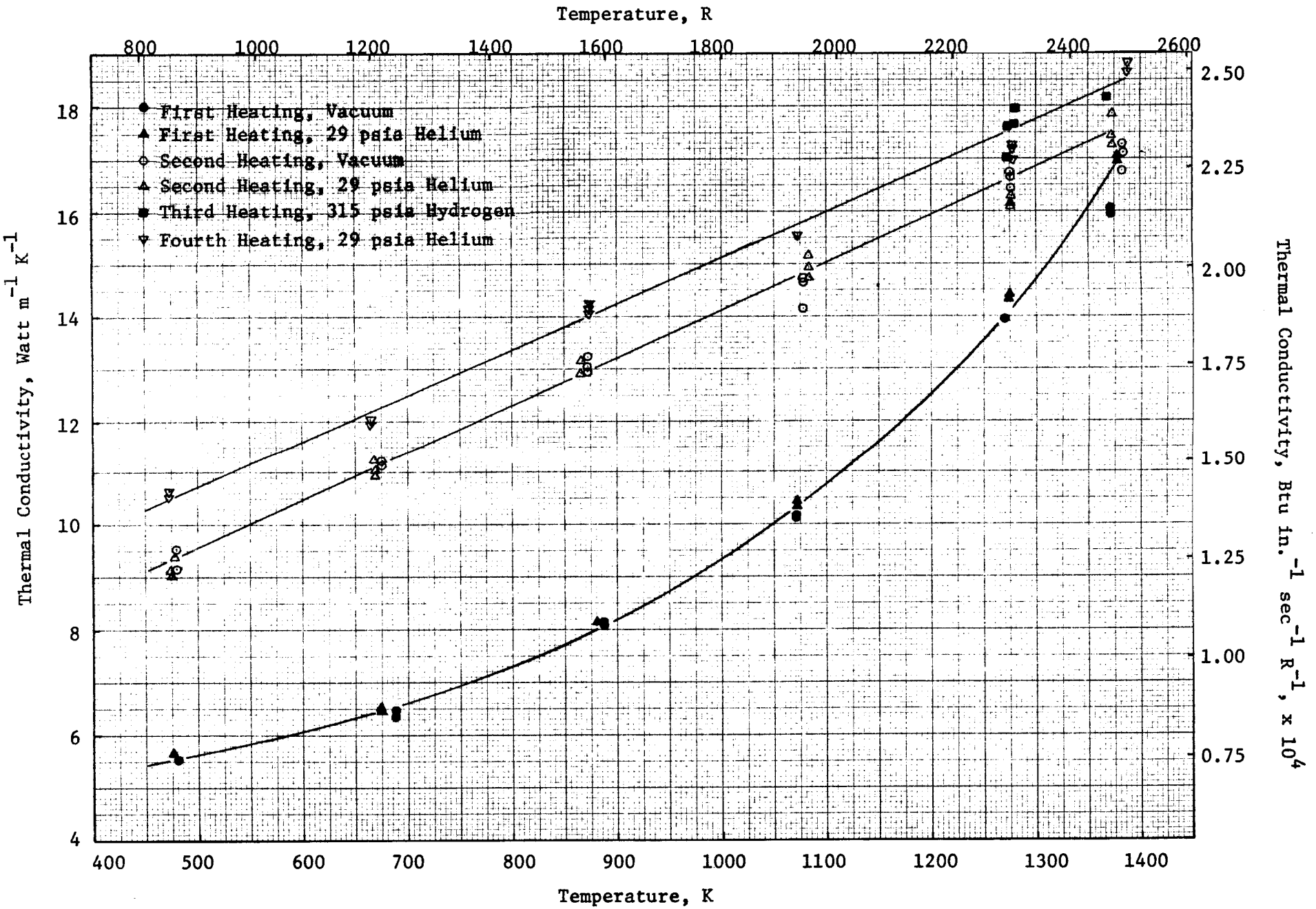

FIGURE 84. THERMAL CONDUCTIVITY OF PLASMA-SPRAYED NICHROME

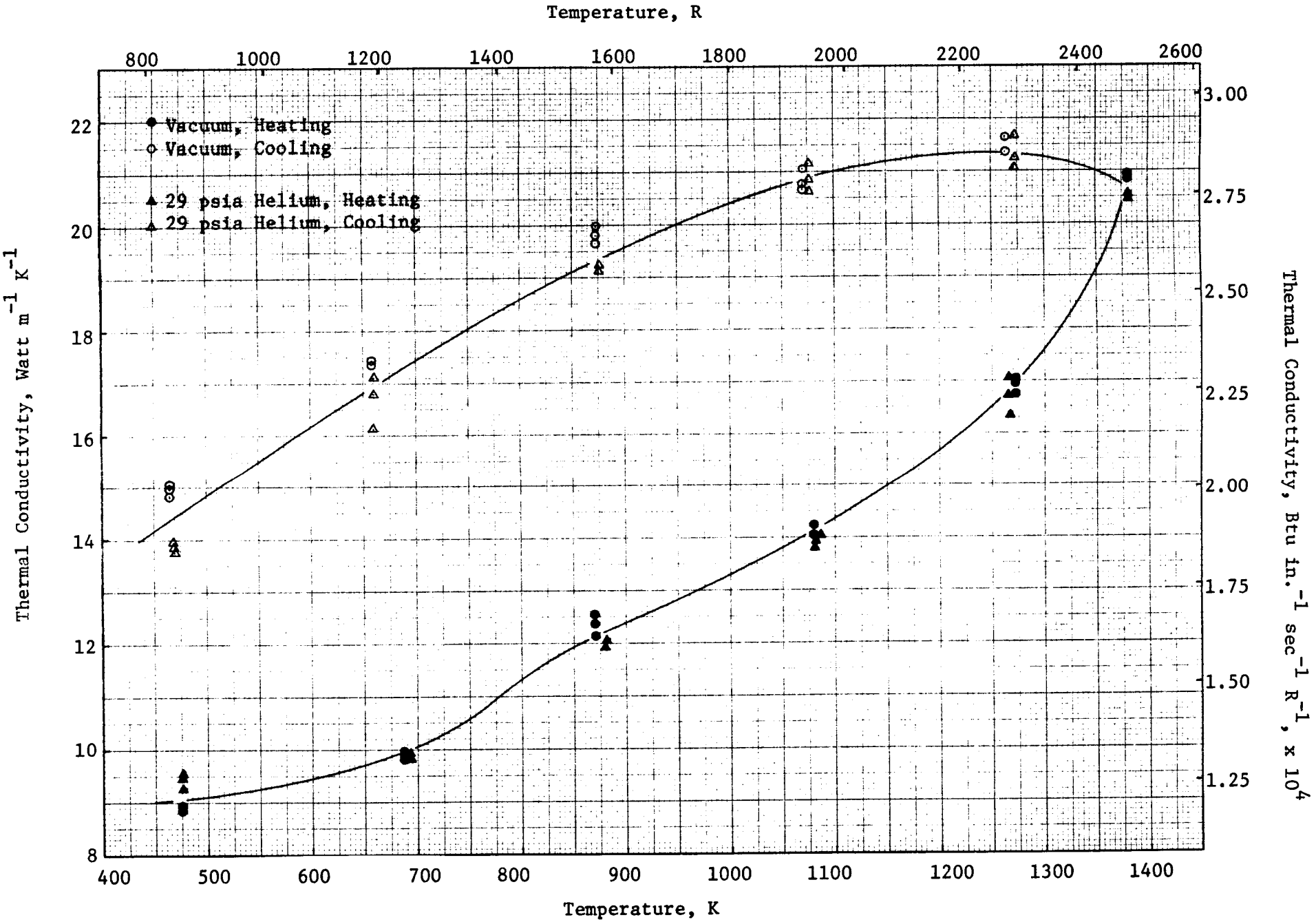

FIGURE 85. THERMAL CONDUCTIVITY OF PLASMA-SPRAYED NiAl, FIRST THERMAL CYCLE

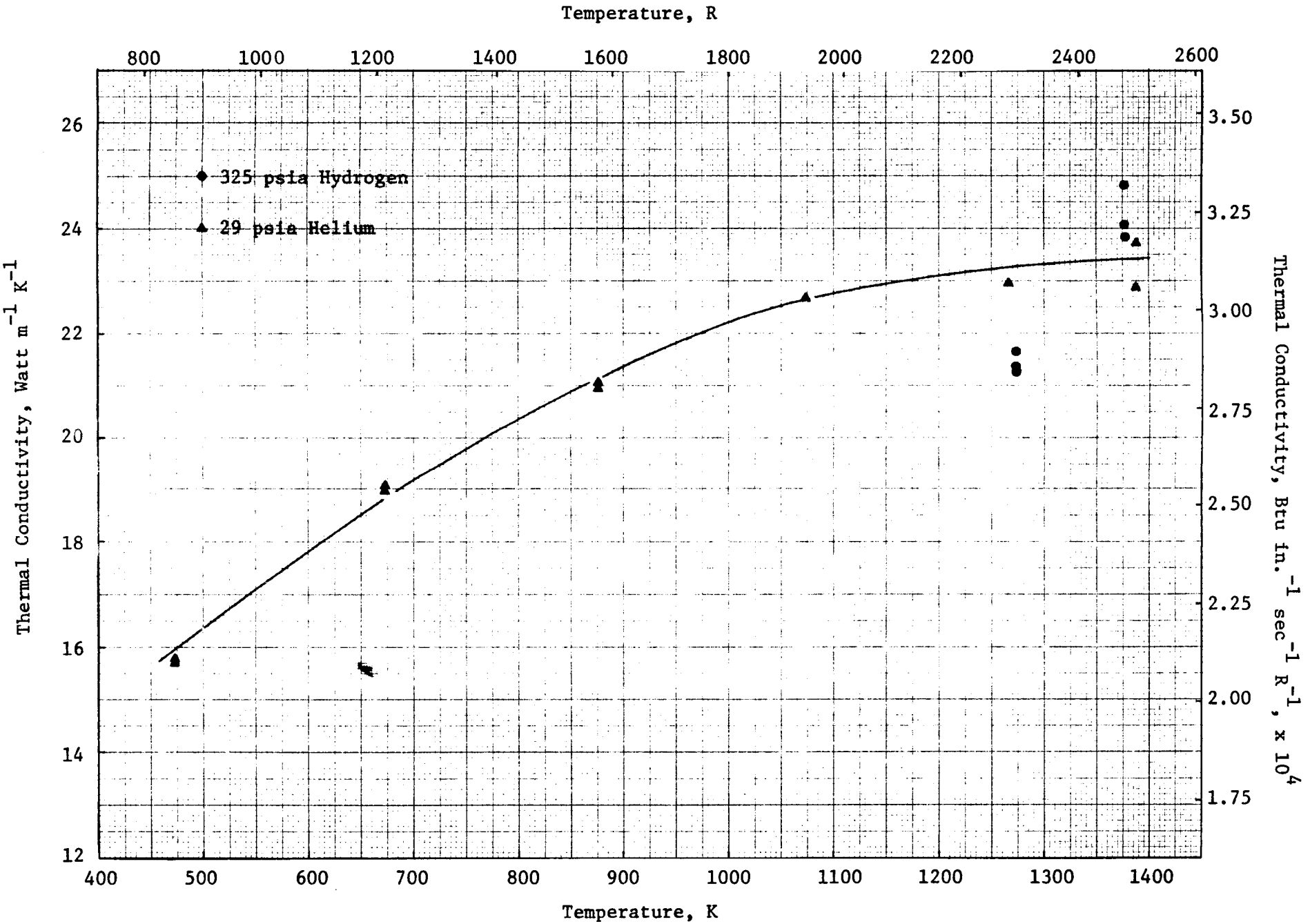

FIGURE 86. THERMAL CONDUCTIVITY OF PLASMA-SPRAYED NiAl, SECOND AND THIRD HEATING

This is also evidenced by the fact that the samples are magnetic, indicating the presence of the α or Ni-rich phase. The equilibrium structure would be a two-phase mixture of the α' or Ni_3Al phase and the α or Ni-rich phase.

The results of specific heat measurements on plasma-sprayed nichrome are given in Figure 87, while similar results for plasma-sprayed NiAl are given in Figure 88. Also shown in Figure 87 are the data of Douglas and Dever[21] for an 80 Ni-20 Cr alloy. The two sets of data are seen to be in excellent agreement above 873 K. The disagreement between the two sets of data below 873 K is less than 6 percent and may be due to differences in heat treatment between the two samples.

Thermal Conductivity Gradient

In order to determine possible thermal conductivity gradients, thermal diffusivity measurements were made in vacuum ($<10^{-5}$ torr) on samples of Y_2O_3-stabilized ZrO_2, HfO_2, and Al_2O_3 of various thicknesses. Physical characteristics of these specimens are given in Table 20. The results of these measurements are given in Figures 89 through 91. The high-temperature data were taken first and the low-temperature data were taken upon cooling. A comparison of the curves shows no obvious trend of conductivity with thickness. The total spread in data at a given temperature on a particular material is at most 13.6 percent. Thus, the effect of coating thickness, if any, is relatively small.

It should also be noted that the ZrO_2 samples changed from white to very dark gray, indicating a change in stoichiometry. Such a change in stoichiometry could account for part of the difference between the data presented in this section for measurements under vacuum and the data presented in an earlier section for measurements under high pressure hydrogen.

Thermal Contact Resistance

Thermal contact resistance studies were conducted on samples consisting of 0.012 in. thick Type 347 stainless steel and approximately equal thicknesses of plasma-sprayed Mo, nichrome, and NiAl. Evaluations of thermal contact conductances are most easily carried out by experimentally measuring $t_{1/2}$, the time required for the back face of a disk specimen to reach one-half its maximum temperature rise on thermal diffusivity measurements. This value of $t_{1/2}$ is then compared with values calculated from Equation (4) using the known properties of the two layers and a range of values for the contact conductance.

The Mo-stainless steel sample consisted of 0.012 in. of stainless steel and 0.0108 in. of plasma-sprayed Mo. A plot of $t_{1/2}$ versus temperature is given in Figure 92. The first measurements were made at 1380 K and then at 1275 K in 365 psia hydrogen. The sample was then transferred to the low-pressure furnace and measurements were made upon heating from 473 to 1373 K with the measuring atmosphere being alternated among vacuum, 15 psia argon, 15 psia helium, and 29 psia helium. Superimposed on this graph are curves of calculated

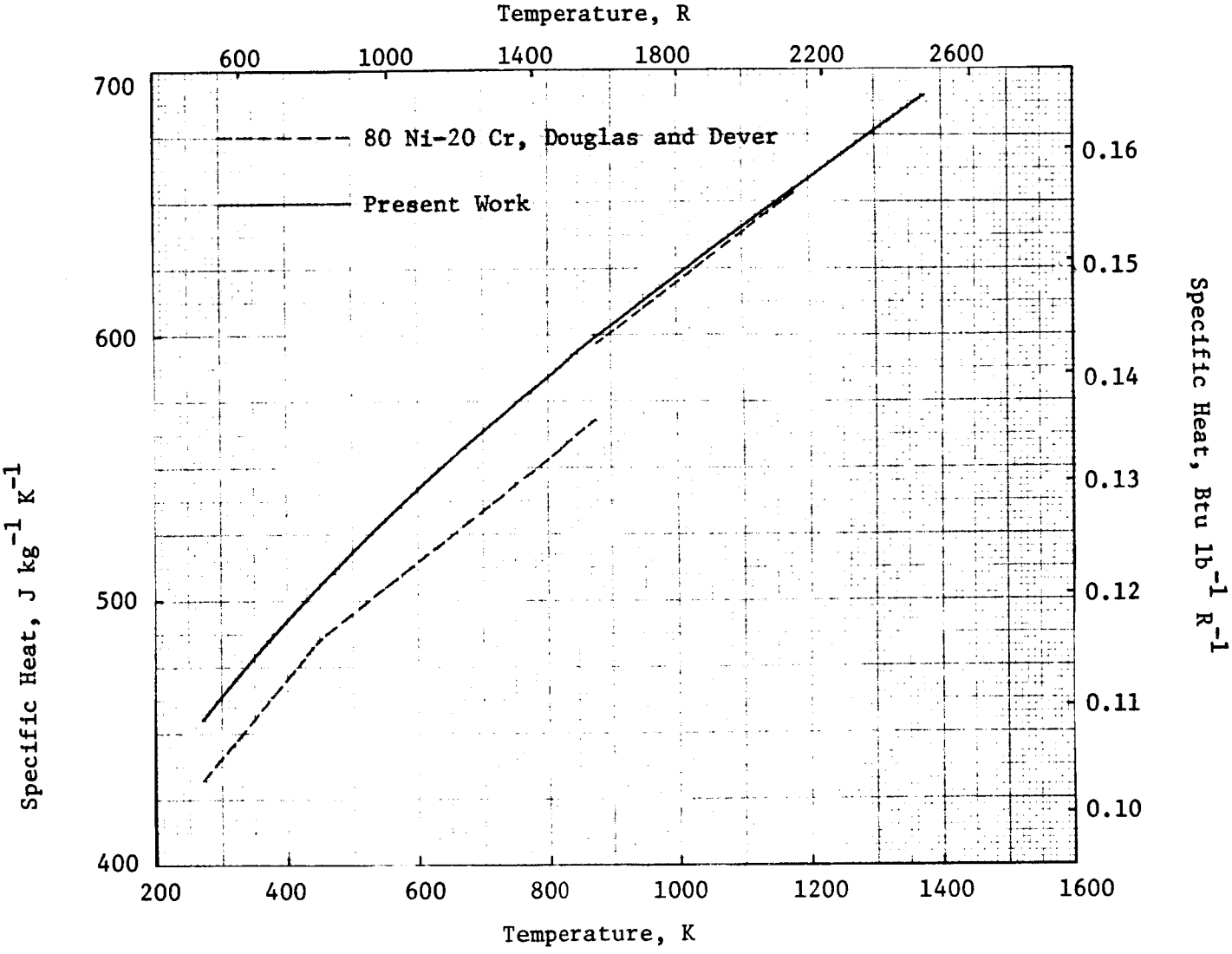

FIGURE 87. SPECIFIC HEAT OF PLASMA-SPRAYED NICHROME

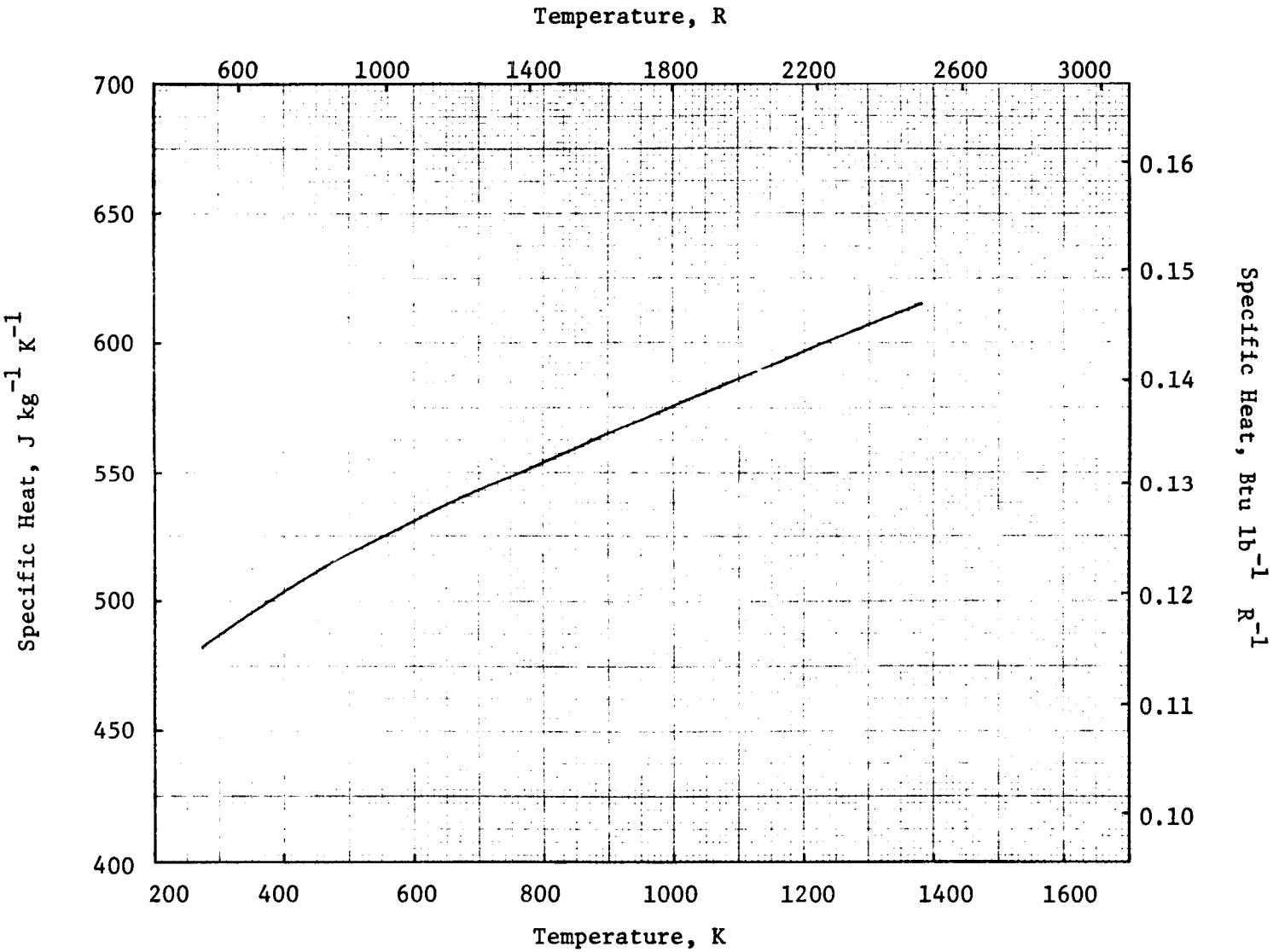

FIGURE 88. SPECIFIC HEAT OF PLASMA-SPRAYED N1A1

TABLE 20. PHYSICAL CHARACTERISTICS OF THERMAL CONDUCTIVITY GRADIENT SAMPLES

	Thickness, cm		Weight, g		Density, g cm^{-3}	
	Pretest	Posttest	Pretest	Posttest	Pretest	Posttest
Y_2O_3-Stabilized ZrO_2						
Sample A	0.0150	0.0150	0.0870	0.0865	4.80	4.94
Sample B	0.0224	0.0224	0.1336	0.1332	4.82	5.05
Sample C	0.305	0.0300	0.1719	0.1711	4.86	5.14
HfO_2						
Sample A	0.0150	0.0145	0.1149	0.1113	6.87	7.64
Sample B	0.0231	0.0221	0.1770	0.1712	6.91	7.66
Sample C	0.0315	0.0302	0.2267	0.2189	6.86	7.61
Al_2O_3						
Sample A	0.0460	0.0937	0.1831	0.1813	3.34	3.68
Sample B	0.0663	0.0630	0.2664	0.2628	3.35	3.69

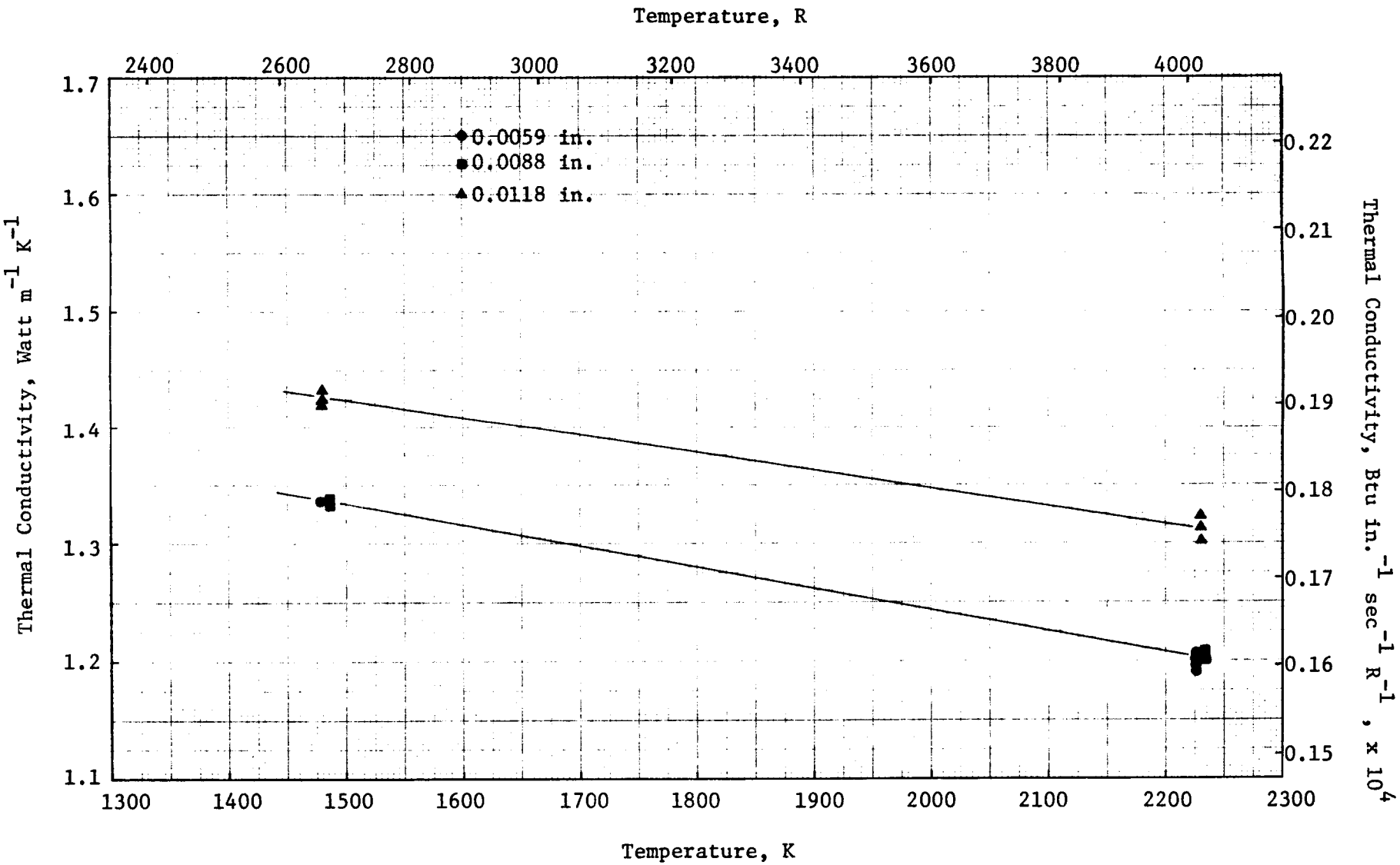

FIGURE 89. THERMAL CONDUCTIVITY OF Y_2O_3-STABILIZED ZrO_2

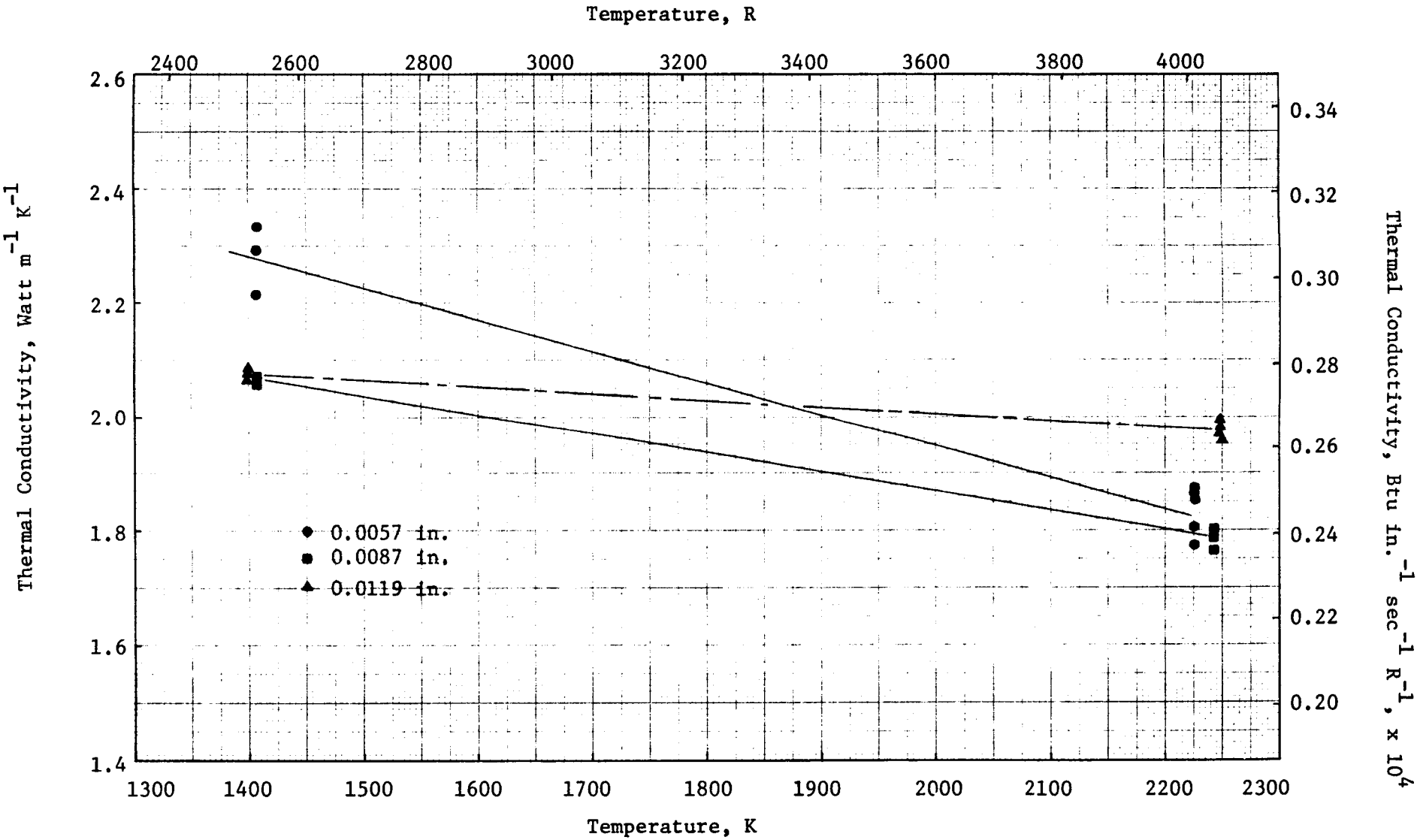

FIGURE 90. THERMAL CONDUCTIVITY OF HfO_2

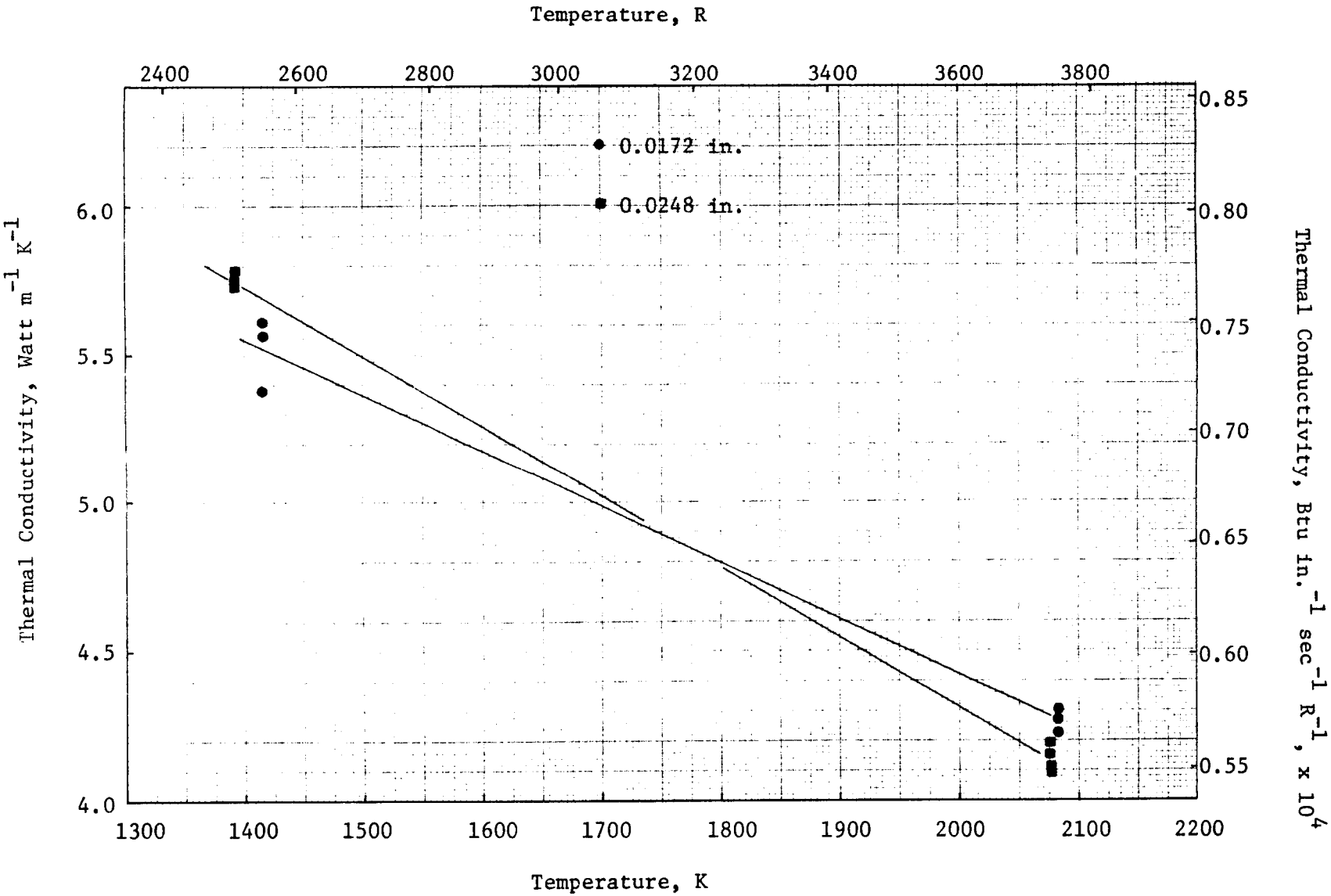

FIGURE 91. THERMAL CONDUCTIVITY OF PLASMA-SPRAYED Al_2O_3

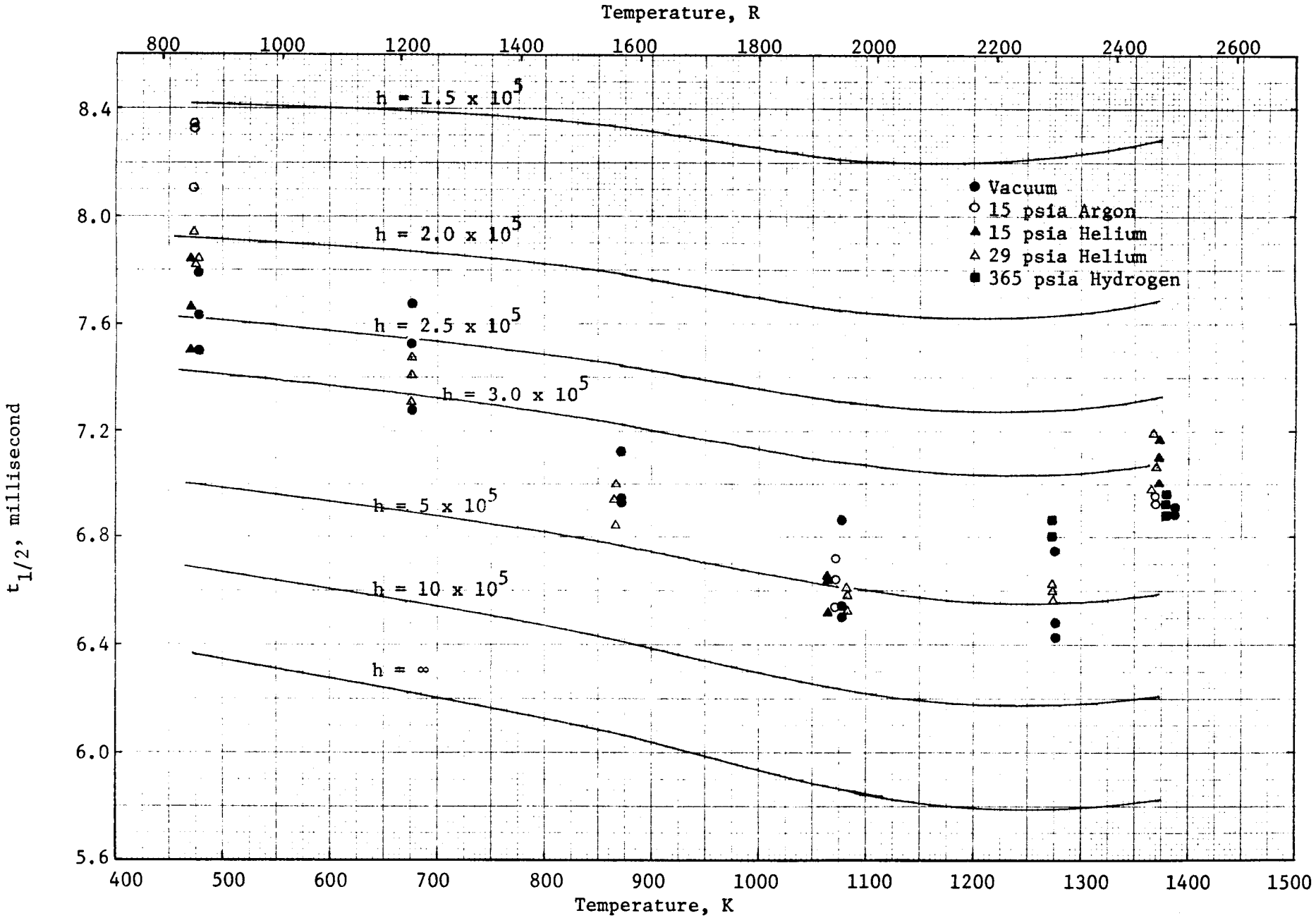

FIGURE 92. HALF-TIME OF STAINLESS STEEL 347 PLASMA-SPRAYED MOLYBDENUM THERMAL CONTACT CONDUCTANCE SPECIMEN

$t_{1/2}$ for thermal contact conductance values of 1.5, 2.0, 2.5, 3.0, 5.0, and 10.0 x 10^5 Watt m^{-2} K^{-1}. The lowest curve is for infinite thermal conductance, i.e., zero thermal resistance. The curves were calculated using the thermal conductivity and specific heat data for Type 347 stainless steel given by Touloukian[22] and the thermal conductivity and specific heat data for molybdenum given in Figures 57 and 58. These latter data should be applicable since the molybdenum in the two samples was given essentially identical heat treatments. Thermal contact conductance values derived from these measurements are given in Figure 93. Two points should be noted. First, there is no obvious dependence upon measurement environment. Second, the values are very high, being greater than 1.5 x 10^5 Watt m^{-2} K^{-1}. In general, these values are much higher than the literature values reviewed by Fried.[23]

The nichrome-stainless steel sample consisted of 0.012 in. of stainless steel and 0.0108 in. of plasma-sprayed nichrome. A plot of measured $t_{1/2}$ versus temperature is given in Figure 94. The measurements were made upon heating from 473 to 1373 K with the measuring atmosphere being alternated among vacuum, 15 psia argon, 15 psia helium, and 29 psia helium. The specimen was then remeasured at 473 K following the above heating sequence. The curve shown on this figure is a plot of $t_{1/2}$ calculated from Equation (3) (i.e., $h = \infty$) using the thermal conductivity and specific heat data for nichrome given in Figures 84 and 87. It can be shown that as the contact conductance decreases, the value of $t_{1/2}$ increases; also, negative values of contact conductance are physically unrealistic. Since almost all the measured values of $t_{1/2}$ are lower than the calculated values, it is not possible to derive values of contact conductance. The discrepancies between the calculated and experimental values are small and could be partly due to experimental errors both in the measurement of $t_{1/2}$ and in the property values used in the calculations. Another possibility for the discrepancy is that the nichrome in the composite sample is not in exactly the same state as the nichrome sample used in obtaining the data in Figures 84 and 87. The only conclusion that can be reached from these data is that the contact resistance between the two layers is small and is probably negligible.

The NiAl-stainless steel sample was made up of 0.012 in. of stainless steel and 0.0127 in. of plasma-sprayed NiAl. The measured values of $t_{1/2}$ are shown in Figure 95, along with the calculated curve for zero contact resistance. This curve was calculated using the thermal conductivity and specific heat data for NiAl given in Figures 85 and 88. Again, since most of the measured $t_{1/2}$'s are lower than the calculated curve, no values of thermal contact conductance were derived from these measurements.

SUMMARY OF RESULTS

Thermal conductivity values have been determined for the following plasma-sprayed materials: CaO-stabilized ZrO_2, Y_2O_3-stabilized ZrO_2, Al_2O_3, HfO_2, Mo, nichrome, NiAl, and Mo-ZrO_2, and Mo-Al_2O_3 mixtures. In all cases, the thermal conductivity of the as-sprayed material was found to be considerably lower than that of the bulk material and was found to increase as a result of heat treatment at high temperatures, apparently due to sintering effects. These sintering effects also result in significant dimension shrinkages.

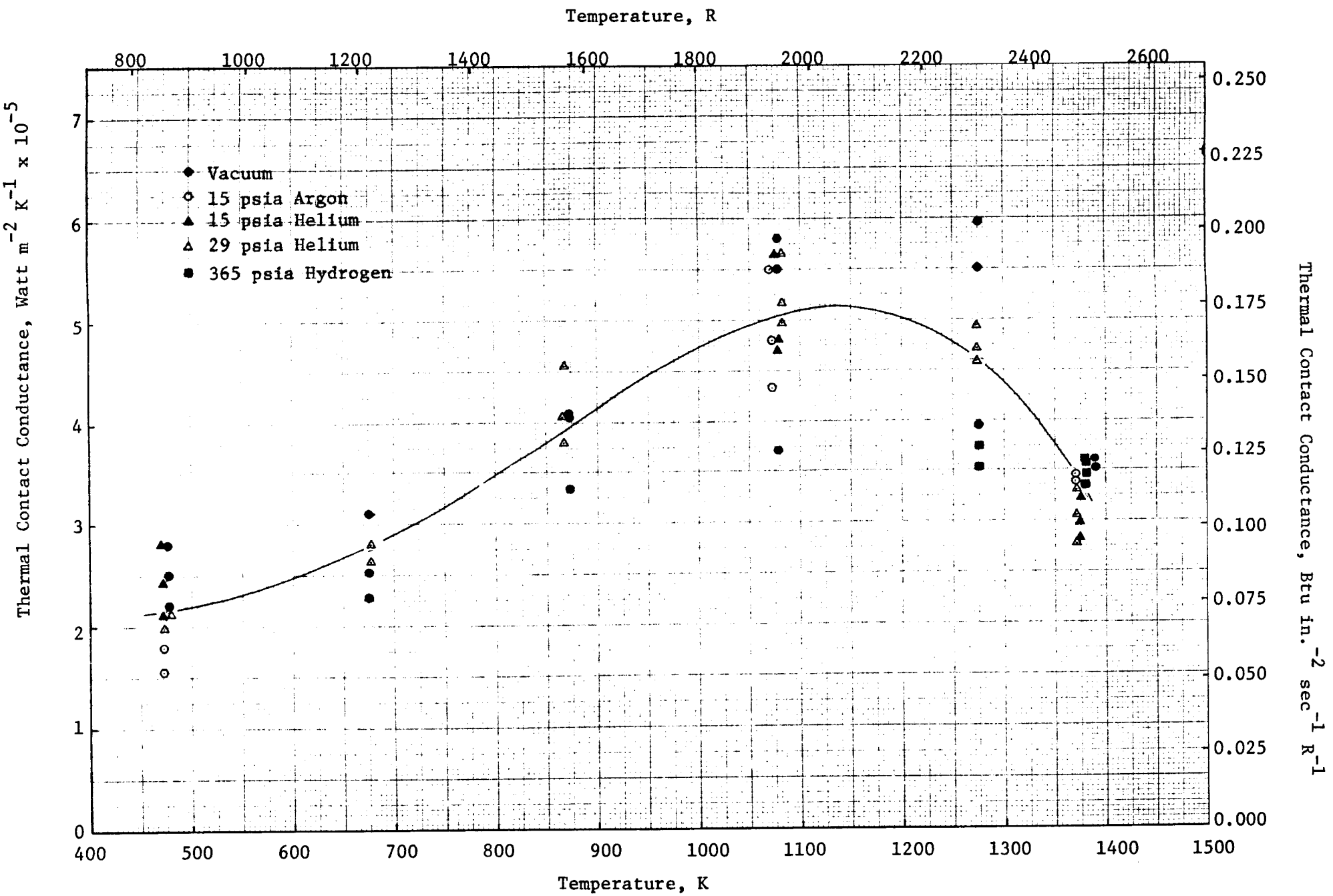

FIGURE 93. THERMAL CONTACT CONDUCTANCE BETWEEN TYPE 347 STAINLESS STEEL AND PLASMA-SPRAYED MOLYBDENUM

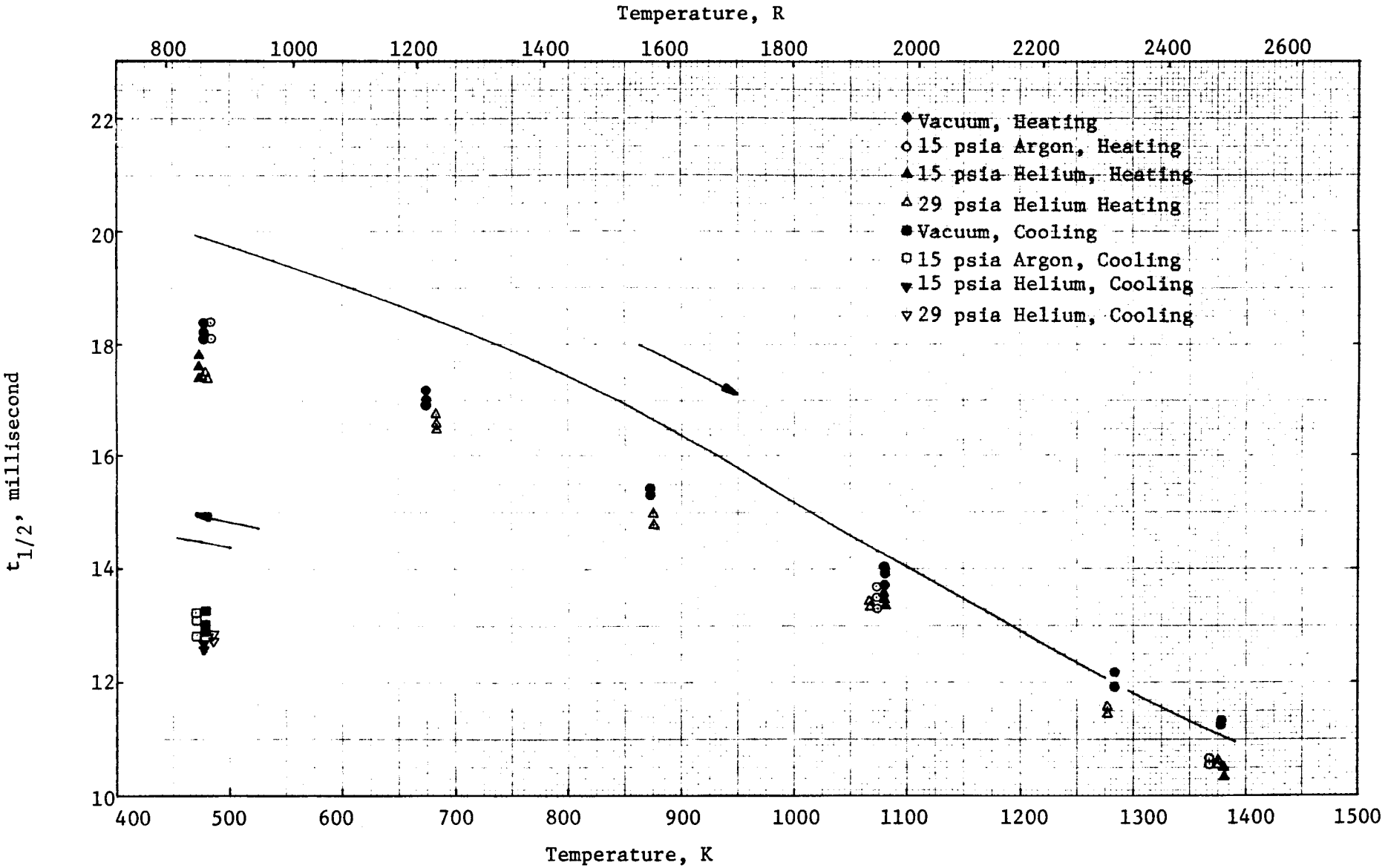

FIGURE 94. HALF-TIME OF STAINLESS STEEL 347-PLASMA SPRAYED NICHROME THERMAL CONTACT CONDUCTANCE SPECIMEN

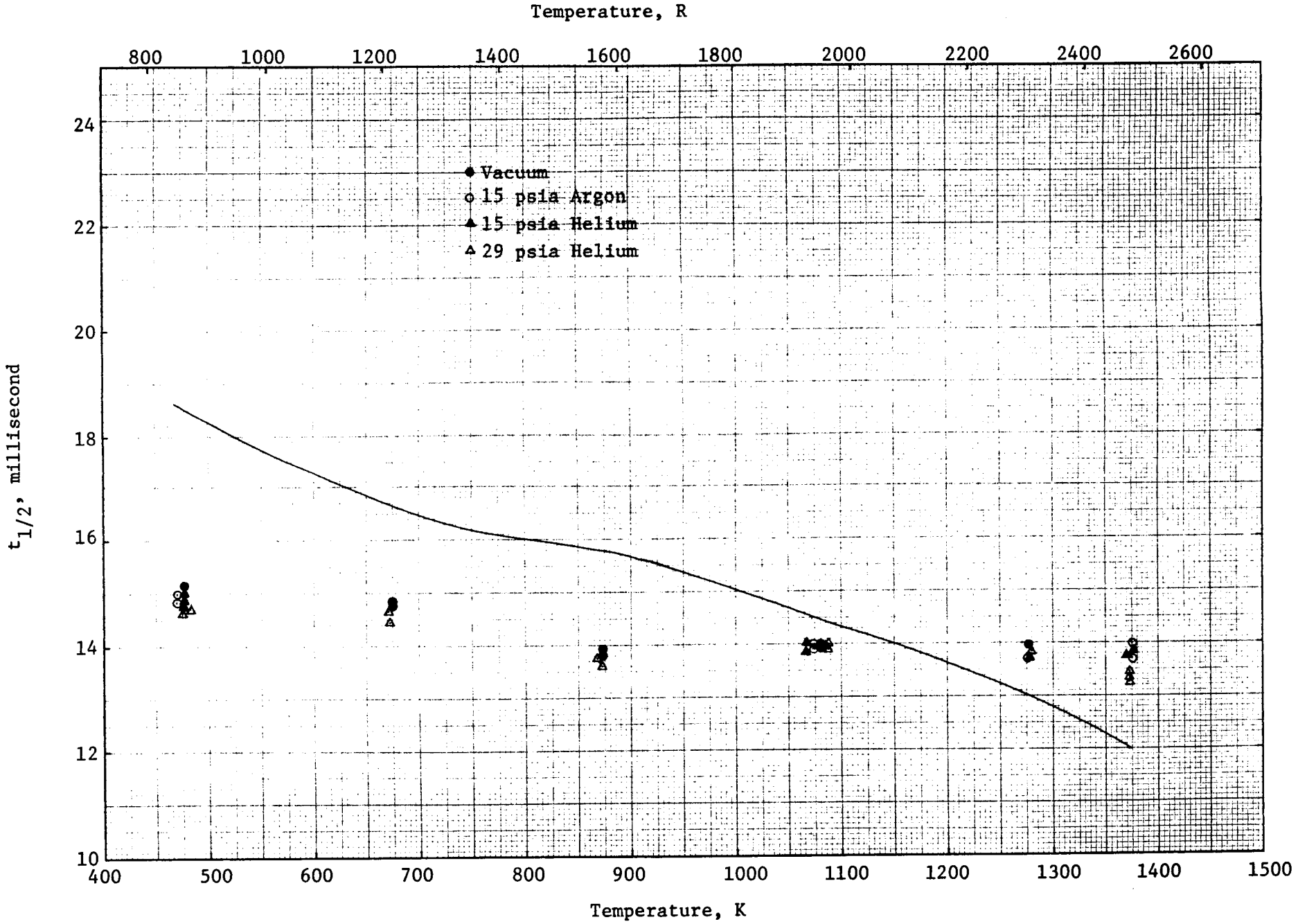

FIGURE 95. HALF-TIME OF STAINLESS STEEL 347-PLASMA SPRAYED NiAl THERMAL CONTACT CONDUCTANCE SPECIMEN

Thermal conductivity increases were found to be functions of heat treatment temperature and heat treatment time. The heat treatment temperature appears to be the major variable, with the heat treatment time producing relatively minor effects. In some cases, the measuring atmosphere (i.e., type and pressure of gas) has a significant influence on the thermal conductivity. High-temperature heat treatments reduce the effect of the atmosphere. It was found that plasma-sprayed coatings containing molybdenum contain significant amounts of oxygen which is removed by heat treatment in hydrogen at fairly moderate temperatures. However, since the water vapor formed by this reaction would probably be removed from the coating system, this effect might not be deleterious to coating performance.

No obvious trend was found for thermal conductivity versus coating thickness for Y_2O_3-stabilized ZrO_2, Al_2O_3, HfO_2. Thus, thermal conductivity gradients, if present at all, are relatively small.

The thermal contact conductance between a stainless steel substrate and a layer of plasma-sprayed molybdenum was found to vary between 1.5×10^5 and 6×10^5 Watt m^{-2} K^{-1}. Corresponding thermal contact resistances would be between 6.7×10^{-6} and 1.7×10^{-6} $Watt^{-1}$ m^2 K. At most, this contact resistance would yield a thermal resistance equivalent to a layer of plasma-sprayed ZrO_2 about 1.3×10^{-5} m (about 0.0005 in.) thick.

REFERENCES

1. Cowan, R. D., "Pulse Method of Measuring Thermal Diffusivity at High Temperatures", J. Appl. Phys., 34, 926-927 (1963).

2. Larson, K. B., and Koyama, K., "Measurement by the Flash Method of Thermal Diffusivity, Heat Capacity, and Thermal Conductivity in Two-Layer Composite Samples", J. Appl. Phys., 39, 4408-4416 (1968).

3. Garvie, R. C., "Zirconium Dioxide and Some of Its Binary Systems", in High Temperature Oxides, Part II, ed. by A. M. Alper, pp 117-166, Academic Press, New York (1970).

4. Pratt, A. W., "Heat Transmission in Low Conductivity Materials", in Thermal Conductivity, Vol. 1, ed. by R. P. Tye, pp 301-313, Academic Press, New York (1969).

5. Touloukian, Y. S., ed., Thermophysical Properties of High Temperature Solid Materials, Vol. 4, Part I, p 916-917, MacMillan, New York (1967).

6. Levinstein, M. A., Gen. Elec. Co. USAF, NADD-TR-60-654, 1-91 (1961), (As quoted in Reference 5, p 915).

7. Borovik, Ye. S. and Usikova, N. G., Fizika. Metallov; Metallovedenie, 13, (3), 470-4 (1962), (As quoted in Reference 5, p 915).

8. Fitzsimmons, E. S., G. E. Aircraft Nuclear Propulsion Dept., DC-61-6-4, 1-9 (1961), (As quoted by Reference 5, pp 968-969).

9. Hobbs, H. A. Plunkett, J. D., and Kingery, W. D., Lexington Lab, Inc, Gen. Elec. Co. Aircraft Nuclear Propulsion Dept., Report No. 6, 1-4 (1961), (As quoted by Reference 5, pp 968-969).

10. Touloukian, Y. S., and Ho, C. Y., editors, Thermophysical Properties of Matter, The TPRC Data Series, 2, p 119, IFI/Plenum, New York (1970).

11. Furukawa, G. T., Douglas, T. B., McCoskey, R. E., and Ginnings, D. C., J. Res. Nat'l. Bur. Std. RP2964, 57, 67-82 (1956).

12. Prophet, H. and Stull, D. R., J. Chem. Eng. Data, 8, (1), 78-81 (1963).

13. Pears, C. D., "The Thermal Properties of Twenty-Six Solid Materials to 5000°F on their Destruction Temperatures", USAF ASD-TDR-62-765, 1-420 (1962).

14. Brown, L. M., and Mazdiyasni, K. S., "Characterization of Alkoxy-Derived Yttria-Stabilized Hafnia", J. Amer. Ceram. Soc., 53 (11), 590-594 (1970).

15. Shunk, F. A., Constitution of Binary Alloys, 2nd Supplement, McGraw-Hill, New York, 517 (1969).

16. Ho, C. Y., Powell, R. W., and Liley, P. E., Thermal Conductivity of Selected Materials, Part 2, NSRDS-NBS 16, U.S. Dept. Comm. p 20 (1968).

17. Taylor, R. E., and Finch, R. A., USAEC, NAA-SR-6034, 1-32 (1961).

18. Kirillin, V. A., Sheivdlin, A. E., and Chekhovshoi, V. Ya., Intern. J. Heat Mass Transfer, 5, 1-9 (1962).

19. Kingery, W. D., Introduction to Ceramics, pp 499-504, Wiley, New York (1960).

20. Hansen, M., Constitution of Binary Alloys, McGraw-Hill, New York, 118 (1958).

21. Douglas, T. B. and Dever, J. L., "Enthalpy and Specific Heat of Four Corrosion-Resistant Alloys at High Temperatures", J. Res. Nat'l Bur. Std. 54, (1), pp 15-19 (1955).

22. Touloukian, Y. S., editor, Recommended Values of the Thermophysical Properties of Eight Alloys, Major Constituents and their Oxides, TPRC Report 16, NBS Subcontract No. CST-7590, NASA Order R-45 (1966).

23. Fried, E., "Thermal Conduction Contribution to Heat Transfer at Contacts", in Thermal Conductivity, 2, ed by R. P. Tye, pp 253-274, Academic Press, New York (1969).